The Effects of Wear on the Morphology and Puncture Force of Shark Teeth

By
Ryan Lucas Sesler
April 3, 2023



Allegheny College
Department of Biology

The Effects of Wear on the Morphology and Puncture Force of Shark Teeth

By
Ryan L. Sesler
April 3, 2023

A Senior Comprehensive Project in Partial Fulfillment of the Requirements for a Bachelor of Science Degree from Allegheny College

I hereby recognize and pledge to fulfill my responsibilities as defined in the Honor Code and to maintain the integrity of both myself and the College community as a whole.

_____
Pledge

Approval by the Senior Thesis Committee:

_____
Dr. Lisa Whitenack, 1st Reader

_____
Dr. Matthew Venesky, 2nd Reader

Acknowledgments

Throughout my four years here at Allegheny College, my family has been my biggest cheerleaders and largest support system. Their dedication to my academics and encouraging support for my dreams have been never-ending. Without my mother, father, and my older brother, Morgan, I am not sure this project would have been finished on time and completed with such care and attention to detail. I am forever grateful for the love and care of my family.

While this project was completed through hard work and dedication, the intricacies of figuring out multiple details would not have been possible without the help of my advisor and first reader, Dr. Lisa Whitenack. Dr. Whitenack has consistently provided crucial guidance and advice during this entire project, and ever since its origins two years ago, she has been one of my closest confidantes and friends. I could not imagine writing this project and soon-to-be published paper without the best advisor and co-author out there.

To Matt Luckiewicz, Tyler Miller, Andreas Vukas, Caleb Moon, and all the brothers of Phi Gamma Delta Fraternity, I owe my deepest gratitude and thanks to you. My fraternity brothers have been with me through all the highs and lows of this project and without them, I do not know what I would do. Thank you to all the FIJIs who have stood by my side.

To conclude my acknowledgements, I would like to thank Allegheny College and its students. I have made lifelong friendships here and without my friends and their unconditional love, I would not be the man I am today. People such as Sarah Pillittieri, Taylor Hayes, Madison Kobylski, Riya Agrawal, Meredythe Baird, Macy White, Abigail Fields, and countless others have made my time here unforgettable.

Allegheny College is, and forever will be, my second home and I cannot wait to see the next generation of marine biology students thrive at this incredible institution. Thank you -

Abstract

Over the course of their lives, sharks replace thousands of teeth. Their teeth have been shown to be structurally and mechanically strong, resisting breakage or fracturing. Based upon this knowledge, the replacement of shark teeth and the frequency at which teeth are replaced could possibly be a consequence of tooth wear, not tooth failure. This project provides an analysis of how tooth wear can affect tooth morphology and puncture performance quantitatively in different species of shark. Individual puncture testing included five teeth each from five species of shark: *Carcharhinus plumbeus*, *C. leucas*, *C. limbatus*, *Sphyrna mokarran*, and *Isurus oxyrinchus*. Puncture testing of each tooth consisted of 400 repeated punctures into a standard prey item. The force of each puncture was recorded at specific intervals, ranging from between 10 to 30 punctures. At each interval, microscopic pictures of the tooth provided photographic evidence of physical wear along the cutting edges and tooth apex. Puncture testing displayed that visible tooth wear occurs over the 400 punctures, however, the rate at which the tooth wore down varied depending on the shark species and specific region of the tooth. Additionally, the puncture force required to complete one puncture increased over the entirety of testing. The data indicated that as the teeth wear down in small increments over time, the ability to function efficiently decreases. Future studies concerning shark tooth replacement rates and the maximum number of bites a tooth can withstand are necessary to complete the link between tooth wear and tooth replacement.

Introduction

While the fossil record of most terrestrial animals' skeletons can be easily studied to understand their morphological characteristics and evolutionary patterns, the skeletons of chondrichthyans, such as sharks, rays, skates, and chimeras, degrade over a period of time due to their cartilaginous composition (Garland et al. 1992; Hunt 2010; Johanson et al. 2012; Voje 2018; Whitenack et al. 2011). These organisms rarely leave behind fossilized skeletons that can be examined for biomechanical evolution or physiological analysis, unless they become mineralized (Johanson et al. 2012). Because of this, fossilized teeth from shark species are some of the few remains which can be found. The study of fossilized teeth across species of sharks has led to new predator-prey interaction discoveries based upon the morphology and functional testing of the teeth (Whitenack et al. 2011). Furthermore, utilizing fossilized teeth and comparing them to teeth found in modern-day species, one can follow the morphological changes to that species' teeth as feeding behavior and prey availability fluctuated throughout history (Cappetta 1987; Hunt 2010; Johanson et al. 2012; Lowe et al. 1996; Moss 1970; Motta et al. 2008; Rasch et al. 2016). Fundamentally, the efficiency of a shark's tooth, or any predator's feeding apparatus by this definition, has a direct correlation to the survival of that organism and its fitness level (Whitenack and Motta 2010).

Shark Tooth Morphology & Function

With an evolutionary history of over 400 million years, sharks are one of the world oceans' apex predators and have fascinated humans with their innate hunting behaviors and jaws filled with razor-sharp teeth (Huber et al. 2009). Rivaling that of mammals, shark teeth carry distinct diversity between species to the point where a majority of species identification can be done via teeth alone (Corn et al. 2016; Frazzetta 1988; Moss 1972; Moss 1977). There are

exceptions to this specific identification technique within certain taxonomic designations of sharks, as seen in many requiem sharks (Order Carcharhiniformes, Family Carcharhinidae) which include species like spinner sharks (*Carcharhinus brevipinna*), blue sharks (*Prionace glauca)*, and silky sharks (*Carcharhinus falciformis*). These species follow a similar tooth morphology pattern like the majority of this family; each species is equipped with serrated, somewhat triangular teeth which vary in size (Cappetta 1987; Corn et al. 2016; Frazzetta 1988; Moss 1972; Moss 1977; Motta et al. 2008; Whitenack et al. 2011).

Chondrichthyan teeth are often grouped into the distinct, overall categories of clutching, puncturing, slicing, crushing, and grinding (Bergman et al. 2017; Cappetta 1987; Enax et al. 2012; Frazzetta 1988; Moss 1972; Moss 1977; Whitenack and Motta 2010). These categories, outlined by studies such as Whitenack and Motta (2010), sort teeth based upon their functional morphologies. For example, the teeth of the short-fin mako shark (*Isurus oxyrinchus*) are non-serrated and utilized to firmly grasp and puncture prey items, but are less effective when slicing (Frazzetta 1988; Whitenack and Motta 2010). Serrated teeth, such as those of the bull shark (*Carcharhinus leucas*), exemplify the slicing category for their ability to remove larger sections of flesh from prey items (Abler 1992; Bergman et al. 2017; Cappetta 1987; Enax et al. 2012; Whitenack and Motta 2010).

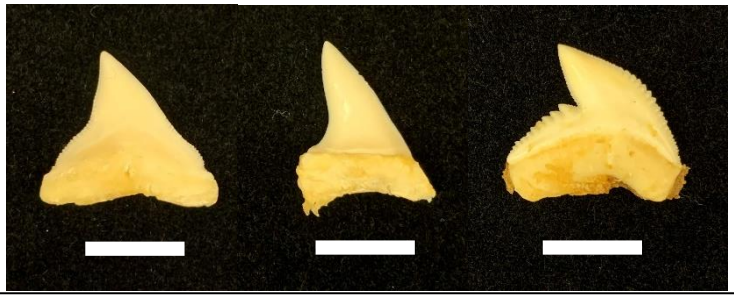


Figure 1: The diverse morphology of shark teeth is a physical indicator of various predator-prey interactions.

The tooth of *Carcharhinus leucas* (left) displays the morphology of serrated and somewhat triangular. The non-serrated *Isurus oxyrinchus* tooth (middle) is efficient at puncturing prey. The uniquely designed *Galeocerdo cuvier* tooth (right) is specific for various prey items. The white bars signify a scale of 1 centimeter.

While many sharks in the family Carcharhinidae have triangular-shaped teeth (e.g., bull shark teeth, *C. leucas*, in Figure 1), other taxonomic families can range from non-serrated daggers (e.g., short-fin mako shark teeth, *I. oxyrinchus*, in Figure 1) to angular teeth with distinct notches and a "bent" appearance (e.g., great hammerhead teeth, *Sphyrna mokarran*) (Cappetta 1987; Corn et al. 2016; Frazzetta 1988). Additional factors can divide shark teeth into more functional subcategories, such as specific types of teeth which require lateral motion or shaking of the head to efficiently cut utilizing serrations (Moyer and Bemis 2017). These subcategories can blend within each other, differing not by their function, but by their morphology (Bergman et al. 2017; Cappetta 1987; Moss 1972; Moyer and Bemis 2017). For example, the teeth of *Galeocerdo cuvier* are shaped like can-openers (Figure 1), characterized by a deep notch on the distal side of the tooth and the presence of large serrations including both primary and secondary serrations (Moyer and Bemis 2017). These teeth are most spectacularly utilized in the hunting and consumption of sea turtles, as the teeth are able to efficiently puncture through the sea turtle's hard shell (Corn et al. 2016; Heithaus 2001; Lowe et al. 1996; Simpfendorfer et al. 2001). Further examples include the presence of serrations on the teeth of large requiem sharks (Family Carcharhinidae), which hunt for larger fish and utilize their teeth for prey apprehension and

tearing capabilities (Bergman et al. 2017; Frazzetta 1988; Wilga et al. 2007). These sharks, like *C. leucas* and *C. plumbeus*, rely on the combination of lateral motion and the teeth serrations to efficiently cut through their prey (Bergman et al. 2017; Cappetta 1987; Ferrara et al. 2011; Frazzetta 1988; Whitenack and Motta 2010). Predator-prey morphology relationships, such as the examples of *G. cuvier* and requiem sharks, have been proposed numerous times with various shark species, usually citing the teeth as being closely associated with the capture of specific prey (Corn et al. 2016; Enax et al. 2012; Mcelroy et al. 2006; Moss 1972).

It has been hypothesized that tooth shape is a direct indicator of feeding behavior in multiple species of cartilaginous fish, including sharks (Ferrara et al. 2011; Motta and Wilga 2001; Whitenack and Motta 2010; Wilga et al. 2007). It is still widely unknown whether these predator-prey relationships exist due to correlations between adaptations found throughout the evolutionary history of sharks or due to species dentition characteristics (Ferrara et al. 2011). However, with these predator-prey relationships, few have actually successfully tested the effects of morphology-based cutting efficiency on specific prey species associated with different sharks (Anderson and LaBarbera 2008; Dean et al. 2008). Frazzetta (1988) focused on the theoretical categorization of shark tooth cutting ability, but overall experimentation was limited (Anderson and LaBarbera 2008). It was not until Abler (1992) that serrated teeth were tested for cutting capabilities (Anderson and LaBarbera 2008). Because of this lack in research, the overall link between tooth morphology, function, and feeding behavior is widely unknown and understanding this link could increase our current knowledge of these ocean predators' feeding mechanics (Abler 1992; Corn et al. 2016; Moss 1972; Motta and Wilga 2001).

Shark Tooth Mechanics

Ferrara et al. (2011) affirms that the mechanical performance of a shark's jaw, and thereby its teeth, affects the capture of prey items, accounting for behavioral and physical characteristics. A majority of chondrichthyans rely on the continuous replacement of functional teeth as a major factor in each species' survival rate (Ferrara et al. 2011; Rasch et al. 2016). This replacement of teeth evolved out of an ancestral, slower tooth replacement designed for smaller prey (Bergman et al. 2017). As larger prey became common within chondrichthyan diets, a simultaneous process of moving a new tooth forward to replace the old tooth allowed for sharper, less worn teeth to occupy the functional row (Bergman et al. 2017; Corn et al. 2016; Rasch et al. 2016; Whitenack et al. 2011). Once in the functional position of the jaw, the "cycle" of tooth replacement restarts as the sharp, new teeth begin usage during prey capture (Abler 1992; Bergman et al. 2017). Shark teeth, like any finely sharpened edge, possess an inverse relationship with natural wear patterns; very sharp, new functional teeth have the disadvantage of dulling at a faster rate, while more worn or blunt teeth wear down at a slower rate (Anderson and LaBarbera 2008; Anderson 2018; Corn et al. 2016; Galloway et al. 2016).

While the teeth themselves are unlikely to break under mechanical stress when puncturing or tearing prey items, the biomechanical reason they are replaced has remained unknown (Whitenack et al. 2011). This process of tooth replacement and the rate of new teeth moving forward varies across different taxa of sharks, ranging from one week to almost three months (Luer et al. 1990; Moss 1970; Reif et al. 1978; Wass 1973). The tooth replacement rates of certain species have been theoretically calculated. For example, *Carcharhinus plumbeus* and *Negaprion brevirostris* replace their functional row of teeth every 14 days or 36 days respectively (Luer et al. 1990; Moss 1970; Motta et al. 1997; Motta et al. 2008; Reif et al. 1978).

This cycle of constant tooth replacement has been hypothesized to stay ahead of tooth failure resulting from breakage (Whitenack et al. 2011). However, previous studies have shown that shark teeth can undergo immense mechanical stress before fracturing or cracking due to their unique arrangement of fluorapatite, which is far more durable than bioapatite, the biomineral which makes up mammalian teeth (Enax et al. 2012; Whitenack et al. 2011; Wilmers et al. 2021). While shark teeth are comparatively "harder", the structural stability and internal strength of the individual tooth is correlated with its shape (Paig-Tran et al. 2022). These varying physical attributes of shark teeth have led to the testing of different species' teeth in performance and wear examination by means of puncturing or cutting prey items (Bergman et al. 2017; Dean et al. 2008; Enax et al. 2012; Ferrara et al. 2011; Whitenack and Motta 2010; Whitenack et al. 2011).

During the time that a predator is using its teeth, mechanical wear forces, such as friction, compound and are centered around certain areas on their teeth (Anderson 2018; Galloway and Porter 2021; Whitenack et al. 2011). These localized areas of concentrated forces begin to wear down and consequently increase in surface area, changing the morphology and efficiency of a tooth (Anderson and LaBarbera 2008; Whitenack et al. 2011). The resulting morphological pattern causes a decrease in the overall stress yielded by the tooth itself (Whitenack et al. 2011). In order for a puncture to occur, a specific force must be reached by an object to not only break through the item's surface, but to overcome the material-specific stress threshold of that item (Paig-Tran et al. 2022). These forces of puncture depend upon factors such as sharpness, tip morphology, and the punctured item material (Anderson 2018; Crofts et al. 2019; Galloway and Porter 2021; Galloway et al. 2016). When new, sharp teeth are used for the first time, the area of the tooth tip is at its smallest. This leads to the conclusion that the smaller the area of contact, the higher the stress inside the material (Paig-Tran et al. 2022). Therefore, sharper teeth do not need

to exert as much force during a puncture as duller teeth which possess a larger tip surface area. While these blunt or dull teeth require more force to puncture a prey item, the possible maximum force exerted by a shark's jaw is able to overcome the negative effects of dulling and be able to create a puncture (Anderson and LaBarbera 2008; Bergman et al. 2017; Whitenack and Motta 2010; Whitenack et al. 2011). Consequently, the hypothesis of tooth failure driving the replacement process would not be supported because teeth are still being used while broken, blunt, or chipped (Huber et al. 2009).

For this research study, I examined the effects of wear, such as changes in serration shape and cutting efficiency, on the puncture force and morphology of shark teeth across multiple species. These species were chosen on the basis of availability and tooth diversity, including both serrated and non-serrated varieties as experimental groups. Coupled with previously established data analyzed in Sesler and Whitenack (2022), this project further examined the individual serrations observed on teeth from multiple shark species. It was hypothesized that the continuous usage of a tooth while puncturing a prey species will cause large amounts of wear and damage on the individual serrations and tip of each tooth, in addition to increasing the amount of necessary puncture force. If the serration measurements and the force recordings share a similar relationship, this study will quantitatively support the hypothesis that shark teeth are replaced on the basis of tooth wear and not tooth malfunction, failure, or breakage.

Methods

Selection of Shark Species

The shark species selected for this study were chosen on the basis of jaw availability in the Allegheny College Department of Biology's collection and condition of the individual jaw. Before the removal of any teeth, the total body length of each shark was calculated. The total length was determined by measuring the interdental distance between teeth or the bite circumference of the jaw, and using a log-log regression equation (Lowry et al. 2009). The following methods were conceived and tested during summer 2021 with Lisa Whitenack, Ph.D. The data that was collected during these preliminary tests was expanded upon during this study.

Tooth data were collected from a single jaw from each of five species: bull shark (*Carcharhinus leucas)*, blacktip shark (*C. limbatus*), sandbar shark (*C. plumbeus*), short-fin mako shark (*Isurus oxyrinchus*) and great hammerhead shark (*Sphyrna mokarran*). Teeth from each species were pulled from positions four through six on both the left and right sides of the upper jaw. When selecting teeth to remove, the positions of four through six were chosen based upon the unique dentition of *I. oxyrinchus*. As a lamniform shark, the short-fin mako displays a unique arrangement of teeth, consisting of anterior, intermediate, and lateral teeth (Shimada 2002; Whitenack and Gottfried 2010). These three sets of teeth, which differ in morphology, dictated the selection of positions four through six to be tested as these positions are start of the lateral teeth section (Shimada 2002). These teeth are similar in size and by avoiding the anterior and intermediate teeth, a common morphology was utilized with the non-serrated shark teeth. In removing the teeth from positions four through six, a "middle-ground" section was examined for each species. Five teeth per species were tested, totaling 25 individual teeth subjected to puncture testing. Two teeth each from *C. plumbeus*, *C. limbatus*, and *C. leucas* were tested during the

preliminary research in summer 2021. The remaining Carcharhiniform teeth and all *I. oxyrinchus* and *S. mokarran* teeth were tested during the 2022-2023 academic year.

Performance Testing of Shark Teeth

To remain consistent with natural motion, a PVC apparatus (Figure 2) was constructed to mimic the downward motion of a shark's upper jaw. Standard metal washers were placed in the one end of the tube. Parafilm was utilized as a barrier to keep the weights from moving into the main section of PVC and falling out the other end. By adding washers, one end of the lever weighed more than the other, holding the weighted end on the table and avoiding the possibility of the apparatus resting on the "tooth end". The aforementioned removed teeth were dried and attached to a removable PVC coupler using low-temperature hot glue. The teeth sat for at least one hour to allow for proper adhesion. At the weighted end of the PVC pipe, an eyelet drilled into the PVC provided a loop to attach a digital scale (RGSDS 15/50 LB., Rapala; www.rapala.com). The attached, tarred scale was used to record the minimum force in kilograms required for the tooth to puncture the prey item. The puncture forces were converted from kilograms to Newtons for reporting.



Figure 2: The PVC apparatus built to mimic natural motion of a shark jaw.

Two corrections were included into the final puncture force data to account for differences in the lever arm lengths and the calibration of the Rapala digital scale. To measure the downward puncture force of the tooth end of the lever arm, the upward force of pulling the digital scale was recorded. With the PVC apparatus being a class one lever, the length of the lever arm associated with output force versus input force matters (Figure 3; L_1 and L_2).

By definition, a lever arm is the distance from the fulcrum or axis to the point of force application. If the lever arms are equal in length, then there is a direct measure of force; the upward force of the weighted end is equivalent to the downward force on the tooth end. If the lever arms are unequal in length, as was seen with measuring the lever arm lengths of our apparatus, then the equation: $F_1L_1 = F_2L_2$ (Equation 1) is utilized to find the specific change in force (F) caused by the differences in lever arm length (L). Similar to the methods of Bergman et al. (2017), a calibration of the Rapala scale against additional digital scales was performed. A linear regression was conducted in Microsoft Excel by measuring known masses on the Rapala fishing scale and a balance, yielding an R^2 value of 0.9999 with the equation: $Force_{(calibrated)}=1.008*Force_{(Rapala)}+0.0065$ (Equation 2). Taking scale calibration and lever arm correction into consideration, the upward force measurements from the Rapala scale [$Force_{(Rapala)}$] were first run through Equation 2. The calibrated force [$Force_{(calibrated)}$, F_2] was then run through Equation 1 to find the actual, corrected force of the puncture (F_1).

All teeth punctured a generalized prey item to avoid any data confliction. For this study, porgy fish (*Pagrus major*) were punctured as these fish were readily available through whole-sale fish markets. By using a standard teleost prey item, there were negligible differences in wear based on prey item and muscle anatomy. Punctures were made in the epaxial muscles of the fish,

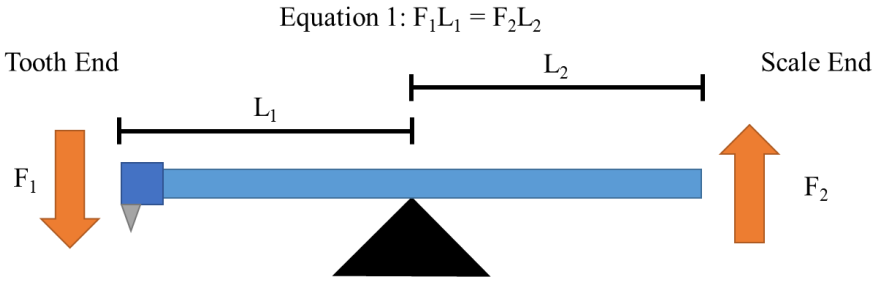


Figure 3: A simple rendition of how Equation 1 was formulated and used for correcting the unequal lever arm lengths.

avoiding organs on the ventral side. The fish were physically repositioned as needed to keep punctures isolated to the epaxial muscles.

Utilizing a Leica DFC295 stereoscope, pictures were taken of each tooth prior to puncture testing to record any pre-existing damages or breakage caused during tooth removal. The performance testing of each tooth consisted of 400 total punctures. The measurement intervals were predetermined during summer 2021 as part of preliminary research. These intervals consisted of measurements taken every 10 punctures during punctures 0-40, every 20 punctures during punctures 40-100, and every 30 punctures during punctures 100-400 (Sesler and Whitenack 2022). At these intervals, a measurement of the force required for puncturing was recorded and additional pictures of the entire tooth were taken to capture visual evidence of any wear done to the tooth during the puncture testing.

Measurement Data Collection

Once puncture testing was completed for each tooth, utilization of ImageJ software allowed for accurate measurements of the serrations and tooth tip. On the tooth, there were seven separate sections, outlined in Sesler and Whitenack (2022), which were measured: distal apron, distal middle, distal apex, tip, mesial apex, mesial middle, and mesial apron (Figure 4).

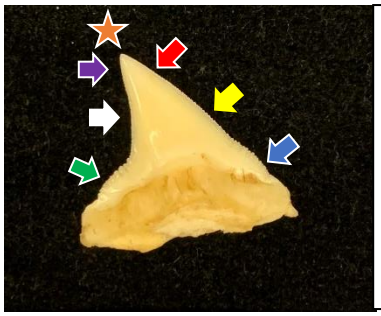


Figure 4: The seven distinct areas of measurement on a *C. plumbeus* tooth.

Each section of five consecutive serrations was measured in one of six cutting edge areas: distal apron (green arrow), distal middle (white arrow), distal apex (purple arrow), mesial apex (red arrow), mesial middle (yellow arrow), and mesial apron (blue arrow). The orange star represents the location of the RoC measurement taken at each tip.

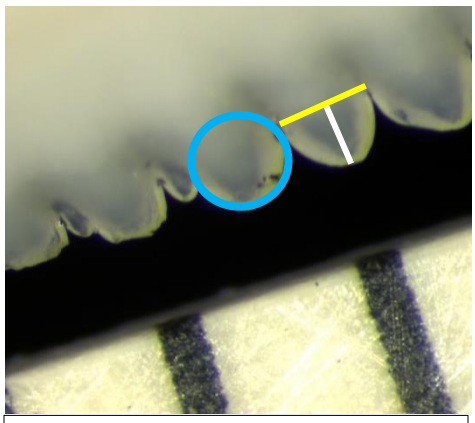


Figure 5: Examples of height and radius of curvature measurements on a *C. leucas* tooth.

The height of each serration (white bar) was drawn from the tip of the serration to the bottom of the "trough" (yellow bar) after setting an accurate scale. The radius of curvature (blue circle) was found by planting three points equidistant on the tip of the tooth or individual serration and creating a circle of best fit based upon Crofts et al. (2019).

The two measurements that were recorded used the line (height) and circle tool [radius of curvature (RoC)] in ImageJ (Figure 5). The height was recorded in micrometers for the serrations only found on the cutting edges. Height was measured from the tip of the rounded serration to the bottom of the "trough". A straight line was drawn between the troughs to mark a consistent bottom line for each serration, allowing for accurate, consistent measurements. For each serration and for the tip, a RoC measurement was recorded in micrometers. To obtain the RoC measurement, a circle of best fit was plotted from equidistant points on the tip or individual serration of the tooth (Crofts et al. 2019). For each section, five consecutive serrations were measured. The teeth of *I. oxyrinchus* are not serrated and therefore, only measurements of the tooth tip were recorded. The same five serrations were labeled, consistently measured over the 400 punctures, and then averaged together to achieve one measurement for each section of tooth for that specific puncture interval.

Statistical Analysis

After all measurements of each tooth were completed, the data was organized in Microsoft Excel. The data for one individual *C. plumbeus* tooth, where the tip of the tooth broke off, was not included in any statistical analysis of the data to avoid discrepancies based on its tip breakage (see Results). Statistical analysis was conducted in JMP Pro Statistical software or PAleontological STatistics (PAST) software. With the compiled data, a paired *t*-test was first

conducted in JMP Pro to identify whether the puncture forces of each species changed the same amount before and after the 400 punctures. Then, correlation analyses were conducted in JMP Pro utilizing the species mean tooth tip RoC and species mean puncture force data.

In order to test for wear trends, the rate of wear (slopes) in each section of the tooth was first calculated through a linear regression in JMP Pro. Once data was complied, the slopes of the lines were tested in PAST using an analysis of covariance (ANCOVA) to identify possible homogeneity of slopes, with puncture number as the covariant. Finally, the measurement differences of the serration areas from before testing and after the 400^{th} puncture were compared with a multivariate analysis of variance (MANOVA) in JMP Pro. This statistical test was run for the data across serrated species only. Additional post-hoc testing differences in JMP Pro of the serration height and radius of curvature, consisting of individual analyses of variance (ANOVA) and Tukey-Kramer pairwise analyses, were included for any differences that displayed a significant change. Separate ANOVAs were run for all species on tip RoC and puncture force.

Results

Tooth Puncture Force and Tip Radius of Curvature

All teeth were able to successfully puncture the prey item. Over the span of 400 punctures, each tooth displayed measurable wear in each region. Gradual increases were seen for puncture force (N), as well as tip radius of curvature (RoC) (µm) (Appendix I). One of the *C. plumbeus* teeth, CplumbR5, experienced a fracturing of the tip while testing, dramatically increasing the tip RoC and puncture force for the remainder of testing. Due to this anomaly, CplumbR5 was not included in species averages. Individual teeth within a species showed remarkably similar trends in puncture force (Figure 6 and Appendix A). Disregarding the one broken *C. plumbeus* tooth, all teeth displayed a significant increase in puncture force from the first puncture to the 400th puncture (paired *t*-test, $df = 23$, $t = -12.144$, $P < 0.0001$).

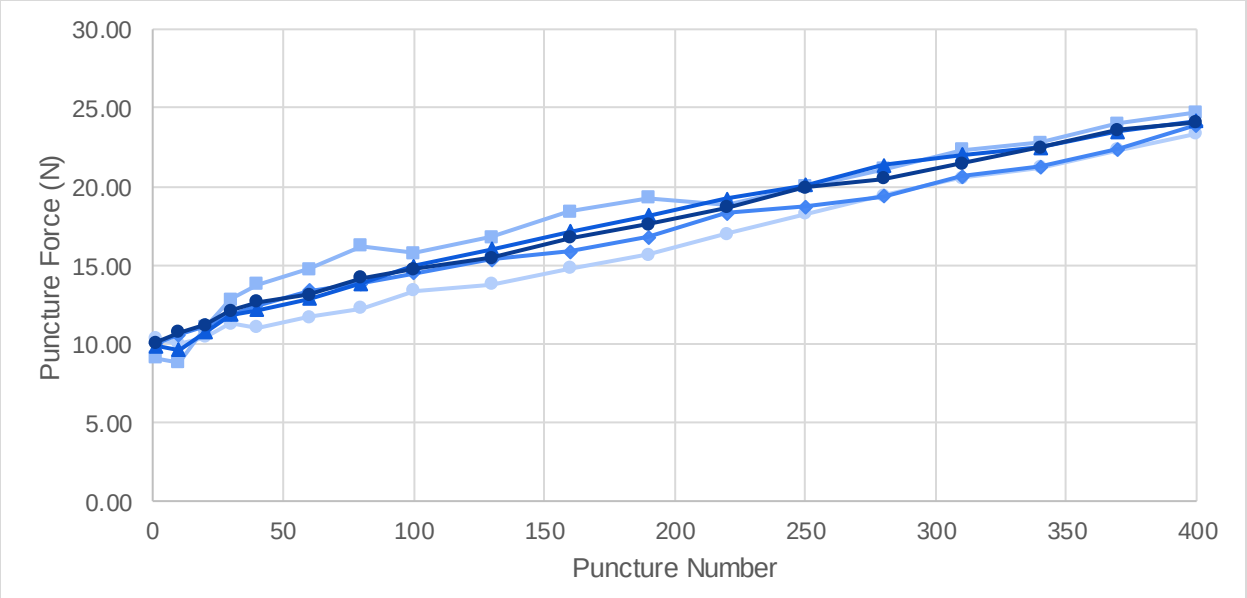


Figure 6: Teeth from *C. leucas* graphically display a positive slope in puncture force (N). All five teeth from *C. leucas* trended in a similar pattern, creating lines which intertwined with each other. Each of the five teeth is individually represented by a different shade of blue and marker shape.

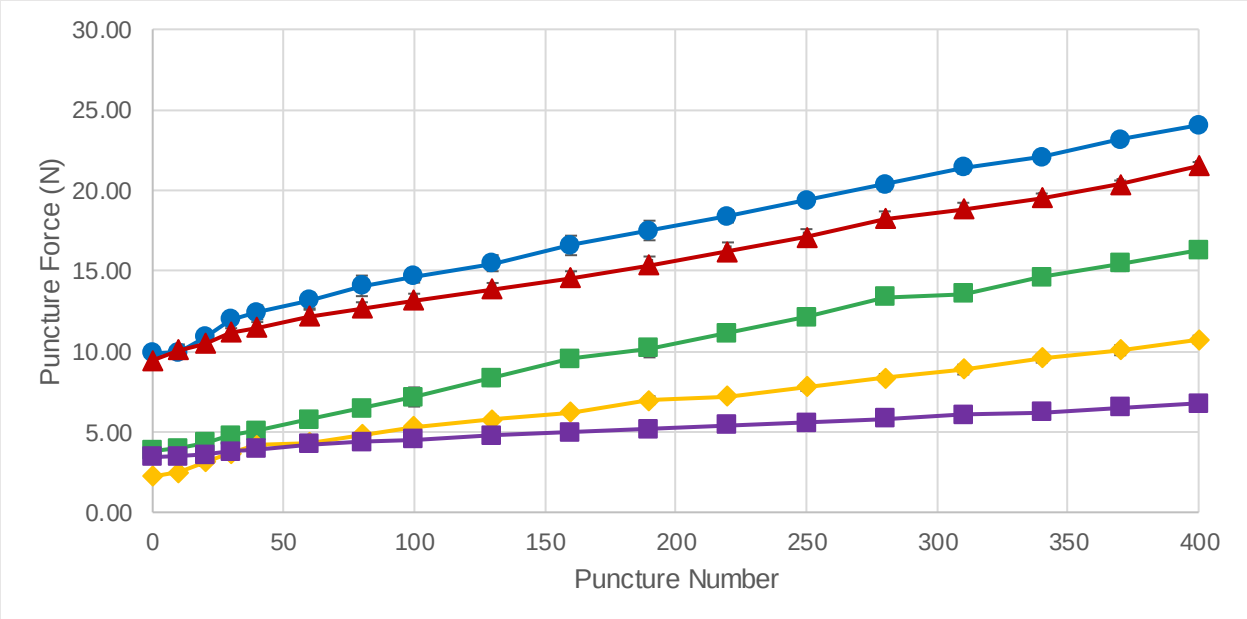


Figure 7: Species average puncture force (N) trends gradually with a positive slope.

Each colored line represents the average puncture force for a single species: *C. plumbeus* (green square), *C. limbatus* (gold diamond), *C. leucas* (blue circle), *I. oxyrinchus* (red triangle), and *S. mokarran* (purple square). Standard error bars (black T-bars) were calculated and added to this and each of the following figures, but are difficult to see due to their small range.

The species averages for puncture force (Figure 7) display positive slopes (Appendix A and Appendix I). For the puncture force measurements (N), a significant difference was seen between a majority of species (one-way ANOVA, $df = 4, 19$, $F = 186.113$, $P < 0.0001$). Post hoc analysis through Tukey-Kramer testing revealed no significant difference between *C. plumbeus* and *I. oxyrinchus* ($P = 0.9038$), but displayed that the average force for *C. leucas* was the highest and the force for *S. mokarran* was the lowest.

When reviewing the tip RoC, the species averages (Figure 8) also display positive slopes (Appendix B and Appendix I). Looking at the difference in tip RoC, further analysis revealed significant differences overall (one-way ANOVA, $df = 4, 19$, $F = 59.8487$, $P < 0.0001$). Post hoc testing with Tukey-Kramer showed that there was no difference between *C. leucas* and *I. oxyrinchus* ($P = 0.1306$) and no difference between *I. oxyrinchus* and *C. limbatus* ($P = 0.8761$).

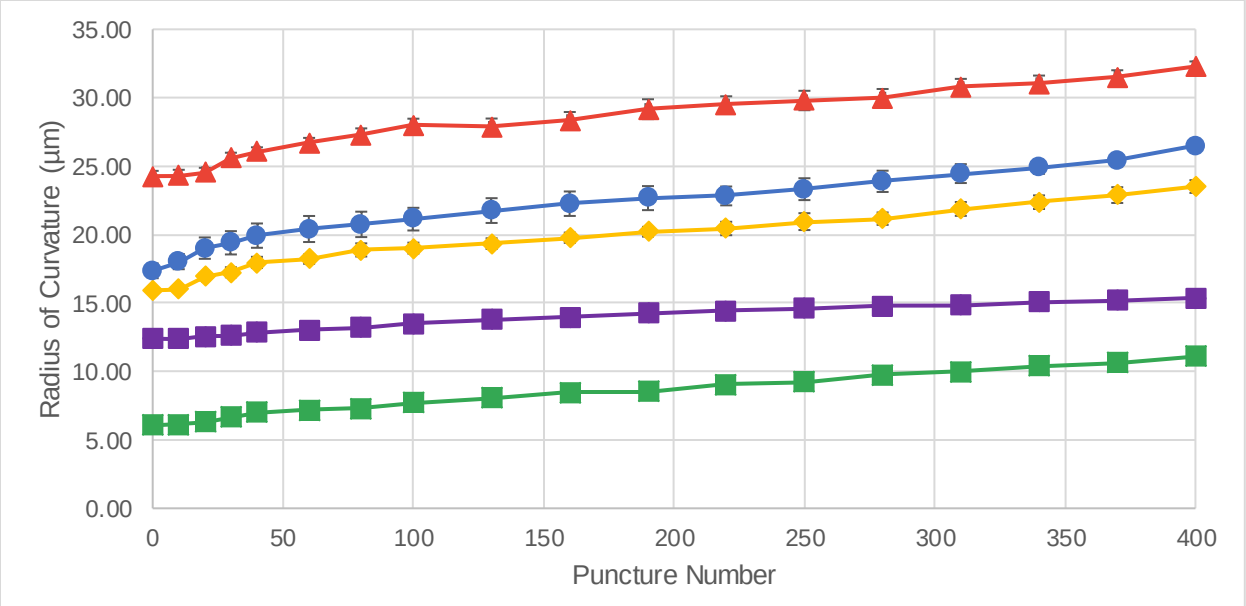


Figure 8: Species average tip RoC (µm) displays a common pattern of a positive slope.

Each colored line represents the average tip radius of curvature for a single species: *C. plumbeus* (green square), *C. limbatus* (gold diamond), *C. leucas* (blue circle), *I. oxyrinchus* (red triangle), and *S. mokarran* (purple square). Standard error bars were calculated and added to the figure.

However, there were significant differences between *C. leucas*, *C. plumbeus*, and *S. mokarran* ($P < 0.0001$). The teeth from *S. mokarran* had the lowest average tip RoC at 2.979 µm, followed by *C. plumbeus*. The teeth from *C. leucas* displayed the highest tip RoC average at 9.149 µm. When analyzing puncture force (N) and tip radius of curvature (µm) over the 400 punctures, a significant positive correlation is present between the change in puncture force and the change in tip RoC for each species (Table 1).

Table 1: Correlation between the change in tip RoC (µm) and puncture force (N).

Species	*R*-value	*df*	*P*-value
C. plumbeus	0.9966	16	<0.0001
C. limbatus	0.9962	16	<0.0001
C. leucas	0.9924	16	<0.0001
I. oxyrinchus	0.9829	16	<0.0001
S. mokarran	0.9939	16	<0.0001

Serration Wear

The data from each of the four serrated species teeth and the six different regions of measurement are included in Appendix C through Appendix H. Figures 9-11 represent three different areas on the tooth and the common patterns seen between the species average serration height and serration radius of curvature. For every regression run, a *P*-value of <0.0001 was calculated (Appendix I). The slopes of the forementioned linear regressions were then analyzed for homogeneity of slopes, indicating equal rate of wear (Table 2). Out of the 14 tests conducted, only one, the mesial apex height, displayed homogeneity of slopes (df = 4,88, F = 0.3931, P = 0.7584). The remaining tests showed non-significant results, indicating the rate of wear was not equal in those regions of the tooth between the species (Table 2).

Table 2: Results from the ANCOVA analysis reveal one measurement of one section having homogeneity of slopes. All ANCOVAs were run with the degrees of freedom being 4, 88.

Region and Measurement Type	*F*-value	*P*-value
Puncture Force	344.6	<0.001
Tip RoC	40.06	<0.001
Distal Apron Height	144.4	<0.001
Distal Apron RoC	107.9	<0.001
Distal Middle Height	58.2	<0.001
Distal Middle RoC	72.65	<0.001
Distal Apex Height	6.843	<0.001
Distal Apex RoC	36.32	<0.001
Mesial Apex Height	0.3931	0.7584
Mesial Apex RoC	90.13	<0.001
Mesial Middle Height	17.29	<0.001
Mesial Middle RoC	31.73	<0.001
Mesial Apron Height	75.52	<0.001
Mesial Apron RoC	60.28	<0.001

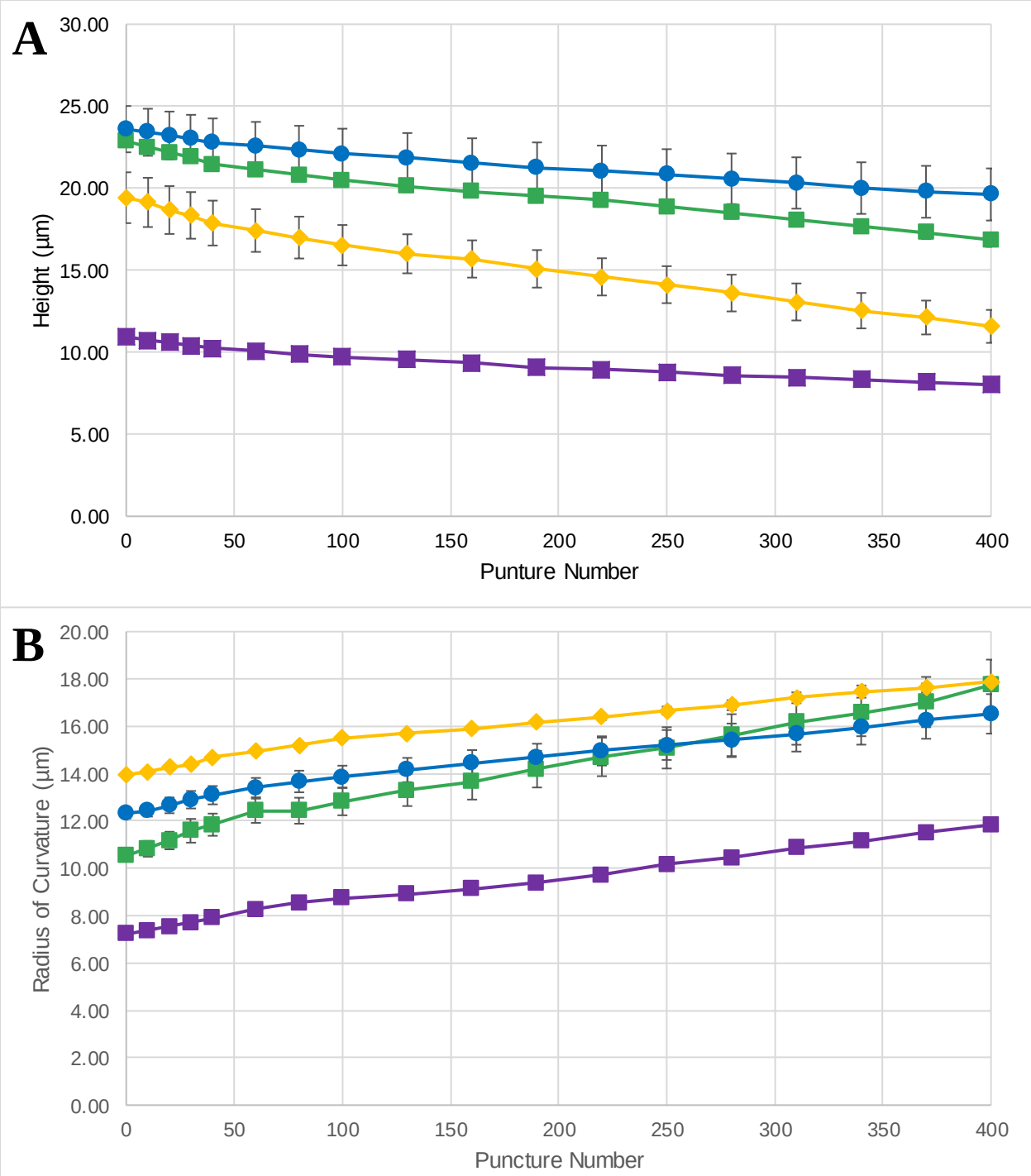


Figure 9: The species averages of serration height (**A**) and radius of curvature (**B**) for the distal apron region, both measured in micrometers.

Each colored line represents measurement averages of the different serrated-teeth species: *C. plumbeus* (green square), *C. limbatus* (gold diamond), *C. leucas* (blue circle), and *S. mokarran* (purple square). Standard errors bars were calculated using the standard deviation and the teeth sample number for each species.

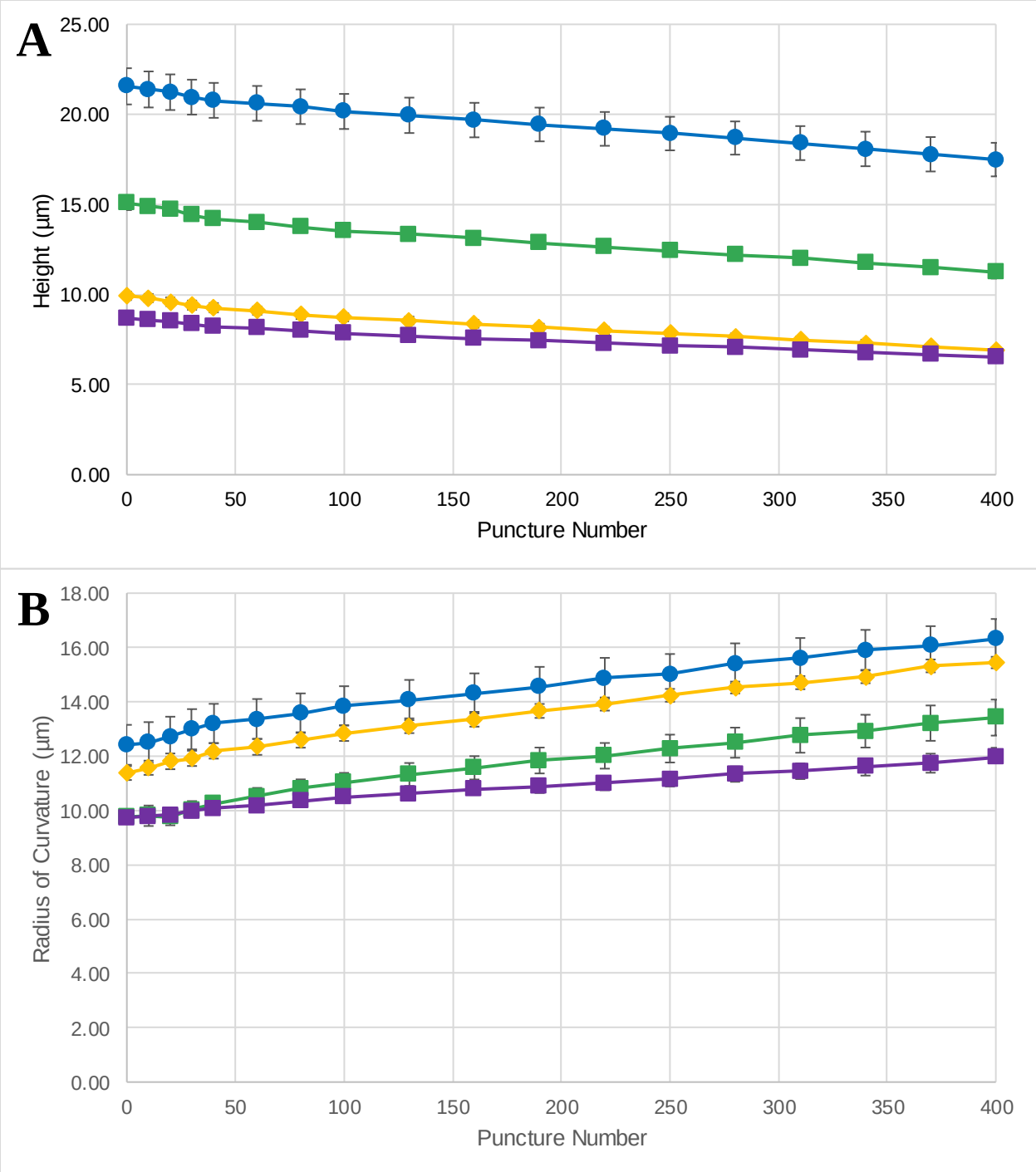


Figure 10: The species averages of the distal middle region for serration height (**A**) and radius of curvature (**B**).

Each colored line represents measurement averages of the different serrated-teeth species: *C. plumbeus* (green square), *C. limbatus* (gold diamond), *C. leucas* (blue circle), and *S. mokarran* (purple square). Standard errors bars were calculated and added to each point.

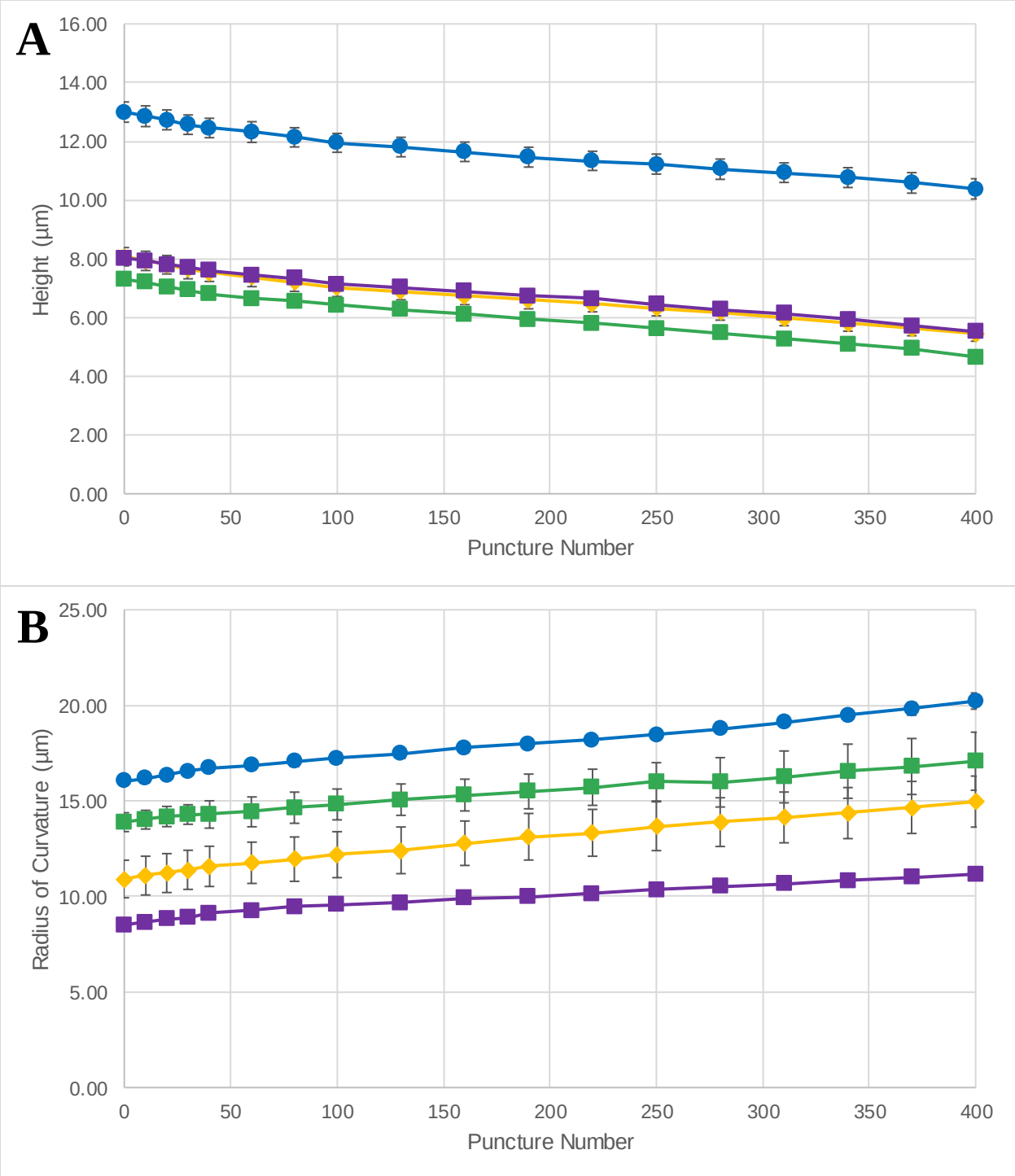


Figure 11: The species averages of the mesial apex region for serration height (**A**) and radius of curvature (**B**).

Each colored line represents measurement averages of the different serrated-teeth species: *C. plumbeus* (green square), *C. limbatus* (gold diamond), *C. leucas* (blue circle), and *S. mokarran* (purple square). Standard errors bars were calculated and added to each point.

To further analyze wear differences among species, a MANOVA was conducted on the measurement differences between "before testing" and "after testing". Only the six serration regions were included in the MANOVA, which showed a significant difference overall for the serration regions among species (MANOVA, Wilks' lambda = 0.0002779, approximate $F = 5.2206$, $P = 0.0016$). With the significant results, preliminary post hoc testing of individual ANOVAs was conducted for each serration region (Table 3). Within these ANOVAs, the only regions which did not show a significant difference were the serration height for the distal apex, mesial apex, and mesial middle. The radius of curvature for the distal apex and mesial apex regions were also not significant with their measurement differences. For all other regions and serration measurement type, the analysis returned significant results (Table 3) and additional post hoc testing using Tukey-Kramer was performed.

Table 3: The individual ANOVAs after the MANOVA reveal that only certain regions of the tooth and each region's two measurements vary in significance. The degrees of freedom for all MANOVAs were 3, 18. The asterisk (*) denotes the region and type of measurement that continued through to post hoc testing through Tukey-Kramer tests.

Region and Measurement Type	*F*-value	*P*-value
Distal Apron Height	23.4591	<0.0001*
Distal Apron RoC	12.7684	0.0002*
Distal Middle Height	8.0179	0.002*
Distal Middle RoC	11.0298	0.0004*
Distal Apex Height	2.1417	0.1377
Distal Apex RoC	3.004	0.0636
Mesial Apex Height	0.1706	0.9146
Mesial Apex RoC	1.576	0.2367
Mesial Middle Height	1.2312	0.333
Mesial Middle RoC	6.9811	0.0037*
Mesial Apron Height	10.5538	0.0006*
Mesial Apron RoC	3.3675	0.0468*

Looking first at Tukey-Kramer results of the distal apron region, there was no significant difference in serration height between *S. mokarran* and *C. leucas*. These species had a lower mean height difference than the other non-significant grouping of *C. plumbeus* and *C. limbatus* (Figure 12). The distal apron RoC revealed that of the four species, *C. plumbeus* had the only significantly different RoC change which was greater than the others. Next, the distal middle region had overall significance from the first round of post hoc testing. However, when looking at the height differences, *S. mokarran* was only significantly different from *C. leucas* and *C. plumbeus*, with *S. mokarran* having a lower mean height than both species. The distal middle RoC showed that *S. mokarran* was the only significantly different species from the other three, having a lower mean serration RoC difference than the three carcharhinid sharks.

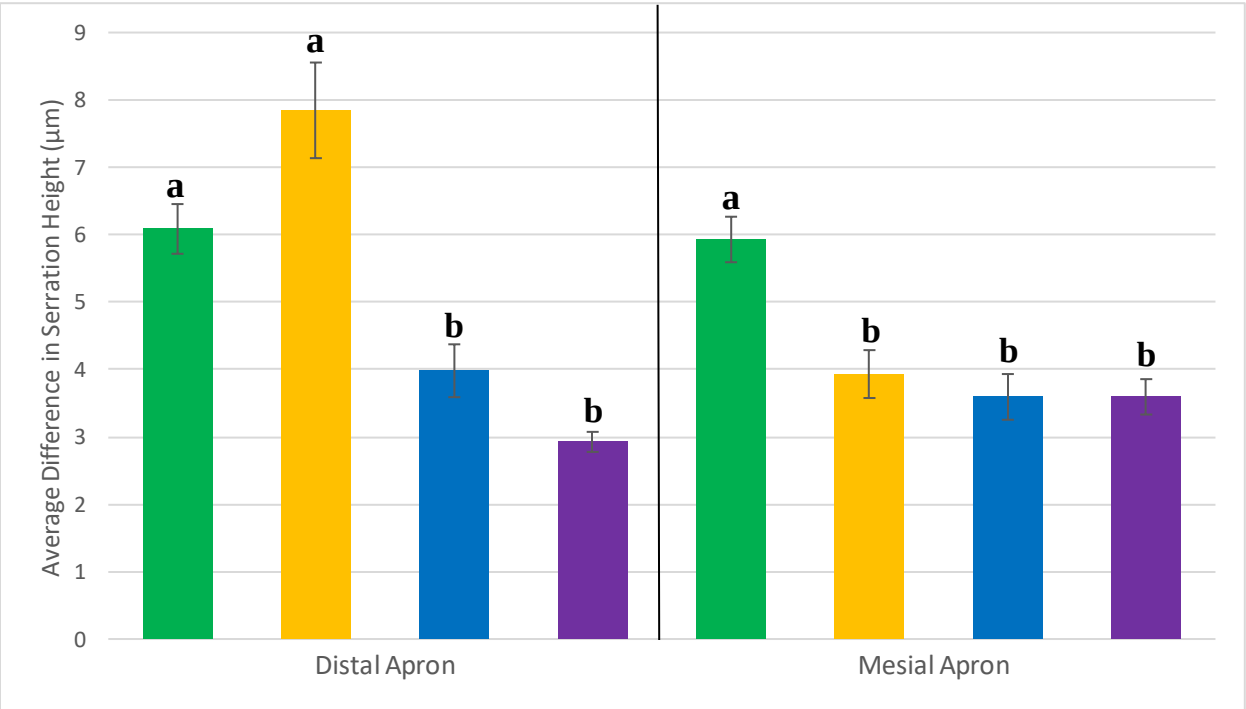


Figure 12: The average differences in serration height (µm) of the distal apron and mesial apron regions, separated by the black bar, display varying significance between the shark species.

Each colored bar represents average height differences from the different serrated-teeth species: *C. plumbeus* (green), *C. limbatus* (gold), *C. leucas* (blue), and *S. mokarran* (purple). Standard errors bars were calculated, added to each bar, and labeled according to post hoc testing utilizing Tukey-Kramer. Bars for each region with the same letter are differences that are not significant.

Working around the tooth, the next region that displayed significant results was the RoC of the mesial middle region. Here, the Tukey-Kramer testing revealed that only *C. limbatus* was significantly different against the other species, displaying a mean serration RoC difference greater than the other species. The last region, the mesial apron, displayed significant differences in both height and RoC. Post hoc testing found that *C. plumbeus* was significantly different than the other three species of shark in serration height, displaying a greater average height difference (Figure 12). However, when looking at the radius of curvature of this region, *C. plumbeus* and *C. leucas* were the only two species that were different from each other, with *C. plumbeus* having a greater mean RoC difference than *C. leucas*.

Discussion

The results of this study demonstrate that while different species of shark teeth wear at different rates, they are able to puncture a standard prey item even with significant wear. The mechanical performance of teeth, such as their ability to puncture, has been previously analyzed in the context of performance, cutting ability, and morphology (Abler 1992; Bergman et al. 2017; Cappetta 1987; Frazzetta 1988; Galloway et al. 2016; Huber et al. 2009; Moss 1977; Motta et al. 1997; Motta et al. 2008; Whitenack and Motta 2010; Wilmers et al. 2021). This study specifically analyzed how tooth wear occurs over 400 punctures, focusing on the entire tooth, not one specific region.

Tooth Puncture Force

All teeth included in this study were able to puncture a prey item regardless of how many punctures the tooth had previously endured during testing. The results show that over 400 punctures, gradual increases are seen in puncture forces for each individual tooth (Appendix A) and their species averages (Figure 7). The significant changes in puncture force from the first puncture to the 400th puncture can be related to the efficiency of the tooth. An increase in puncture force suggests that the tooth is becoming less efficient as the shark would need to exert more force in the bite in order for the tooth to successfully puncture, and thus expend more energy. These observations support the proposed hypothesis that the replacement of shark teeth is driven by tooth wear to maintain a sharp functional row of teeth (Bergman et al. 2017; Galloway and Porter 2021; Whitenack et al. 2011).

When analyzing the puncture force data from this study, different forces were seen for the tested species. The larger teeth of *C. plumbeus*, *C. leucas*, and *I. oxyrinchus* (Figure 1) required more force to puncture at the start of testing, distinguishing them as less efficient than

the smaller, narrower teeth from *C. limbatus* and *S. mokarran*. These results, which present larger teeth as less efficient at puncturing, are consistent with other studies that compared puncture capabilities for some of the same shark species (Bergman et al. 2017; Ferrara et al. 2011; Whitenack and Motta 2010). Additionally, when comparing this study's force data for *I. oxyrinchus*, *C. leucas*, and *C. plumbeus* (Appendix A), similarities in force magnitudes and puncture force means were seen between these results and those of previous studies such as Whitenack and Motta (2010) and Bergman et al. (2017). The force measurements of this study for *S. mokarran* and *C. limbatus* were lower than the results of the aforementioned publications.

Recent findings analyzing the maximum bite force in mammals demonstrates the accessibility to which bite force in terrestrial mammals, including humans, can be measured (Edmonds and Glowacka 2020). Due to the difficulty of testing maximum bite forces in the wild in an aquatic species, studying the individual teeth of chondrichthyans in a controlled setting allows for average bite forces to be suggested (Ferrara et al. 2011; Huber et al. 2009; Huber and Motta 2004). It is important to note that the amount of force measured in this study, at each interval over 400 punctures (Figure 6), is less than what sharks such as *C. leucas* are theorized to produce in terms of bite force. These theoretical bite forces, while not exerted in every bite, can range from 36 to 2128 N, with extreme scenarios producing bite forces up to 5914 N (Habegger et al. 2012; Habegger 2009; Huber et al. 2009). The puncture forces measured in this study provide a "minimal" baseline for possible forces exerted to create a puncture, taking into account existing wear and damage caused by previous bites. These minimal puncture force values, in addition to previous findings concerning the forces exerted during a bite, can provide more accurate ranges of an average bite from specific shark species (Bergman et al. 2017; Ferrara et al. 2011; Habegger et al. 2012; Huber et al. 2009; Huber and Motta 2004). While these increasing

minimal puncture force values provide evidence that a shark's tooth becomes less efficient over a series of bites, the increase in force required to create a puncture would hypothetically not impact the shark's ability to capture prey. As shown in the results of this study, all teeth were able to puncture the prey item at varying magnitudes of force, demonstrating that less efficient teeth can still successfully capture and puncture prey.

Tip Radius of Curvature

Over a series of punctures, pointed objects such as a tooth will wear down and its morphology will be altered, not only along its cutting edges, but also on the pointed tip (Crofts et al. 2019). In order to create a puncture, a specific stress threshold must be overcome to rupture the prey (Paig-Tran et al. 2022). Factors such as puncture tool shape, which includes tip surface area, length and size of the tooth, and angular morphologies, dramatically alter how efficiently a puncture can be made. The results of this study show gradual increases in the average tip radius of curvature (RoC) for the tested teeth over 400 punctures (Figure 8 and Appendix B). Given that stress is equal to the amount of applied force divided by the surface area, the increases of tip RoC can be equated as increases in surface area on the tip of each tooth, demonstrating that a tooth becomes less efficient as the tip surface area becomes larger.

When analyzing both sets of measurements, a positive correlation was found between the change in tip RoC and the change in puncture force (Table 1). During the testing, both the measurements of tip RoC and puncture force consistently increased over 400 punctures. This observed positive correlation is based on the mechanical understanding of stress, where an increase in surface area (tip RoC) requires an increase in applied force (puncture force) to generate the necessary stress level. This positive correlation demonstrates that these two aspects of a shark's tooth contribute to its puncture performance and thereby its efficiency.

As shown in the results of this study, the teeth with the lowest tip RoC difference from prior to puncture testing to the 400th puncture all belonged to the same species, *S. mokarran* (Figure 7). Furthermore, *S. mokarran* displayed the lowest difference in puncture forces over the course of testing, demonstrating how a consistently low surface area on the tip of the tooth can allow for more efficient punctures that require less force (Figure 8). Conversely, the chipped *C. plumbeus* tooth CPlumbR5 demonstrated that with an increase in tip RoC measurements, the puncture force increases dramatically (Appendix B [*C. plumbeus* Tip Radius of Curvature]). Losing the tip of the tooth during testing exemplified that a larger tip RoC, a subsequently a larger tip surface area, produced a higher puncture force in order to successfully overcome the stress threshold of the prey. This increase in puncture force due to the tooth performing at a less efficient rate supports the results of previous studies examining puncture performance (Anderson and LaBarbera 2008; Whitenack et al. 2011).

Serration Wear

The serration measurement results from this study are unique as the shark tooth serrations were measured over a series of bites for their size and "dullness". Looking at the overall data, region-specific measurements for radius of curvature and height varied not only across the five species, but additionally on an individual-species basis. By taking the average of five consecutive serrations as the "region measurement", regions with smaller serrations had a higher average due to the presence of one serration being physically larger in size than the others. Factors such as these abnormally-sized serrations and pre-existing damages to the tooth, either from jaw drying or tooth removal, limited the regions of serrations that could be measured properly.

Previous studies examining serrated teeth in therapod dinosaurs, such as *Tyrannosaur* species, have found that serrations on dinosaur teeth are similar to that of modern animal teeth serrations in their characteristic size, shape, and hypothesized usage and wear patterns (Abler 1992; Brink et al. 2015; Farlow et al. 1991). While there is little data available for how much physical wear is caused to fossilized therapod teeth during a singular bite, it is hypothesized that their serrations began to wear down once the teeth were grown into the functional position (Brink et al. 2015). This wear on therapod teeth is similar to how the shark teeth exhibited measurable amounts of wear within the first 40 punctures. However over 400 punctures, the serrations of the shark teeth wore down at differing rates, with only one region and type of measurement (mesial apex height) possessing homogeneity of slopes (Table 2). This conveys that even within the same species, the serrations of separate teeth wear down at different rates.

Over the course of performance testing, visible morphological changes to each tooth occurred in the serrated regions of the teeth (Appendix C through Appendix H). Areas of the tooth displaying the most change were the distal apron and mesial apron regions (Appendix C and Appendix H). In these regions, not only was the difference in measurements significant, but visible chipping or fracturing of serrations was observed in the microscopic imaging. These drastic changes to the serrations could be due to unequal pressure applied on either side of the tooth during the puncture. Since the entire tooth enters the prey item during a puncture, one side of the tooth could experience more wear due to the natural angular morphology of the teeth used in this study. As seen in Figure 1, shark teeth of different species possess varying morphologies, with some teeth having a more "bent" appearance than others. By not entering the prey item completely vertically (e.g., entering at a slight angle due to a bent or curved shape), one side of the tooth would be in contact with the prey item for a longer period of time.

Conversely, the distal apex and mesial apex regions displayed non-significant, minimal measurement differences; visible damages or wear to these regions could not be seen (Appendix E and Appendix F). During a puncture, the apex regions of the tooth are in contact with the prey item for the longest period of time. However, as seen in the data, not even repeated punctures changed the amount of significant wear occurring to the apex regions. This could be due to the smaller size of the serrations on the apex regions, appearing almost flush with the edge of the tooth.

Conclusions

Considering how puncture force, tip RoC, and serrations change over 400 punctures, further research is necessary to expand this study by including additional variables. It is understood that there is wide variation between teleost prey items commonly found in shark's diets (Mcelroy et al. 2006; Moss 1972; Simpfendorfer et al. 2001; Wilga et al. 2007; Wilmers et al. 2021). While this study utilized a standard prey item, further research could introduce other prey items commonly found in each species diet. This alteration could potentially show that the respective shark teeth wear down at different rates when puncturing prey the specific shark regularly consumes. Relating to results found in previous studies, the presence of hard shells or different skin thicknesses could possibly wear the teeth down more, whereas soft-bodied prey could result in less force being utilized to puncture and less wear to the tooth (Bergman et al. 2017; Whitenack and Motta 2010).

The wear caused by repeated bites can be quantified by the methods presented in this study, and subsequent studies should use a similar approach. These methods and similar data could lead to future calculations predicting the amount of wear to a tooth based upon the tooth's morphology and the chosen prey item or puncturing material. Predictive wear calculations have

been conducted on human and mammalian teeth (Borrero-Lopez et al. 2014), but analyzing the wear on shark teeth could potentially assist in creating a timeline for teeth found with existing wear and when the teeth were first used in bites.

Upon review of the data and the patterns seen between serration wear and puncture force, the possibility of a linkage between puncture force and serrations could be examined in alternate studies. These two variables were analyzed throughout this study separately, but by comparing the measurements with each other, one could find if the presence of serrations increases the amount of puncture force necessary for the first puncture and vice versa. However with natural shark teeth, this would be extremely difficult due to the entire tooth experiencing puncture wear simultaneously. Modeling the teeth with alternative materials and accounting for this wear by changing one variable at a time through precision cutting would allow for this hypothesis to be tested. The tooth model could then be cut in a different pattern to either increase or decrease serration size, allowing the tip of the tooth to stay sharp and not wear down.

In conclusion, over a series of punctures or simulated "bites", shark teeth exhibit a multitude of changes in their morphology and puncture performance. Over time, the minimal puncture force necessary to create a puncture increases. Moreover, the radius of curvature at the tip of the tooth follows this similar trend of a positive slope, displaying a gradual increase in surface area. When reviewing the data for the serrated species, constant change can be seen as serration height and radius of curvature fluctuated over the series of punctures. By subjecting new, replacement teeth to a series of punctures, the results of this study show quantitative evidence that over time, teeth become more worn and less efficient. This data thereby supports the hypothesis that sharks replace their teeth not on the basis of tooth failure, but on tooth wear. At this time, the number of days it takes for a shark to lose its teeth or the number of bites taken

in a day are largely unknown (but see Luer et al. 1990; Moss 1970; Motta et al. 1997; Motta et al. 2008; Reif et al. 1978 for tooth replacement rates in lemon sharks and nurse sharks). However, combining the findings of this study with results from previous publications could potentially unlock a better understanding of how shark teeth work and the specific driving forces behind their unique tooth replacement cycle.

References

Abler WL. 1992. The Serrated Teeth of Tyrannosaurid Dinosaurs, and Biting Structures in Other Animals. Paleobiology. 18(2):161-83.

Anderson PSL. 2018. Making a point: Shared mechanics underlying the diversity of biological puncture. Journal of Experimental Biology. 221(22):jeb187294.

Anderson PSL, LaBarbera M. 2008. Functional consequences of tooth design: Effects of blade shape on energetics of cutting. Journal of Experimental Biology. 211(22):3619-26.

Bergman JN, Lajeunesse MJ, Motta PJ. 2017. Teeth penetration force of the tiger shark *Galeocerdo cuvier* and sandbar shark *Carcharhinus plumbeus*. Journal of Fish Biology. 91(2):460-72.

Borrero-Lopez O, Pajares A, Constantino PJ, Lawn BR. 2014. A model for predicting wear rates in tooth enamel. Journal of the Mechanical Behavior of Biomedical Materials. 37:226-34.

Brink KS, Reisz RR, LeBlanc ARH, Chang RS, Lee YC, Chiang CC, Huang T, Evans DC. 2015. Developmental and evolutionary novelty in the serrated teeth of theropod dinosaurs. Scientific Reports. 5(1):12338.

Cappetta H. 1987. Chondrichthyes II. Handbook of Paleoichthyology. New York: Gustav Fischer Verlag.

Corn KA, Farina SC, Brash J, Summers AP. 2016. Modelling tooth-prey interactions in sharks: the importance of dynamic testing. Royal Society Open Science. 3(8):160141.

Crofts SB, Lai Y, Hu Y, Anderson PSL. 2019. How do morphological sharpness measures relate to puncture performance in viperid snake fangs? Biology Letters. 15(4):20180905.

Dean MN, Ramsay JB, Schaefer JT. 2008. Tooth reorientation affects tooth function during prey processing and tooth ontogeny in the lesser electric ray, *Narcine brasiliensis*. Zoology. 111(2):123-34.

Edmonds HM, Glowacka H. 2020. The ontogeny of maximum bite force in humans. Journal of Anatomy. 237(3):529-42.

Enax J, Prymak O, Raabe D, Epple M. 2012. Structure, composition, and mechanical properties of shark teeth. Journal of Structural Biology. 178(3):290-9.

Farlow JO, Brinkman DL, Abler WL, Currie P. 1991. Size, shape, and serration density of theropod dinosaur lateral teeth. Modern Geology. 16(1-2):161-98.

Ferrara TL, Clausen P, Huber DR, McHenry CR, Peddemors V, Wroe S. 2011. Mechanics of biting in great white and sandtiger sharks. Journal of Biomechanics. 44(3):430-5.

Frazzetta TH. 1988. The mechanics of cutting and the form of shark teeth (Chondrichthyes, Elasmobranchii). Zoomorphology. 108(2):93-107.

Galloway KA, Porter ME. 2021. Predator–Prey interactions examined using lionfish spine puncture performance. Integrative Organismal Biology. 3(1):obaa049.

Galloway KA, Anderson PSL, Wilga CD, Summers AP. 2016. Performance of teeth of lingcod, *Ophiodon elongatus*, over ontogeny. Journal of Experimental Zoology. 325(2):99-105.

Garland T, Harvey PH, Ives AR. 1992. Procedures for the analysis of comparative data using phylogenetically independent contrasts. Systematic Biology. 41(1):18-32.

Habegger ML, Motta PJ, Huber DR, Dean MN. 2012. Feeding biomechanics and theoretical calculations of bite force in bull sharks (*Carcharhinus leucas*) during ontogeny. Zoology. 115(6):354-64.

Habegger ML. 2009. Bite Force in Two Top Predators, the Great Barracuda, *Sphyraena barracuda* and Bull Shark *Carcharhinus leucas*, During Ontogeny. Scholar Commons.

Heithaus MR. 2001. The biology of tiger sharks, *Galeocerdo cuvier*, in Shark Bay, Western Australia: Sex ratio, size distribution, diet and seasonal changes in catch rates. Environmental Biology of Fishes. 61(1):25-36.

Huber DR, Claes JM, Mallefet J, Herrel A. 2009. Is extreme bite performance associated with extreme morphologies in sharks? Physiological and Biochemical Zoology. 82(1):20-8.

Huber DR, Motta PJ. 2004. Comparative analysis of methods for determining bite force in the spiny dogfish *Squalus acanthias*. Journal of Experimental Zoology. 301A(1):26-37.

Hunt G. 2010. Evolution in Fossil Lineages: Paleontology and The Origin of Species. The American Naturalist. 176(S1):S61-76.

Johanson Z, Kearsley A, den Blaauwen J, Newman M, Smith MM. 2012. Ontogenetic development of an exceptionally preserved Devonian cartilaginous skeleton. Journal of Experimental Zoology. 318B(1):50-8.

Lowe CG, Wetherbee BM, Crow GL, Tester AL. 1996. Ontogenetic dietary shifts and feeding behavior of the tiger shark, *Galeocerdo cuvier*, in Hawaiian waters. Environmental Biology of Fishes. 47(2):203-11.

Lowry D, de Castro A, Mara K, Whitenack L, Delius B, Burgess G, Motta P. 2009. Determining shark size from forensic analysis of bite damage. Marine Biology. 156(12):2483-92.

Luer CA, Blum PC, Gilbert PW. 1990. Rate of tooth replacement in the nurse shark, *Ginglymostoma cirratum*. Copeia. 182-91.

Mcelroy WD, Wetherbee BM, Mostello CS, Lowe CG, Crow GL, Wass RC. 2006. Food habits and ontogenetic changes in the diet of the sandbar shark, *Carcharhinus plumbeus*, in Hawaii. Environmental Biology of Fishes. 76(1):81-92.

Moss ML. 1970. Enamel and bone in shark teeth: with a note on fibrous enamel in fishes. Acta Anatomica (Basel). 77(2):161-87.

Moss SA. 1977. Feeding mechanisms in sharks. American Zoologist. 17(2):355-64.

Moss SA. 1972. The feeding mechanism of sharks of the family Carcharhinidae. Journal of Zoology. 167(4):423-36.

Motta P, Tricas T, Summers R. 1997. Feeding mechanism and functional morphology of the jaws of the lemon shark *Negaprion brevirostris* (Chondrichthyes, Carcharhinidae). Journal of Experimental Biology. 200(21):2765-80.

Motta PJ, Wilga CD. 2001. Advances in the Study of Feeding Behaviors, Mechanisms, and Mechanics of Sharks. Environmental Biology of Fishes. 60(1-3):131-56.

Motta PJ, Hueter RE, Tricas TC, Summers AP, Huber DR, Lowry D, Mara KR, Matott MP, Whitenack LB, Wintzer AP. 2008. Functional morphology of the feeding apparatus, feeding constraints, and suction performance in the nurse shark *Ginglymostoma cirratum*. Journal of Morphology (1931). 269(9):1041-55.

Moyer JK, Bemis WE. 2017. Shark teeth as edged weapons: serrated teeth of three species of selachians. Zoology. 120:101-9.

Paig-Tran M, Porter ME, Ferry LA, Whitenack LB. 2022. How To Build a Shark: Biomechanics and Bioinspiration. In: Biology of sharks and their relatives. Third edition ed. Boca Raton, FL: CRC Press. 60 p.

Rasch LJ, Martin KJ, Cooper RL, Metscher BD, Underwood CJ, Fraser GJ. 2016. An ancient dental gene set governs development and continuous regeneration of teeth in sharks. Developmental Biology. 415(2):347-70.

Reif W, McGill D, Motta PJ. 1978. Tooth replacement rates of the sharks *Triakis semifasciata* and *Ginglymostoma cirratum*. Zool Jahrb Anat Ontog. 99:151–156.

Sesler R, Whitenack LB. 2022. Chomping at the bit: The effects of wear on shark tooth puncture performance and morphology. The Society Integrative & Comparative Biology Annual Meeting.

Shimada K. 2002. Dental homologies in lamniform sharks (Chondrichthyes: Elasmobranchii). Journal of Morphology (1931). 251(1):38-72.

Simpfendorfer CA, Goodreid AB, McAuley RB. 2001. Size, sex and geographic variation in the diet of the tiger shark, *Galeocerdo cuvier*, from Western Australian waters. Environmental Biology of Fishes. 61(1):37-46.

Voje KL. 2018. Assessing adequacy of models of phyletic evolution in the fossil record. Methods in Ecology and Evolution. 9(12):2402-13.

Wass RC. 1973. Size, growth, and reproduction of the sandbar shark, *Carcharhinus milberti*, in Hawaii. Pacific Science. 27(4):305-18.

Whitenack LB, Gottfried MD. 2010. A Morphometric Approach for Addressing Tooth-Based Species Delimitation in Fossil Mako Sharks, Isurus (Elasmobranchii: Lamniformes). Journal of Vertebrate Paleontology. 30(1):17-25.

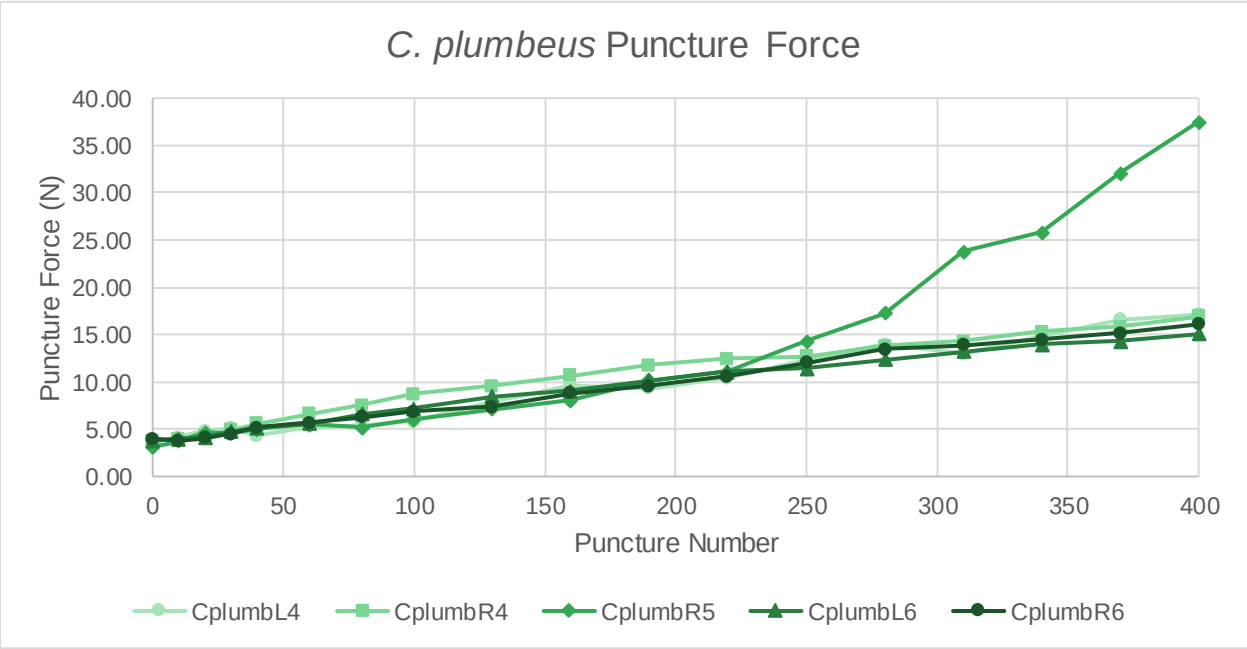
Whitenack LB, Motta PJ. 2010. Performance of shark teeth during puncture and draw: implications for the mechanics of cutting. Biological Journal of the Linnean Society. 100(2):271-86.

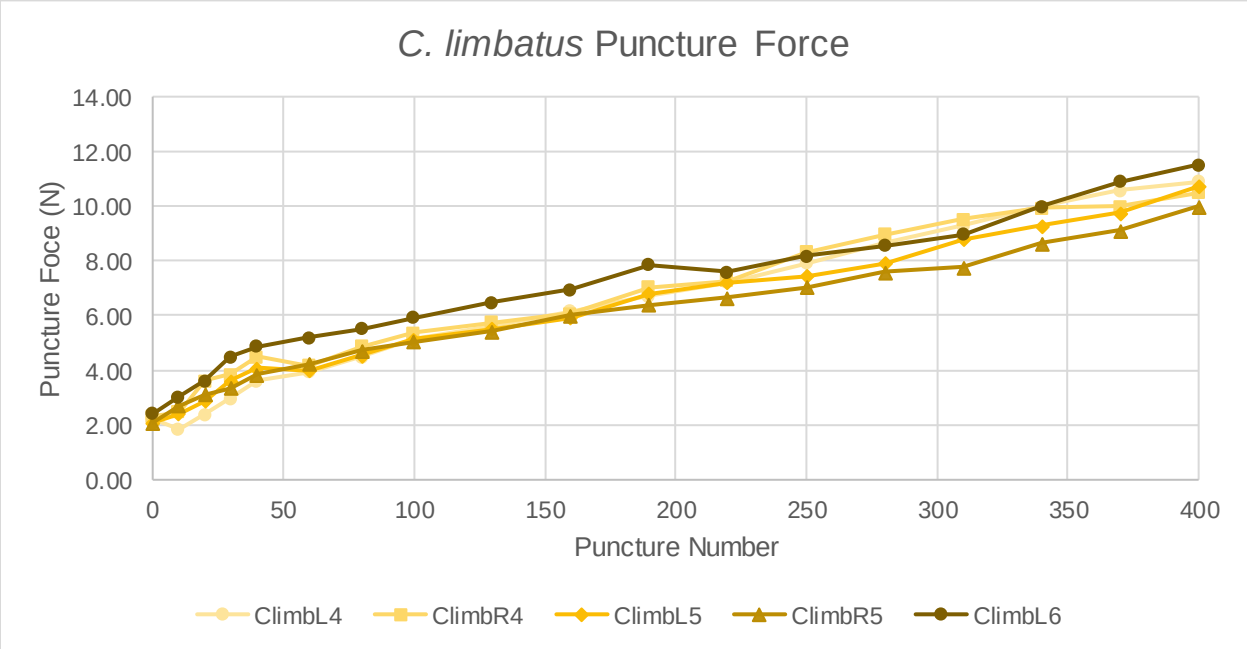
Whitenack LB, Simkins DC, Motta PJ. 2011. Biology Meets Engineering: The Structural Mechanics of Fossil and Extant Shark Teeth. Journal of Morphology. 272(2):169-79.

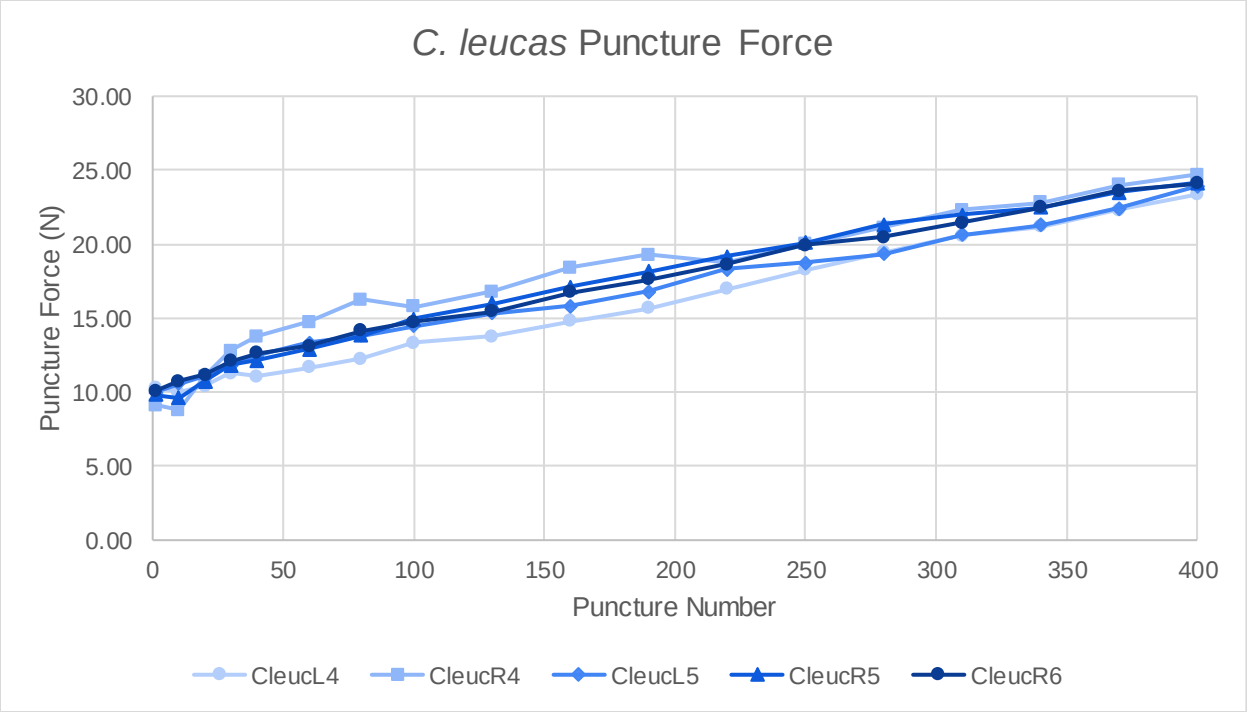
Wilga CD, Motta PJ, Sanford CP. 2007. Evolution and Ecology of Feeding in Elasmobranchs. Integrative and Comparative Biology. 47(1):55-69.

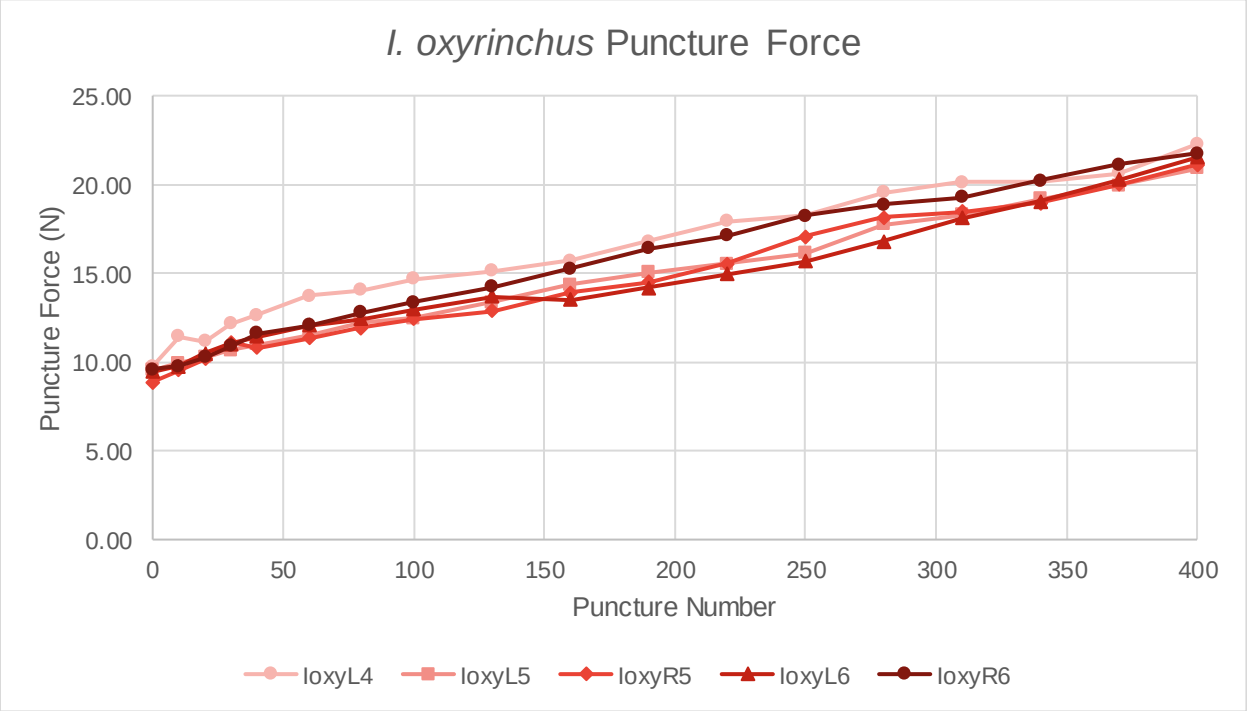
Wilmers J, Waldron M, Bargmann S. 2021. Hierarchical Microstructure of Tooth Enameloid in Two Lamniform Shark Species, *Carcharias taurus* and *Isurus oxyrinchus*. Nanomaterials (Basel, Switzerland). 11(4):969.

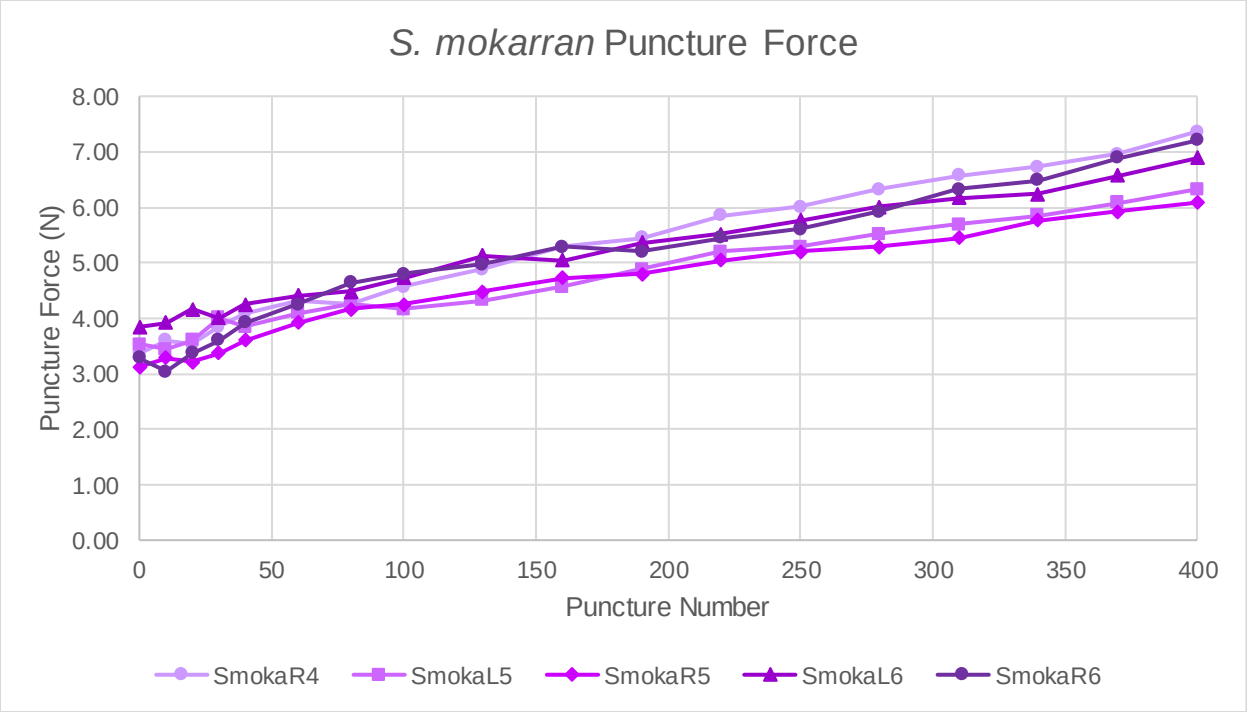
Appendix A: Puncture Force

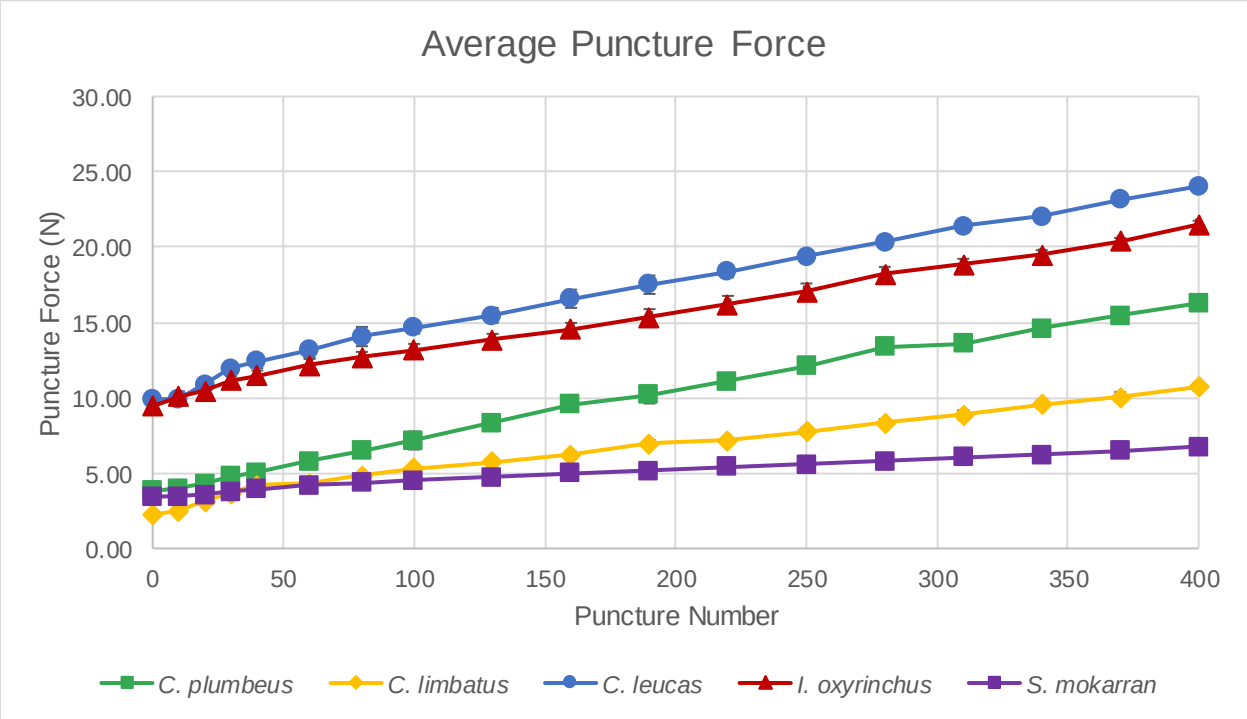




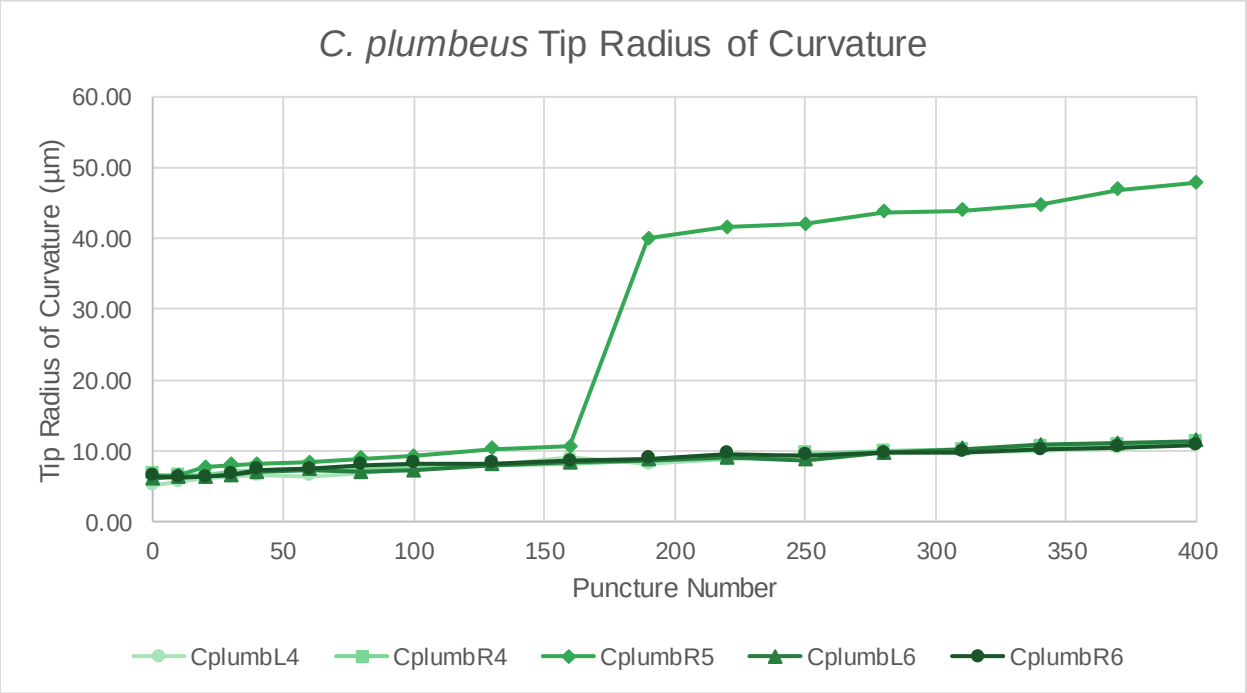

C. leucas Puncture Force
Puncture Force (N)
30.00
25.00
20.00
15.00
10.00
5.00
0.00
0
50
100
150
200
250
300
350
400
Puncture Number
CleucL4
CleucR4
CleucL5
CleucR5
CleucR6

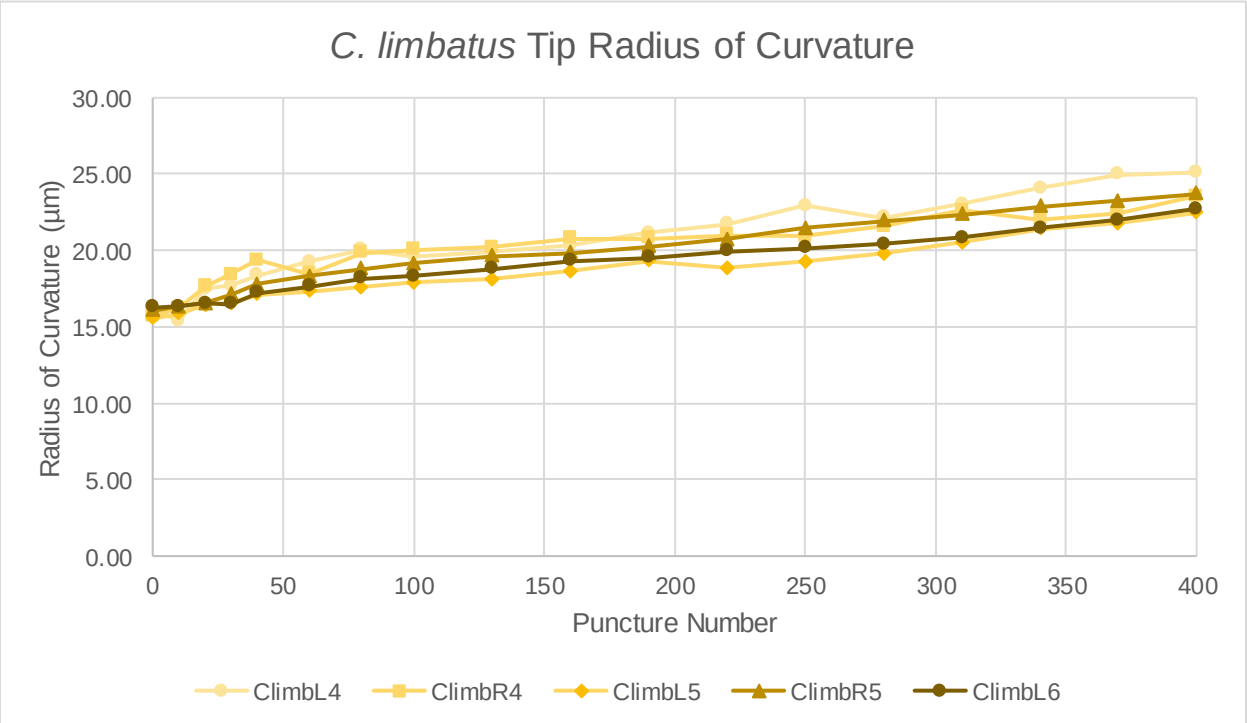

I. oxyrinchus Puncture Force
Puncture Force (N)
25.00
20.00
15.00
10.00
5.00
0.00
0
50
100
150
200
250
300
350
400
Puncture Number
IoxyL4
IoxyL5
IoxyR5
IoxyL6
IoxyR6

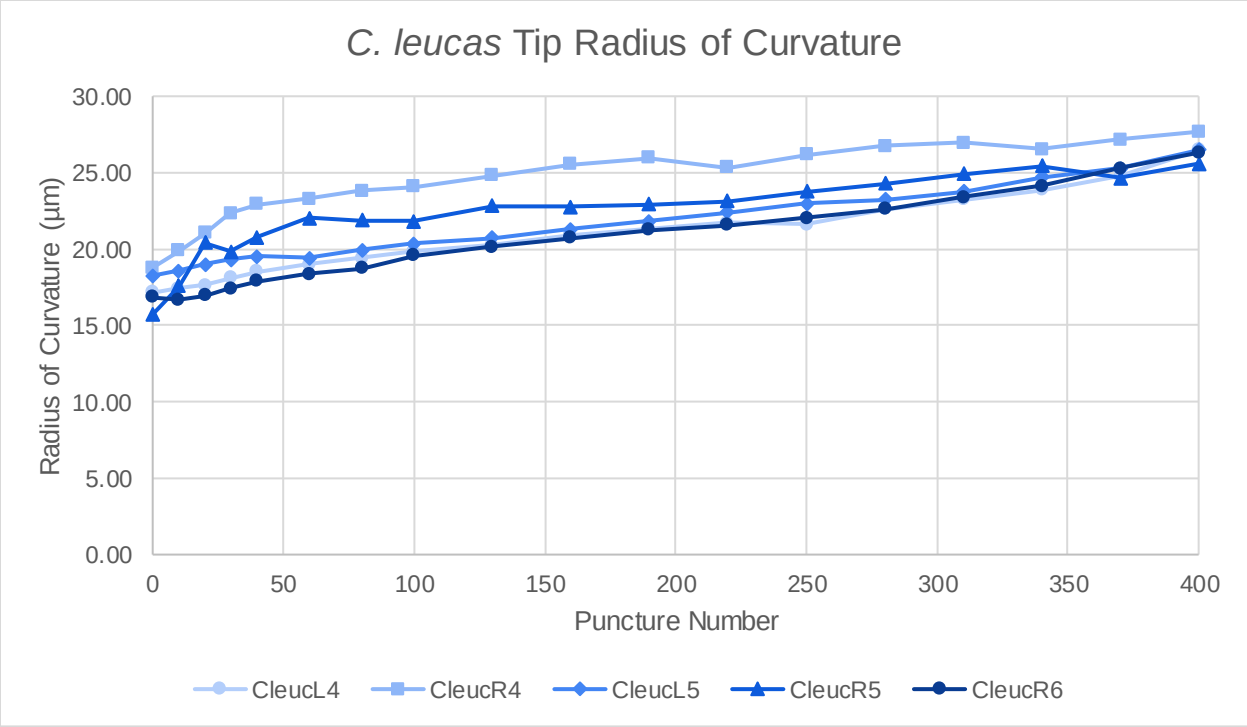

S. mokarran Puncture Force
Puncture Force (N)
8.00
7.00
6.00
5.00
4.00
3.00
2.00
1.00
0.00
0
50
100
150
200
250
300
350
400
Puncture Number
SmokaR4
SmokaL5
SmokaR5
SmokaL6
SmokaR6

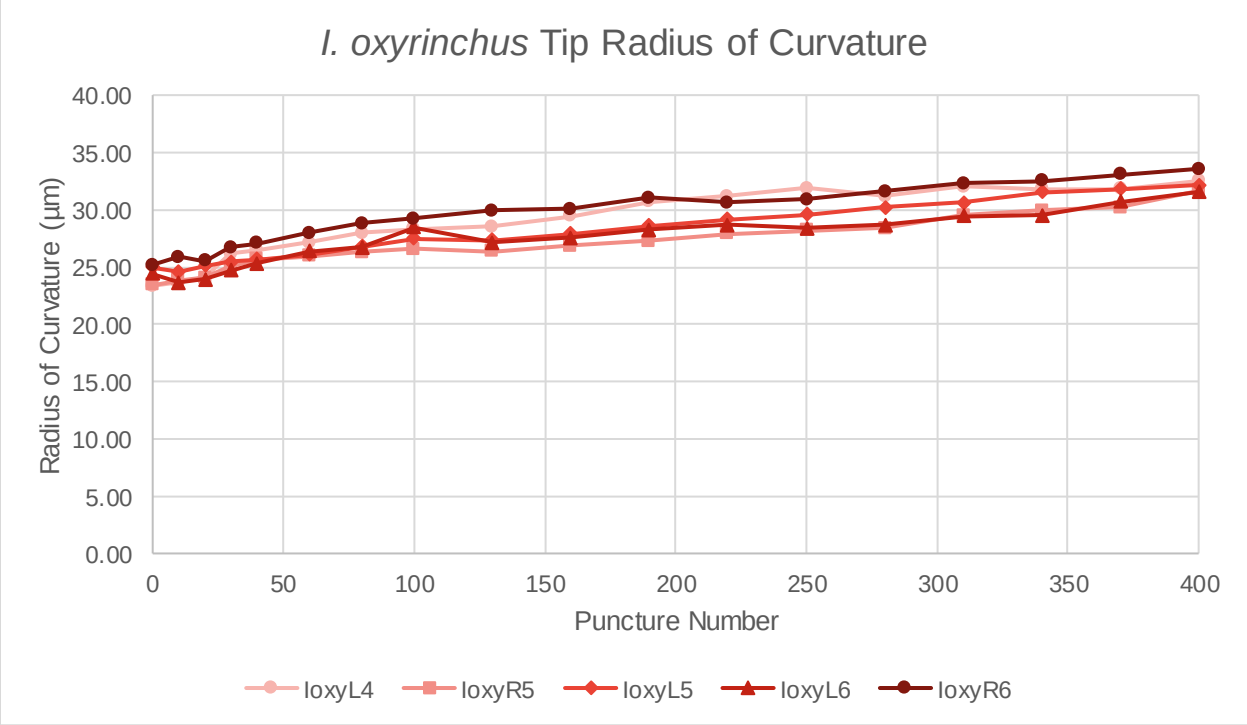

Average Puncture Force
Puncture Force (N)
30.00
25.00
20.00
15.00
10.00
5.00
0.00
0
50
100
150
200
250
300
350
400
Puncture Number
C. plumbeus
C. limbatus
C. leucas
I. oxyrinchus
S. mokarran

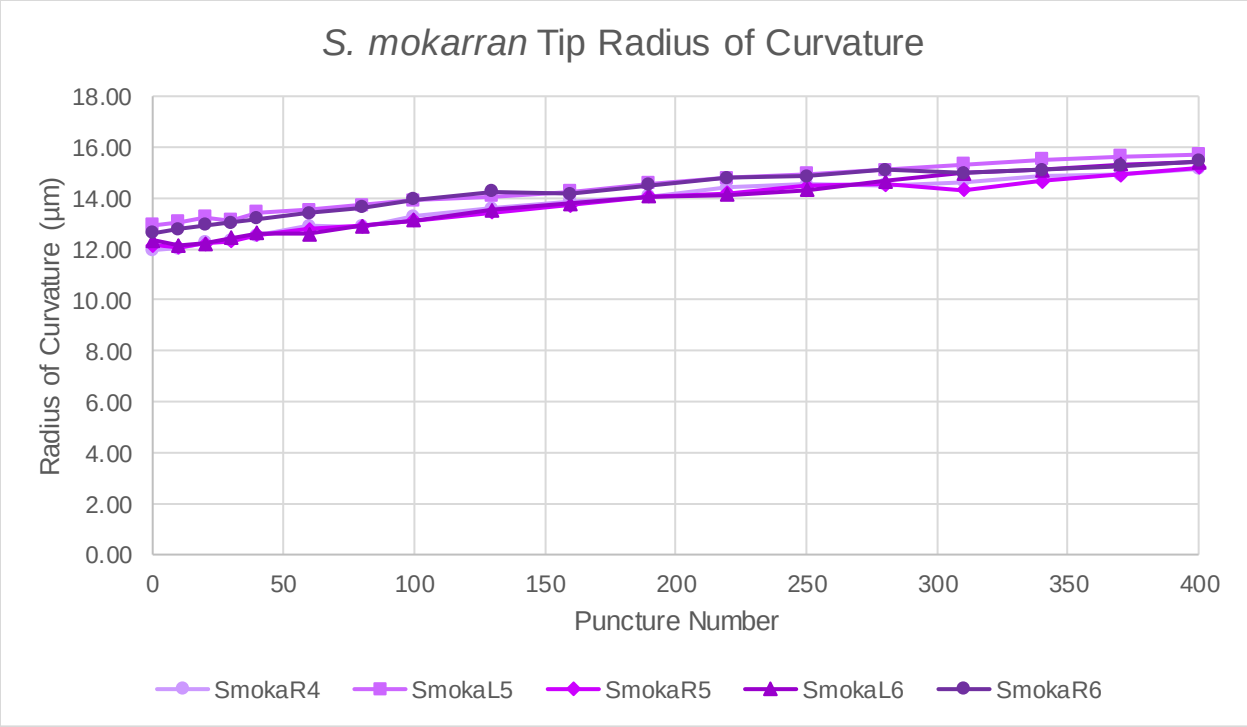
Appendix B: Tip Radius of Curvature

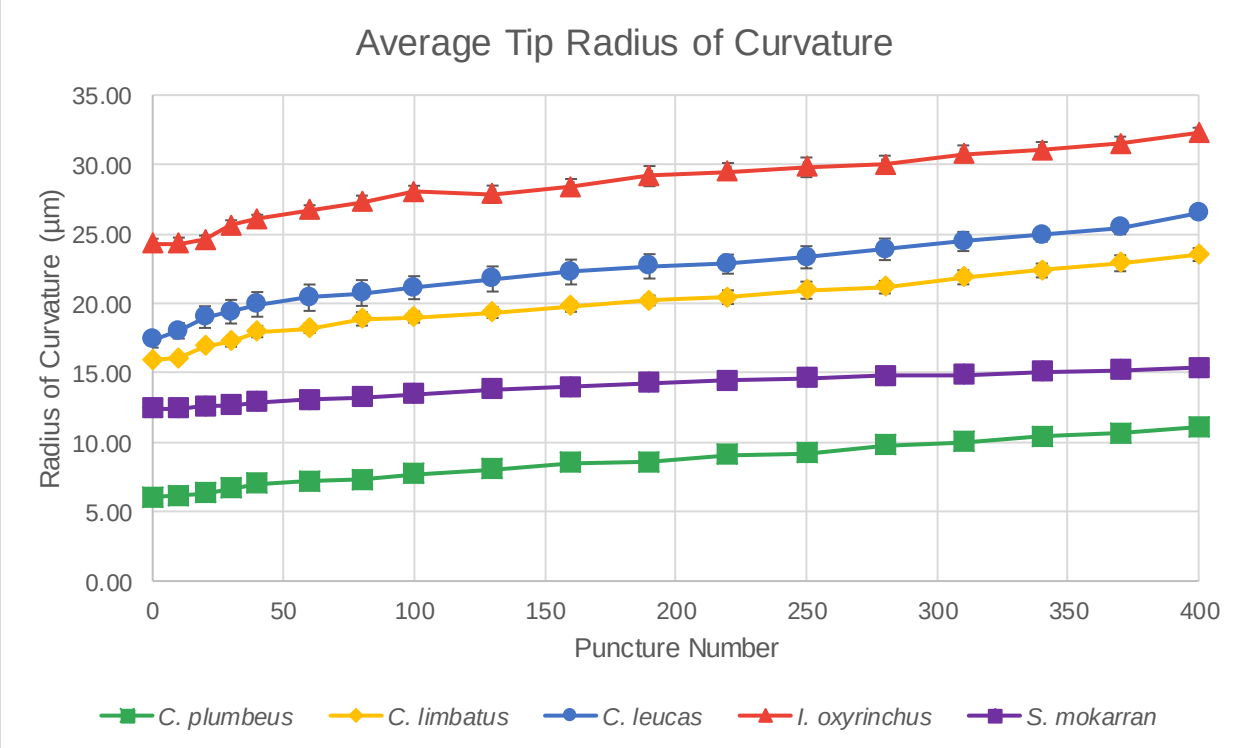




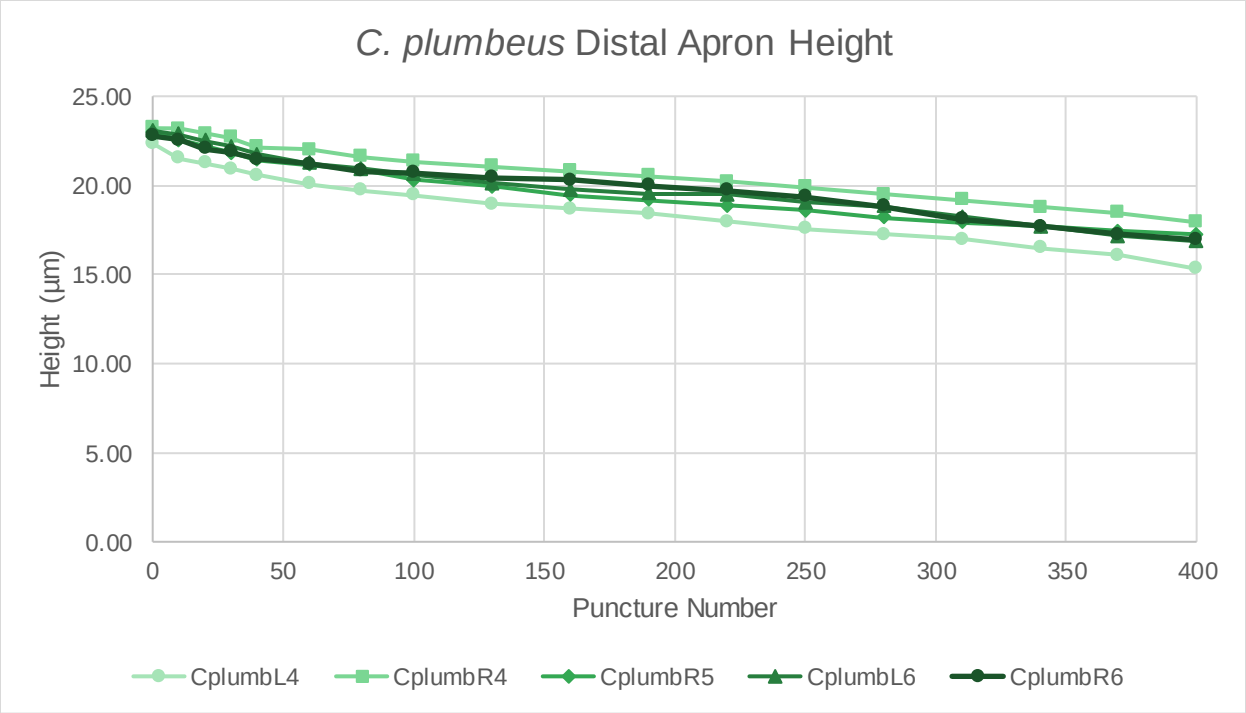

C. leucas Tip Radius of Curvature
Radius of Curvature (µm)
30.00
25.00
20.00
15.00
10.00
5.00
0.00
0
50
100
150
200
250
300
350
400
Puncture Number
CleucL4
CleucR4
CleucL5
CleucR5
CleucR6

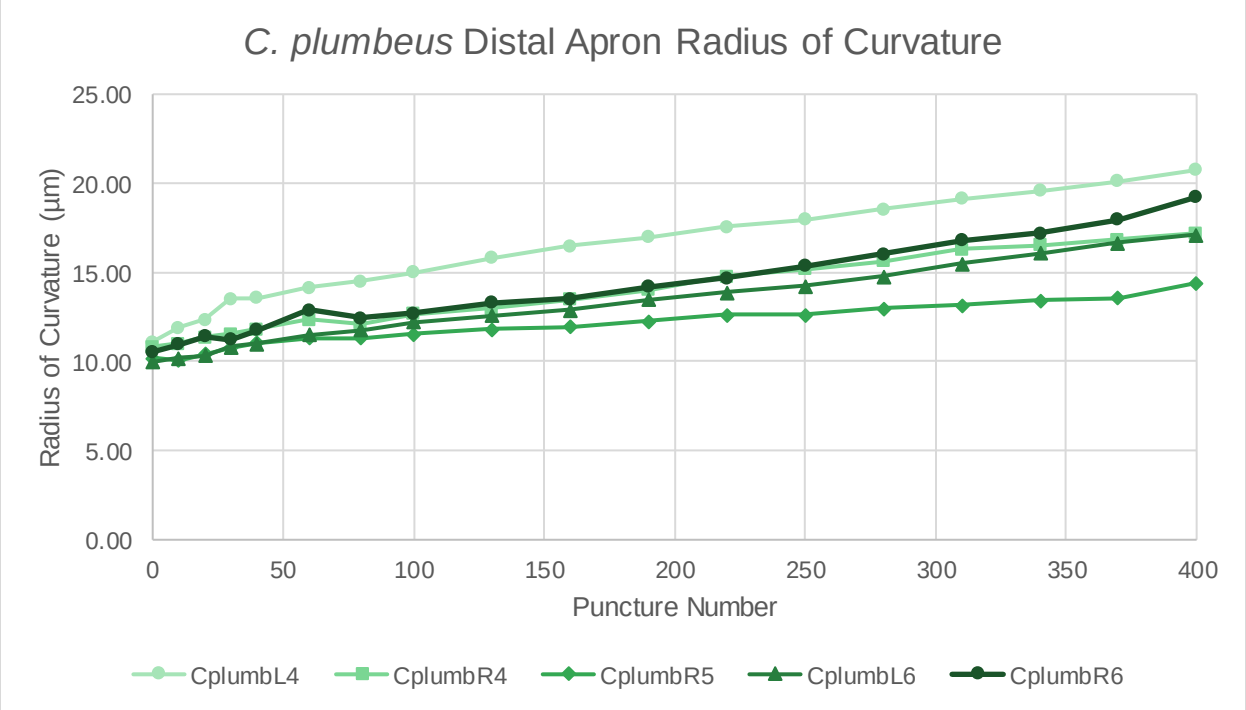

I. oxyrinchus Tip Radius of Curvature
Radius of Curvature (µm)
40.00
35.00
30.00
25.00
20.00
15.00
10.00
5.00
0.00
0
50
100
150
200
250
300
350
400
Puncture Number
IoxyL4
IoxyR5
IoxyL5
IoxyL6
IoxyR6

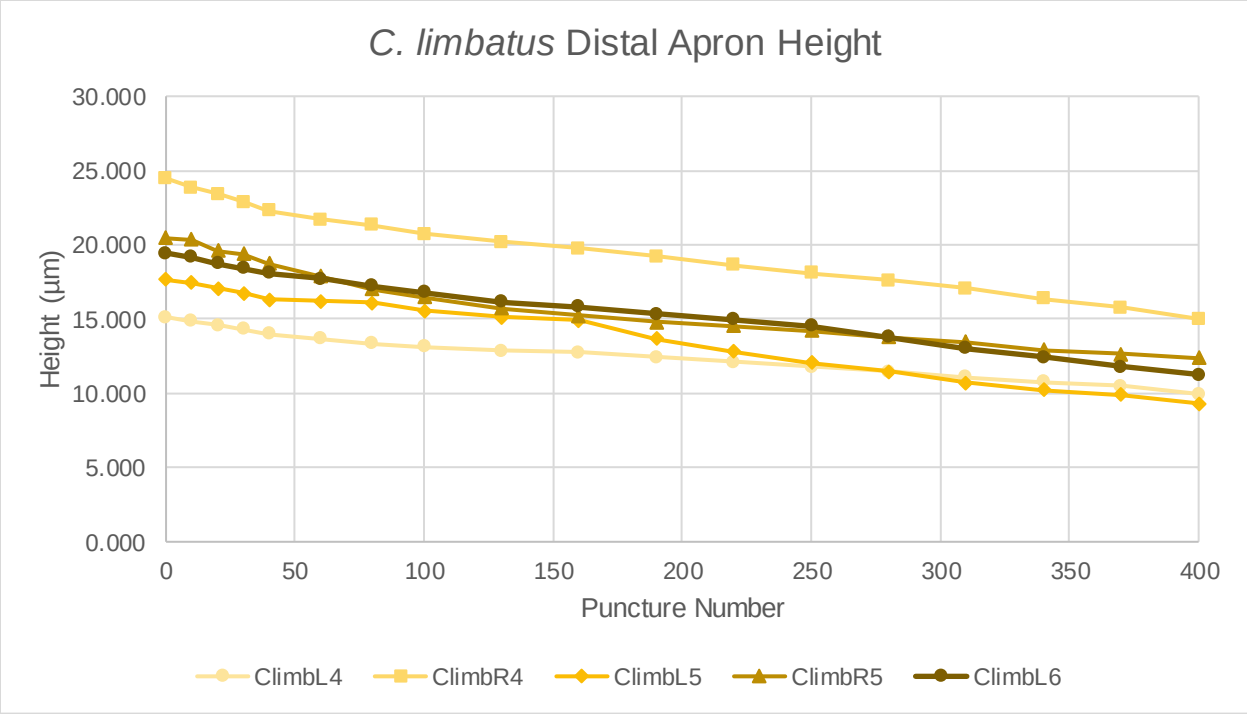

S. mokarran Tip Radius of Curvature
Radius of Curvature (µm)
18.00
16.00
14.00
12.00
10.00
8.00
6.00
4.00
2.00
0.00
0
50
100
150
200
250
300
350
400
Puncture Number
SmokaR4
SmokaL5
SmokaR5
SmokaL6
SmokaR6

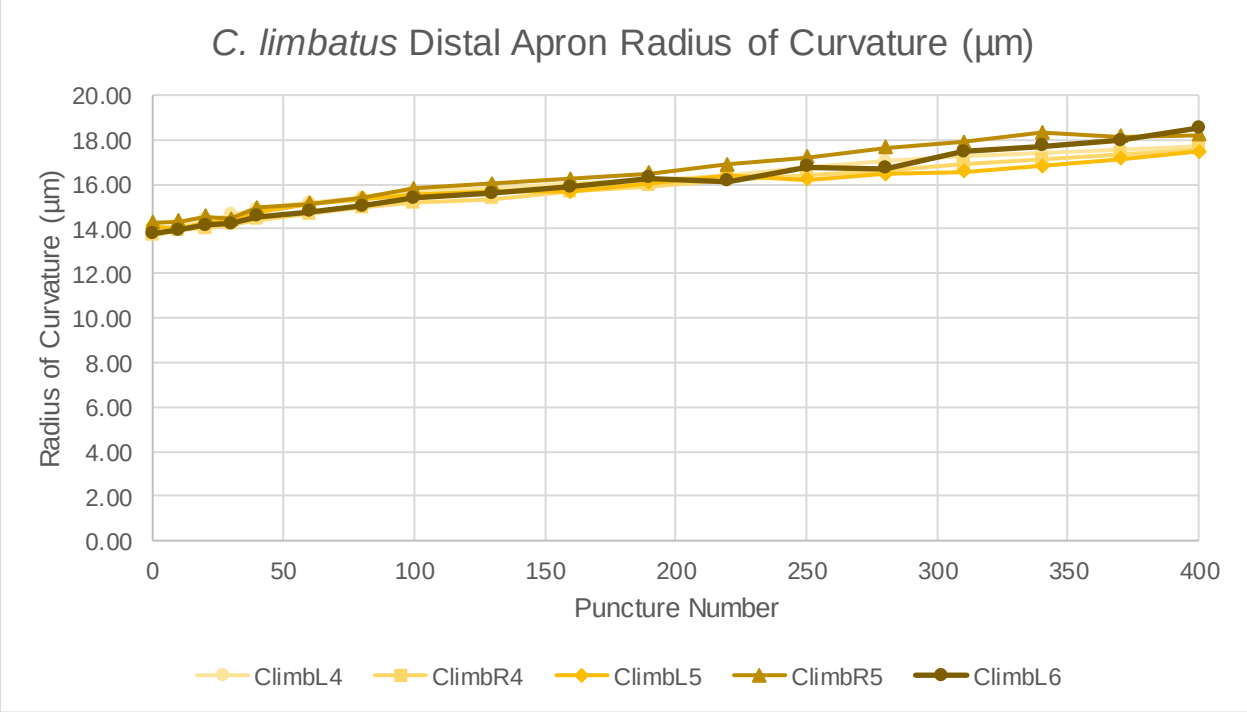

Average Tip Radius of Curvature
Radius of Curvature (µm)
35.00
30.00
25.00
20.00
15.00
10.00
5.00
0.00
0
50
100
150
200
250
300
350
400
Puncture Number
C. plumbeus
C. limbatus
C. leucas
I. oxyrinchus
S. mokarran

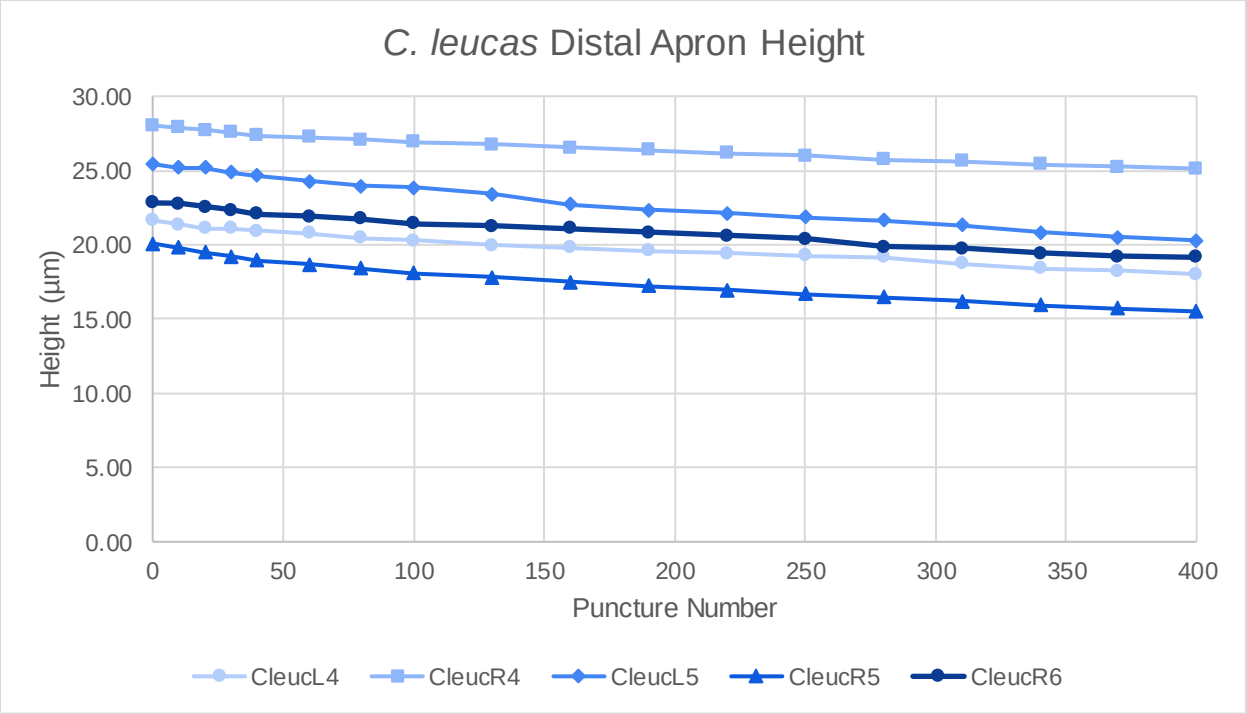
Appendix C: Distal Apron

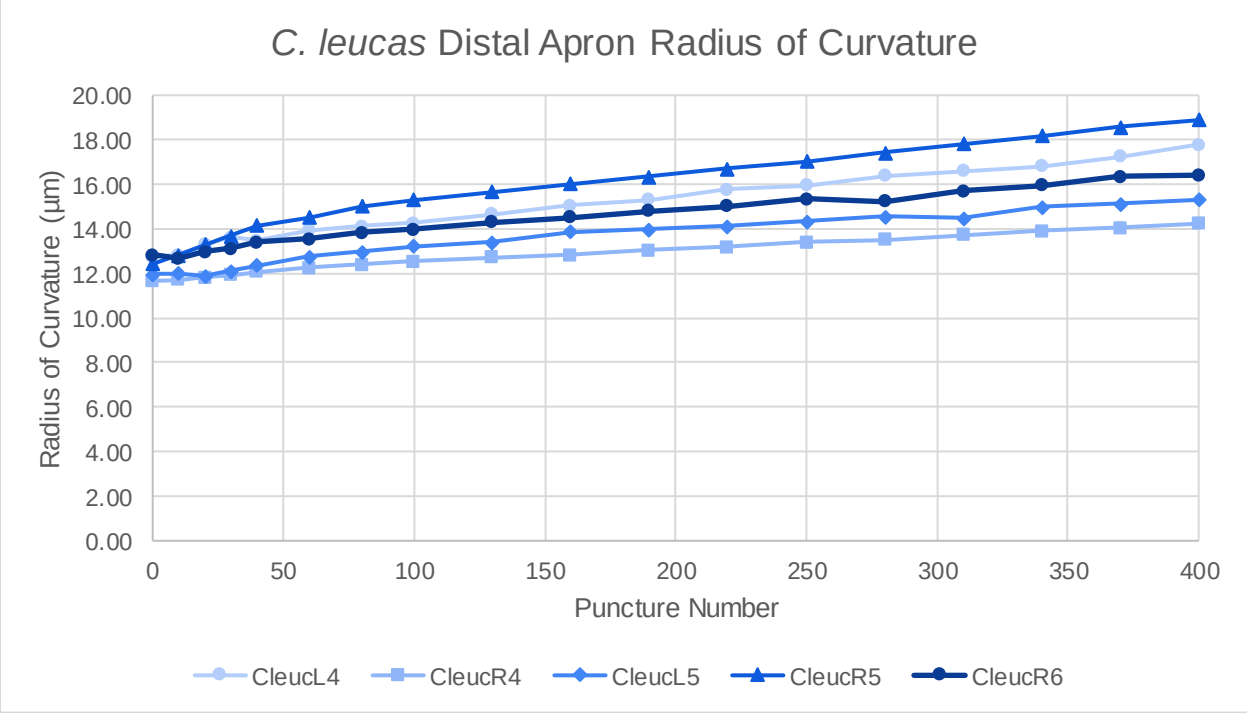


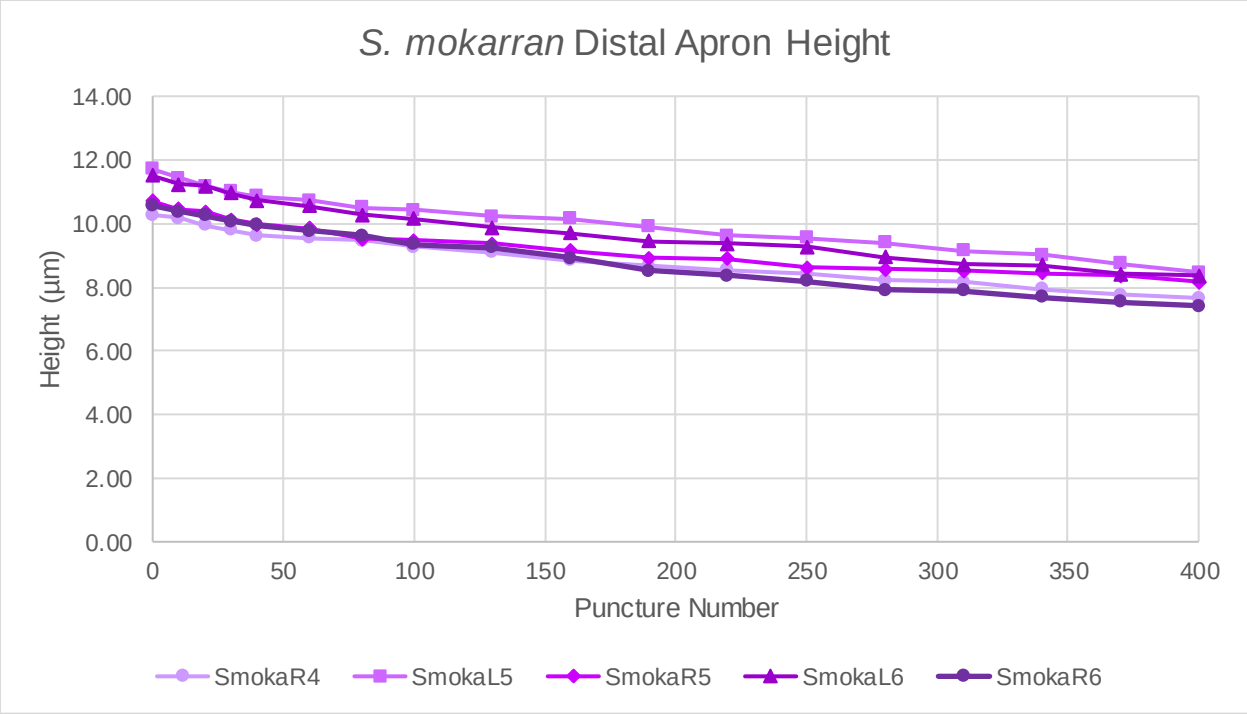


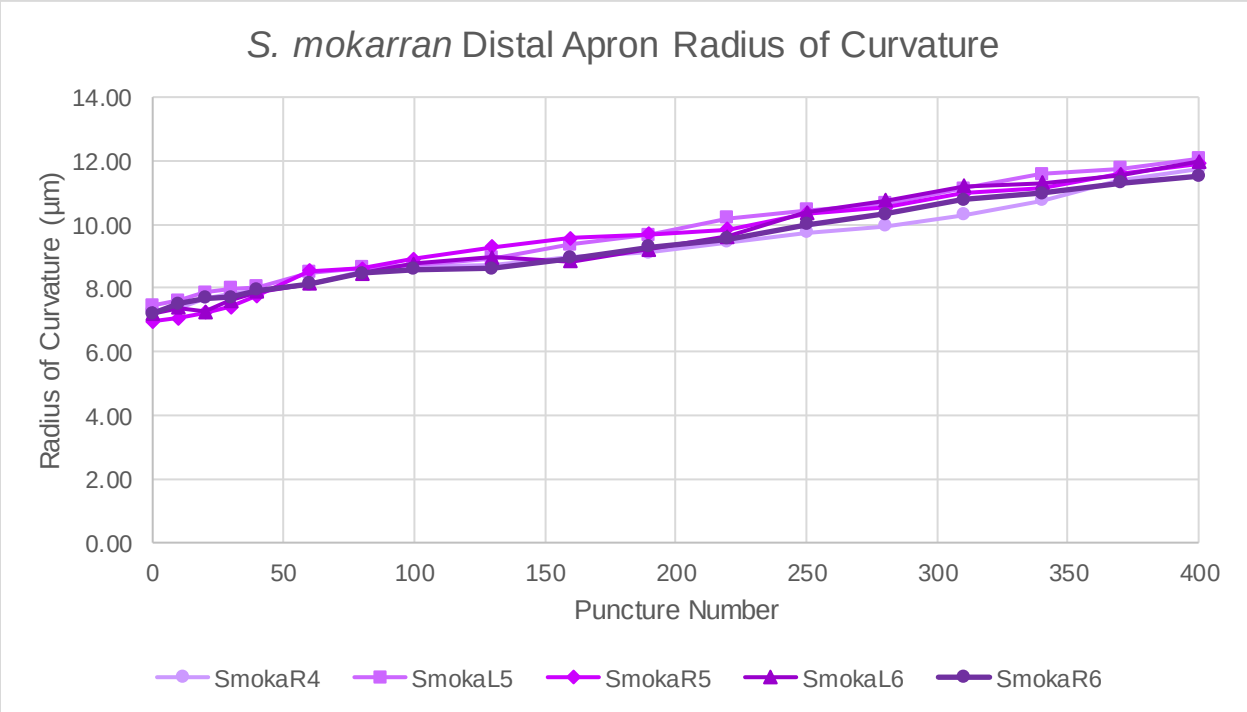

C. limbatus Distal Apron Height
30.000
25.000
20.000
15.000
10.000
5.000
0.000
Height (µm)
0
50
100
150
200
250
300
350
400
Puncture Number
ClimbL4
ClimbR4
ClimbL5
ClimbR5
ClimbL6

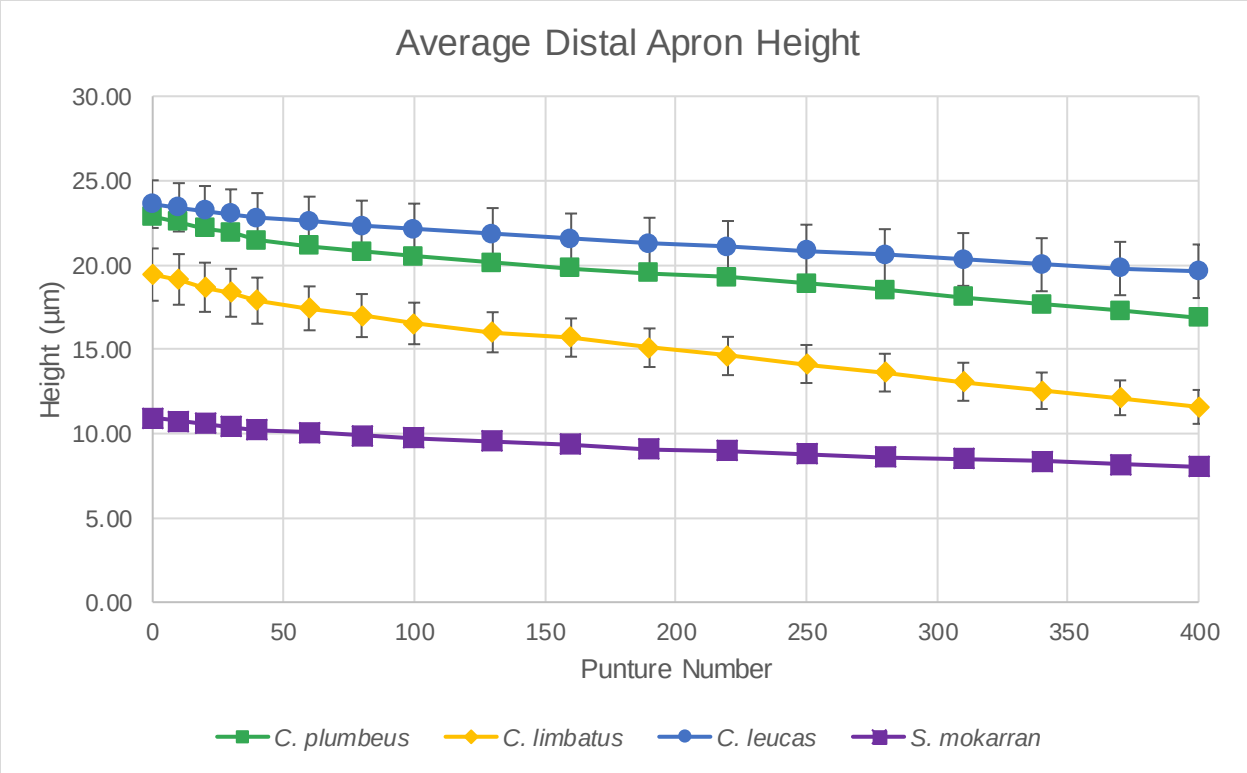

C. limbatus Distal Apron Radius of Curvature (µm)
20.00
18.00
16.00
14.00
12.00
10.00
8.00
6.00
4.00
2.00
0.00
Radius of Curvature (µm)
0
50
100
150
200
250
300
350
400
Puncture Number
ClimbL4
ClimbR4
ClimbL5
ClimbR5
ClimbL6

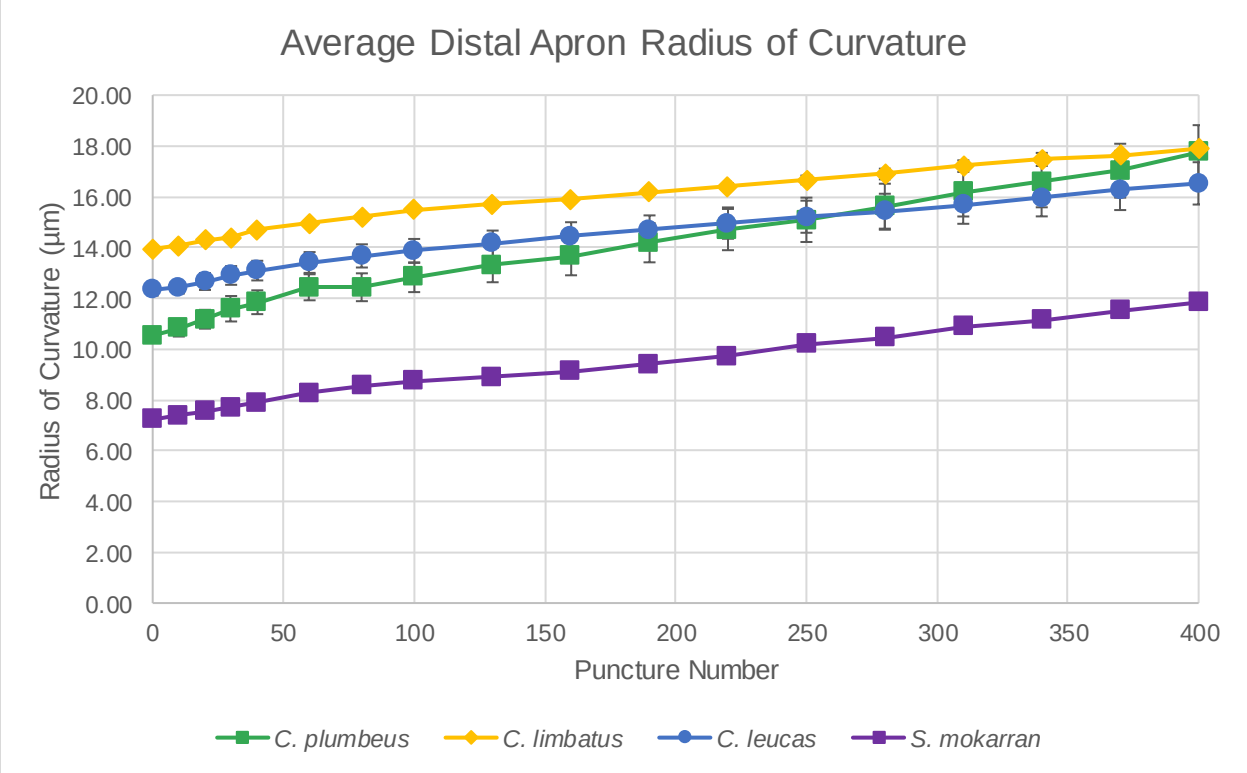

C. leucas Distal Apron Height
Height (µm)
30.00
25.00
20.00
15.00
10.00
5.00
0.00
0
50
100
150
200
250
300
350
400
Puncture Number
CleucL4
CleucR4
CleucL5
CleucR5
CleucR6


C. leucas Distal Apron Radius of Curvature
Radius of Curvature (µm)
20.00
18.00
16.00
14.00
12.00
10.00
8.00
6.00
4.00
2.00
0.00
0
50
100
150
200
250
300
350
400
Puncture Number
CleucL4
CleucR4
CleucL5
CleucR5
CleucR6

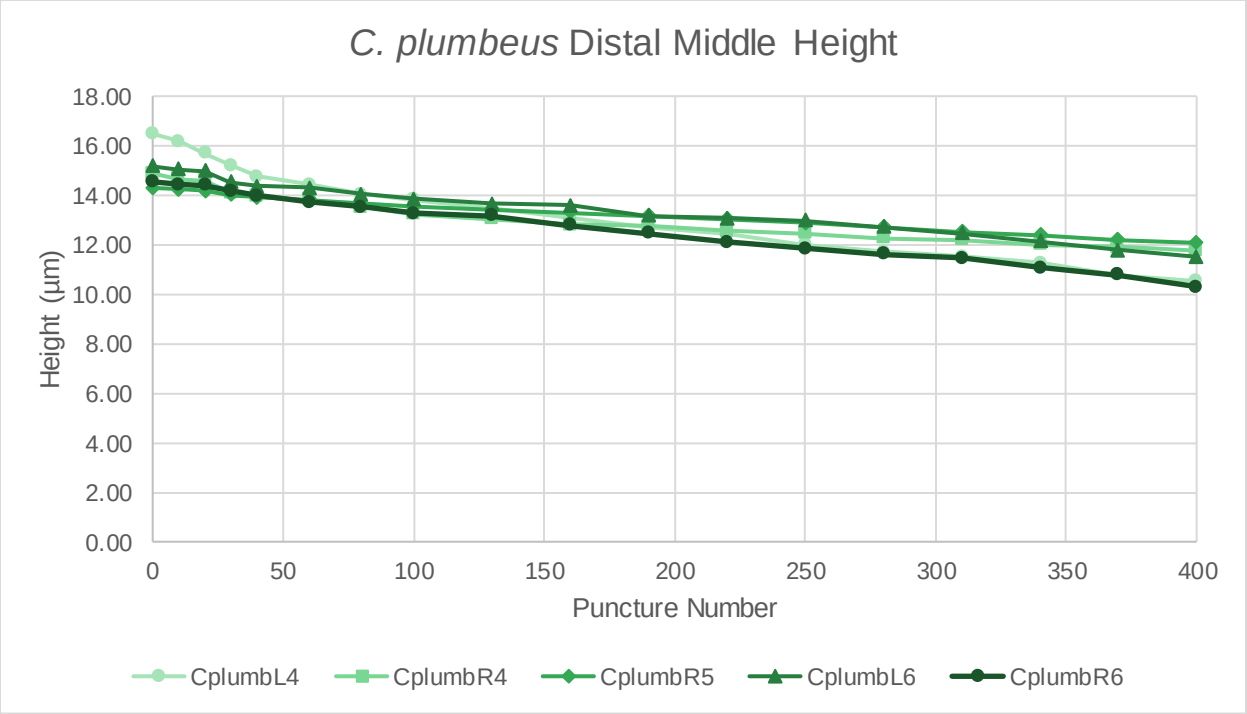

S. mokarran Distal Apron Height
14.00
12.00
10.00
8.00
6.00
4.00
2.00
0.00
Height (µm)
0
50
100
150
200
250
300
350
400
Puncture Number
SmokaR4
SmokaL5
SmokaR5
SmokaL6
SmokaR6

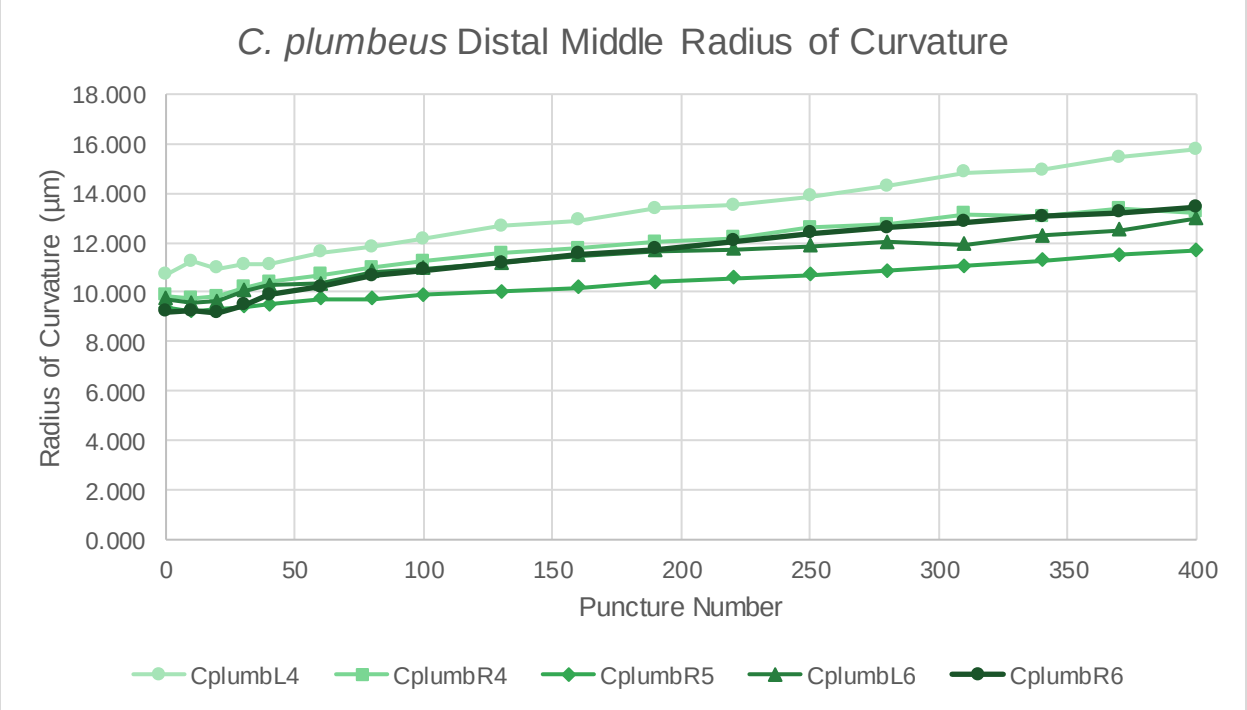

S. mokarran Distal Apron Radius of Curvature
14.00
12.00
10.00
8.00
6.00
4.00
2.00
0.00
Radius of Curvature (µm)
0
50
100
150
200
250
300
350
400
Puncture Number
SmokaR4
SmokaL5
SmokaR5
SmokaL6
SmokaR6

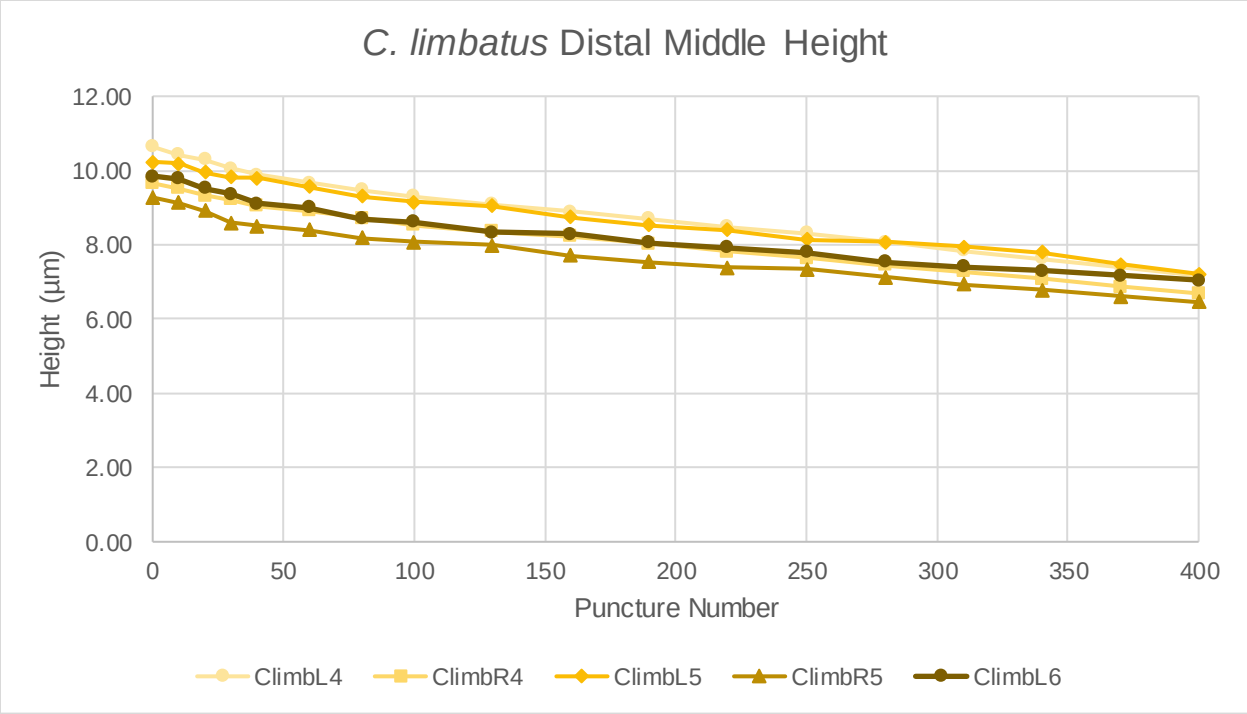

Average Distal Apron Height
Height (µm)
30.00
25.00
20.00
15.00
10.00
5.00
0.00
0
50
100
150
200
250
300
350
400
Punture Number
C. plumbeus
C. limbatus
C. leucas
S. mokarran

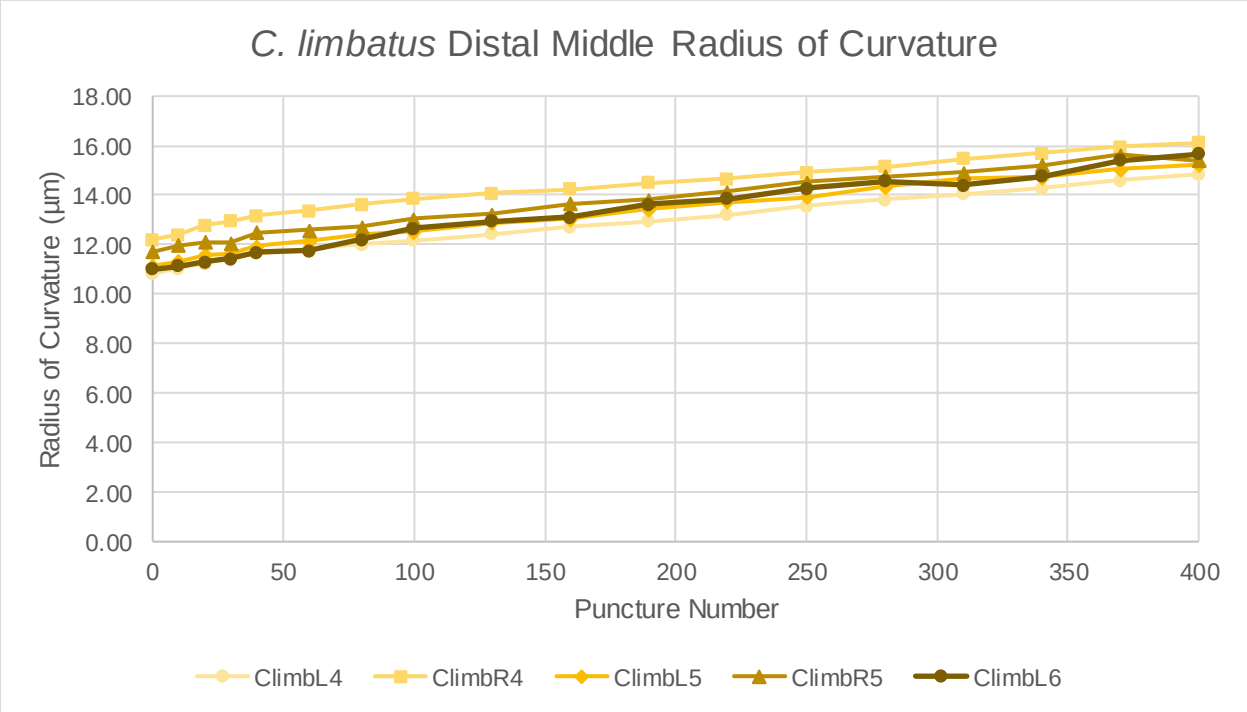

Average Distal Apron Radius of Curvature
Radius of Curvature (µm)
20.00
18.00
16.00
14.00
12.00
10.00
8.00
6.00
4.00
2.00
0.00
0
50
100
150
200
250
300
350
400
Puncture Number
C. plumbeus
C. limbatus
C. leucas
S. mokarran

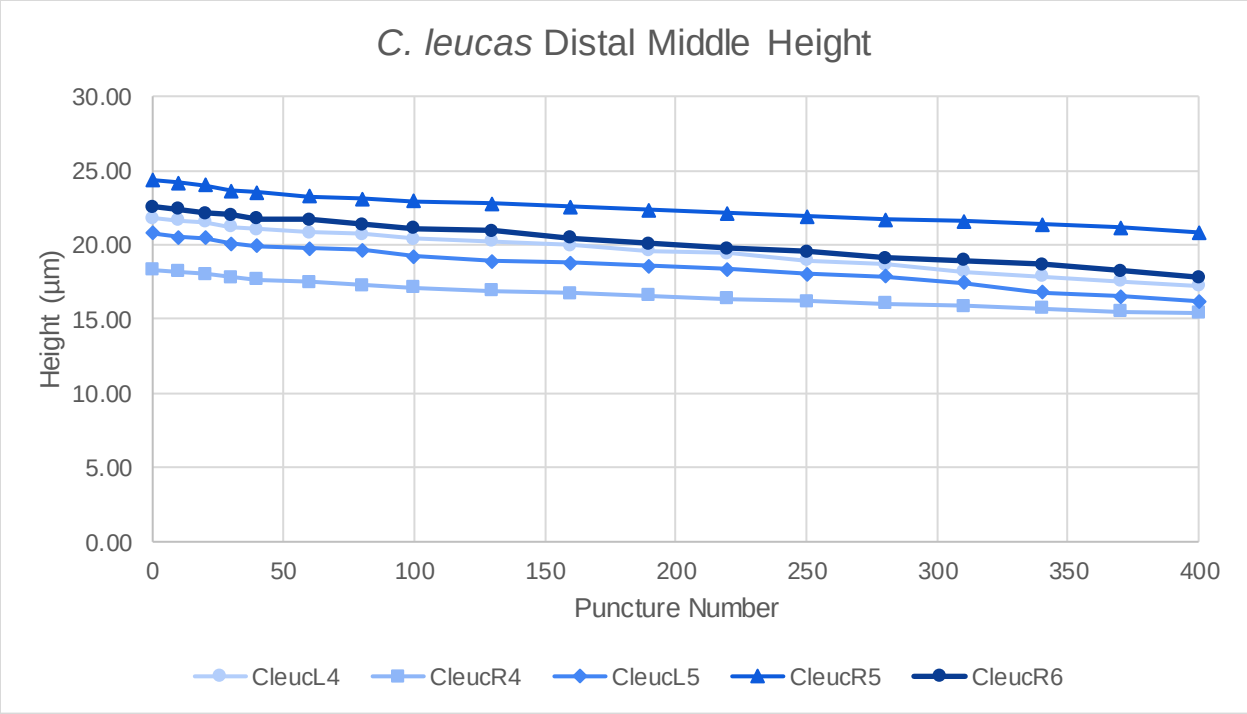
Appendix D: Distal Middle

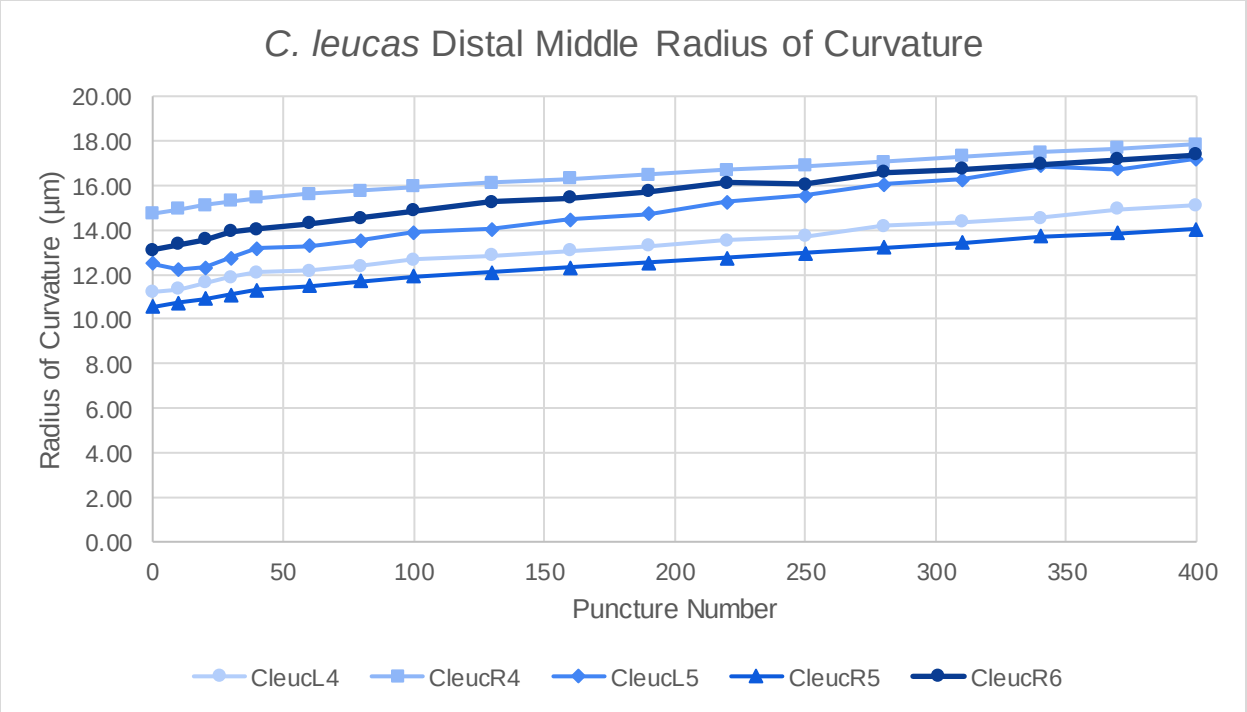


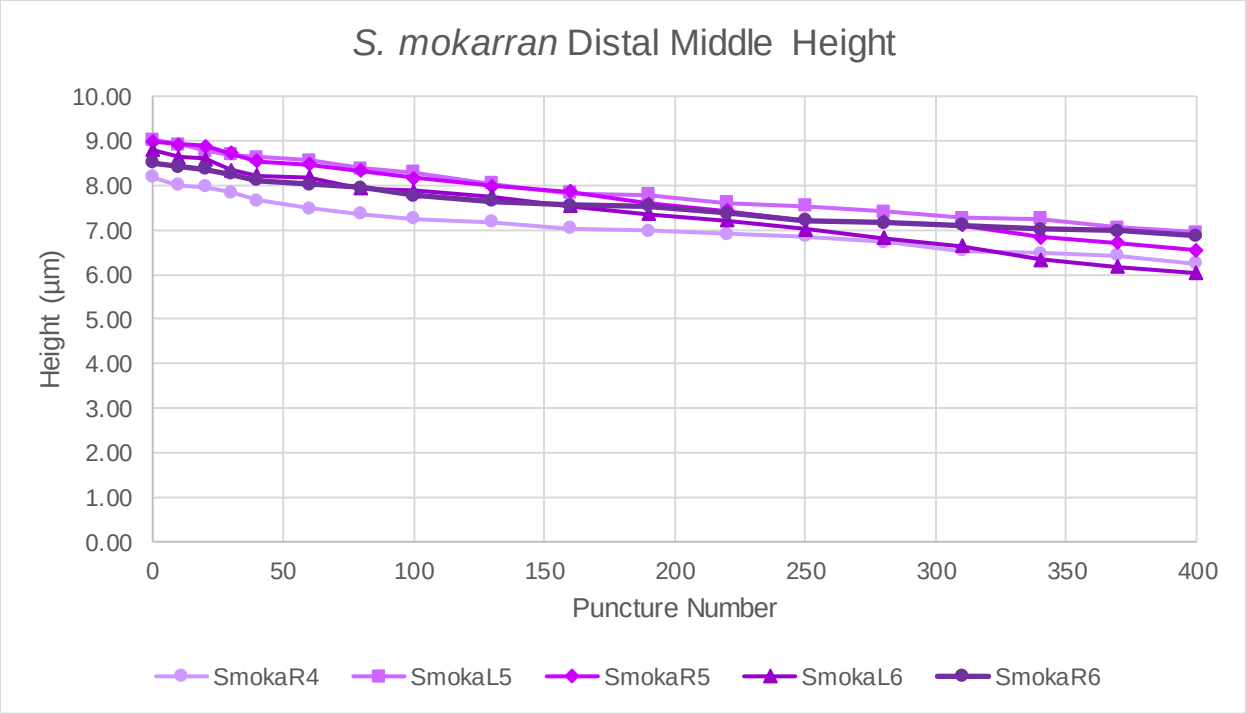


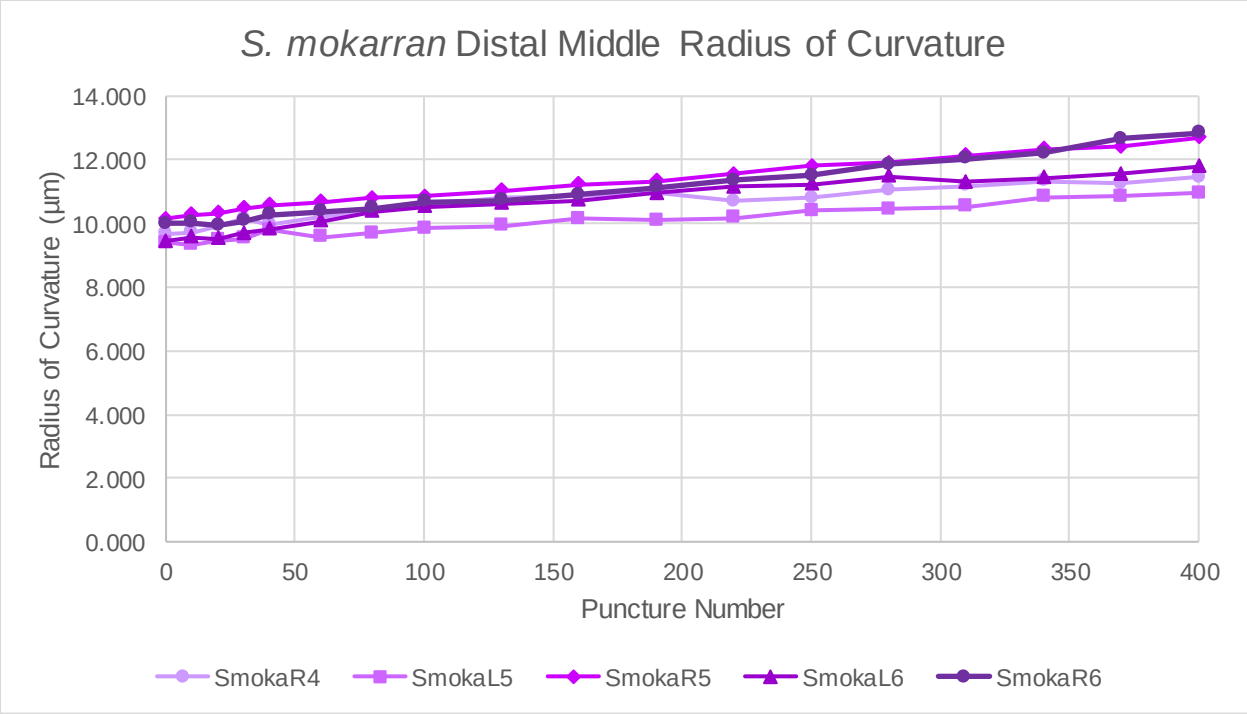

C. limbatus Distal Middle Height
12.00
10.00
8.00
6.00
4.00
2.00
0.00
Height (µm)
0
50
100
150
200
250
300
350
400
Puncture Number
ClimbL4
ClimbR4
ClimbL5
ClimbR5
ClimbL6

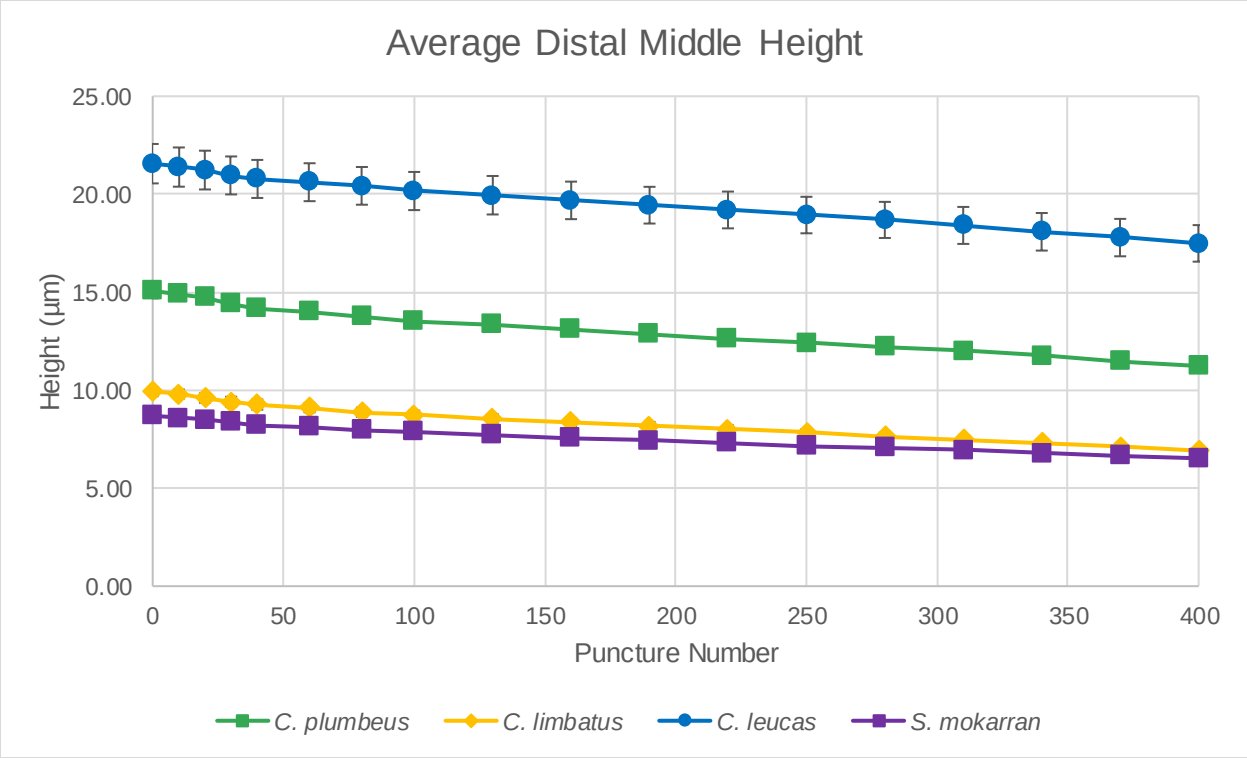

C. limbatus Distal Middle Radius of Curvature
18.00
16.00
14.00
12.00
10.00
8.00
6.00
4.00
2.00
0.00
Radius of Curvature (µm)
0
50
100
150
200
250
300
350
400
Puncture Number
ClimbL4
ClimbR4
ClimbL5
ClimbR5
ClimbL6

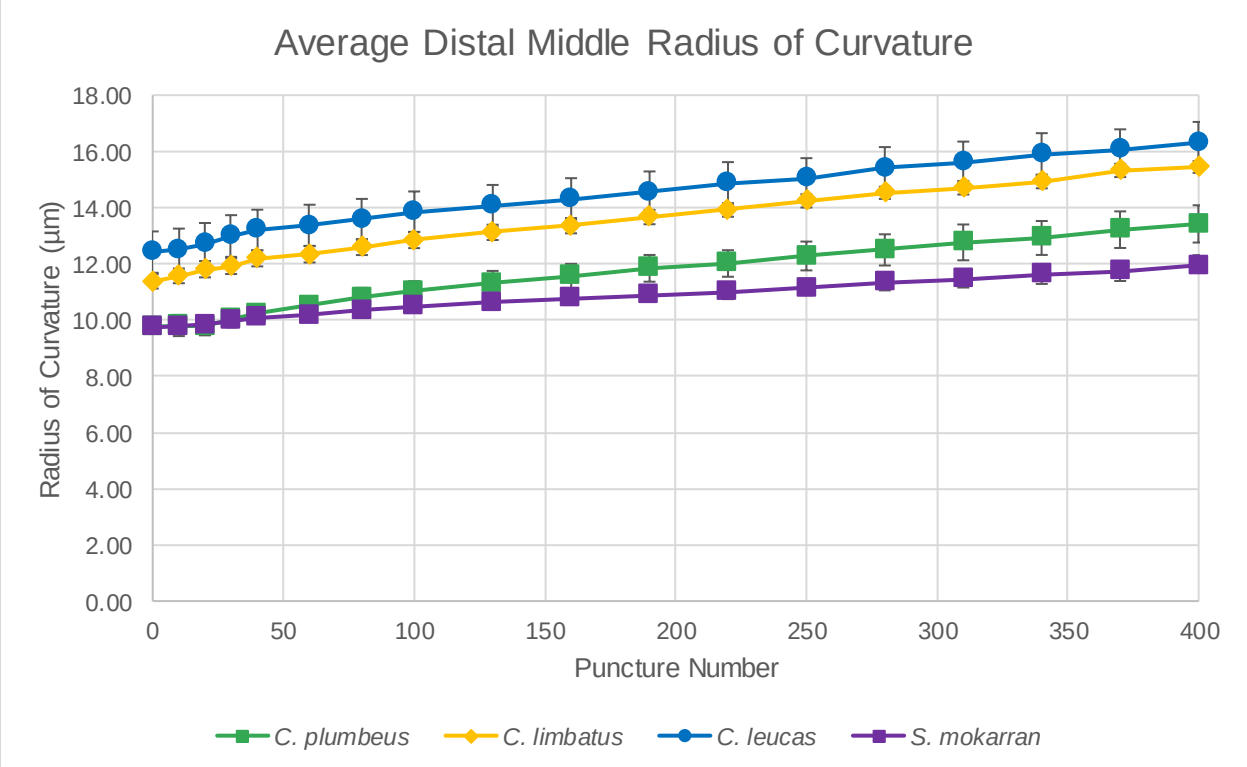

C. leucas Distal Middle Height
30.00
25.00
20.00
15.00
10.00
5.00
0.00
Height (µm)
0
50
100
150
200
250
300
350
400
Puncture Number
CleucL4
CleucR4
CleucL5
CleucR5
CleucR6


C. leucas Distal Middle Radius of Curvature
20.00
18.00
16.00
14.00
12.00
10.00
8.00
6.00
4.00
2.00
0.00
Radius of Curvature (µm)
0
50
100
150
200
250
300
350
400
Puncture Number
CleucL4
CleucR4
CleucL5
CleucR5
CleucR6

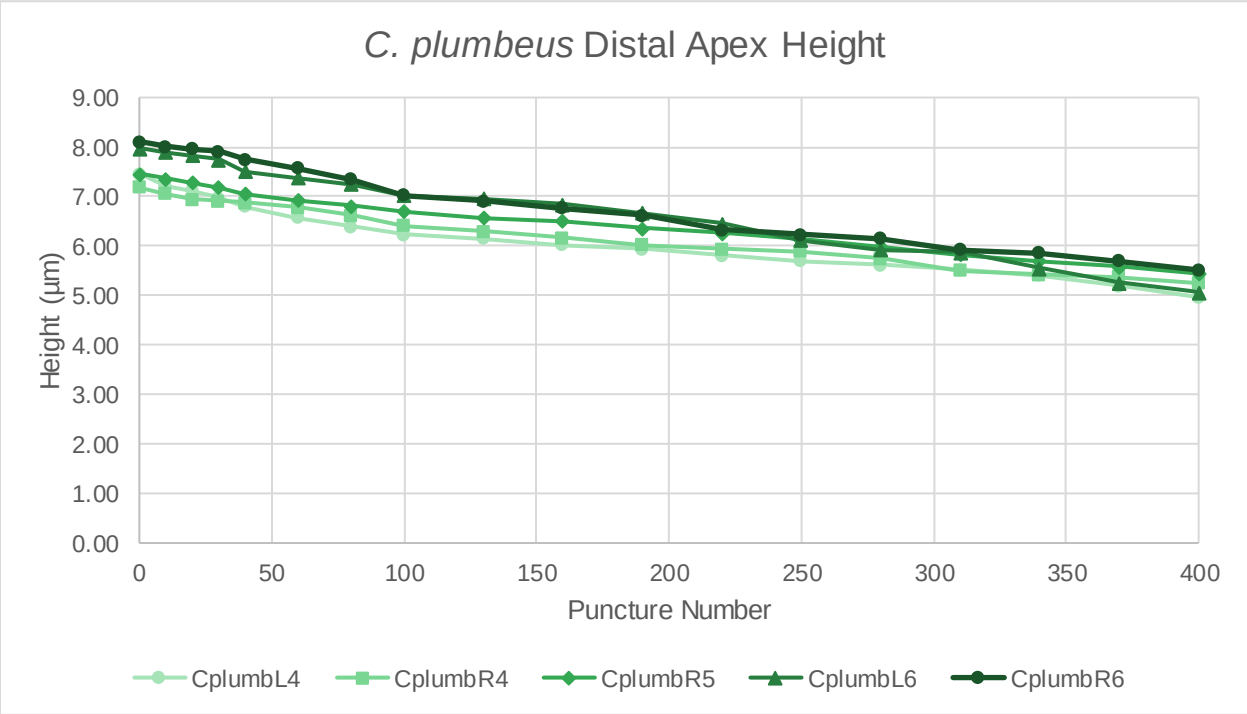

S. mokarran Distal Middle Height
10.00
9.00
8.00
7.00
6.00
5.00
4.00
3.00
2.00
1.00
0.00
Height (µm)
0
50
100
150
200
250
300
350
400
Puncture Number
SmokaR4
SmokaL5
SmokaR5
SmokaL6
SmokaR6

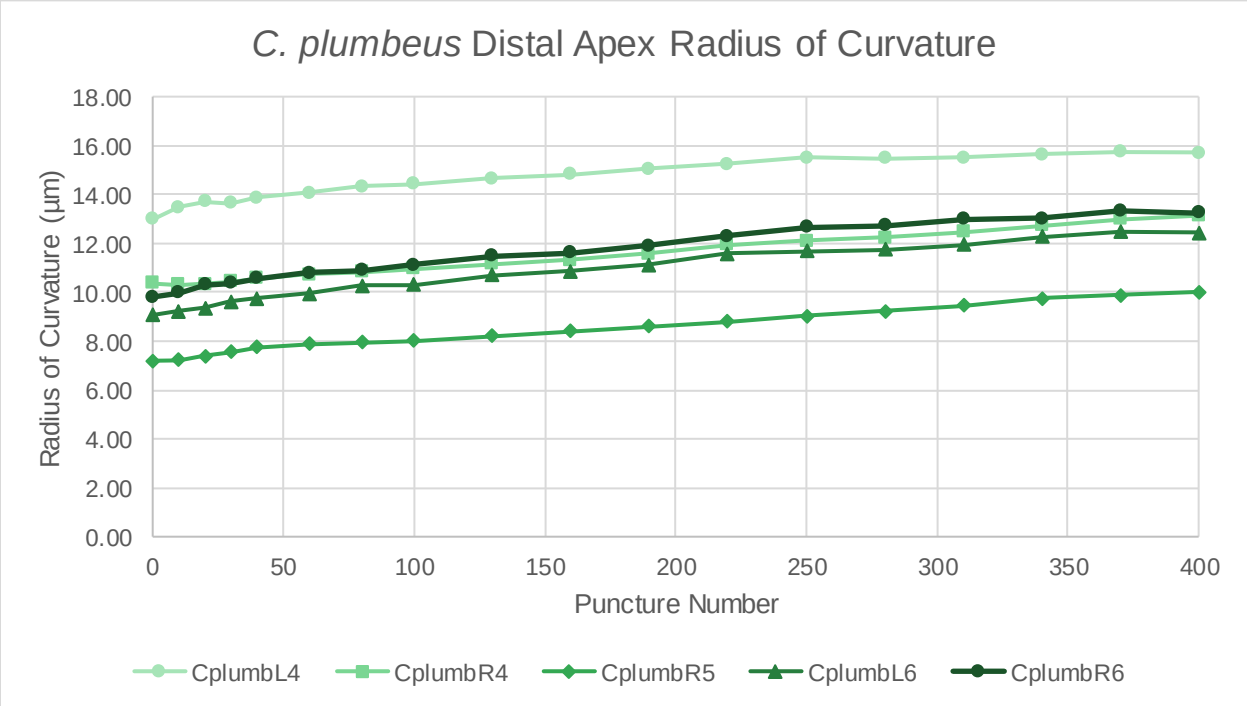

S. mokarran Distal Middle Radius of Curvature
14.000
12.000
10.000
8.000
6.000
4.000
2.000
0.000
Radius of Curvature (µm)
0
50
100
150
200
250
300
350
400
Puncture Number
SmokaR4
SmokaL5
SmokaR5
SmokaL6
SmokaR6

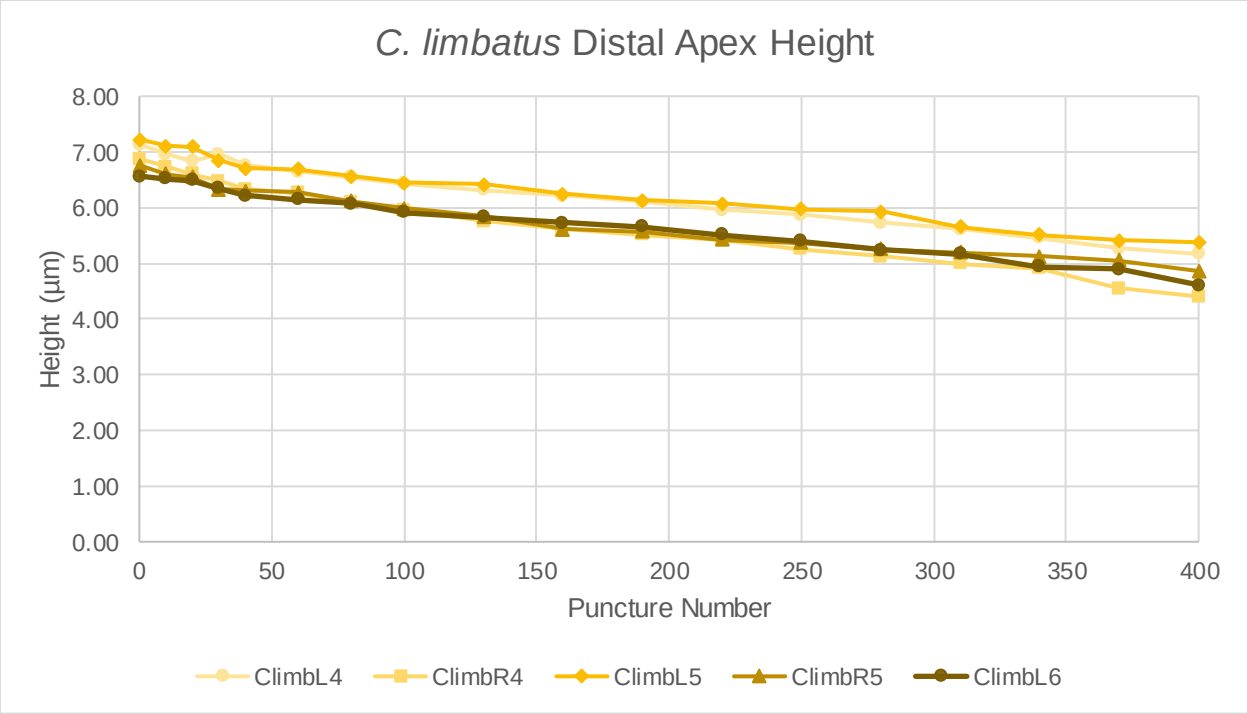

Average Distal Middle Height
25.00
20.00
15.00
10.00
5.00
0.00
Height (µm)
0
50
100
150
200
250
300
350
400
Puncture Number
C. plumbeus
C. limbatus
C. leucas
S. mokarran

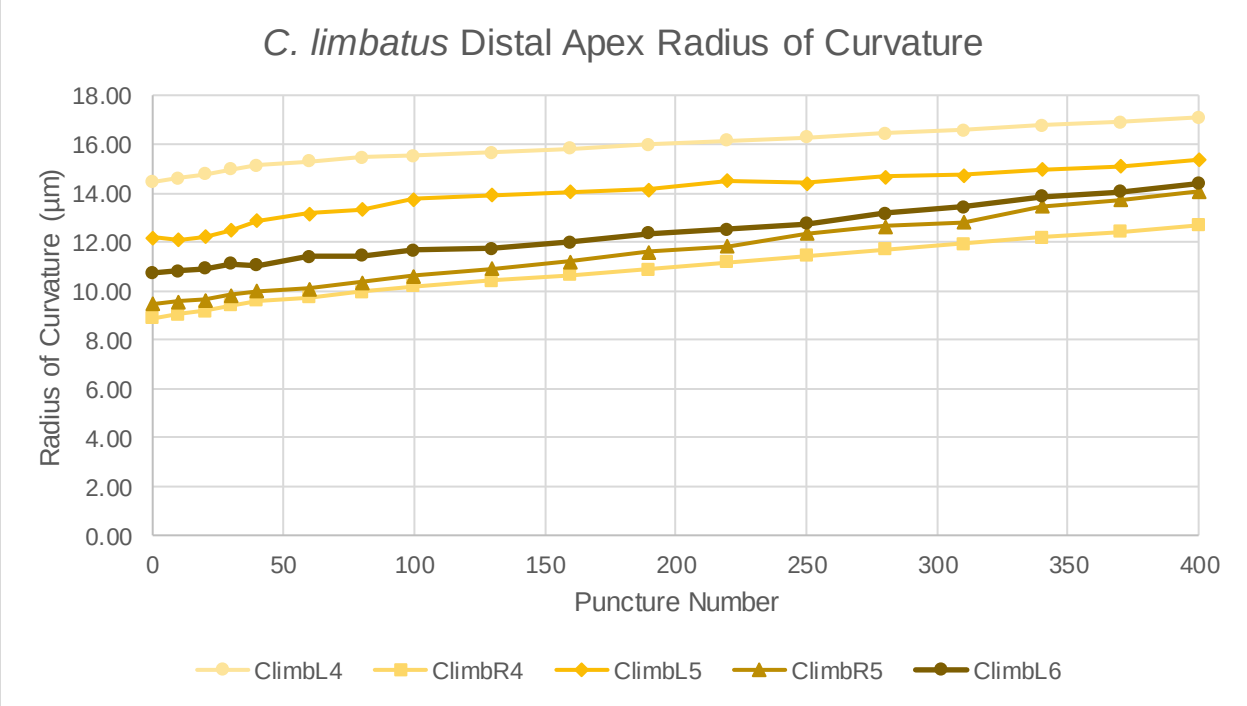

Average Distal Middle Radius of Curvature
18.00
16.00
14.00
12.00
10.00
8.00
6.00
4.00
2.00
0.00
Radius of Curvature (µm)
0
50
100
150
200
250
300
350
400
Puncture Number
C. plumbeus
C. limbatus
C. leucas
S. mokarran

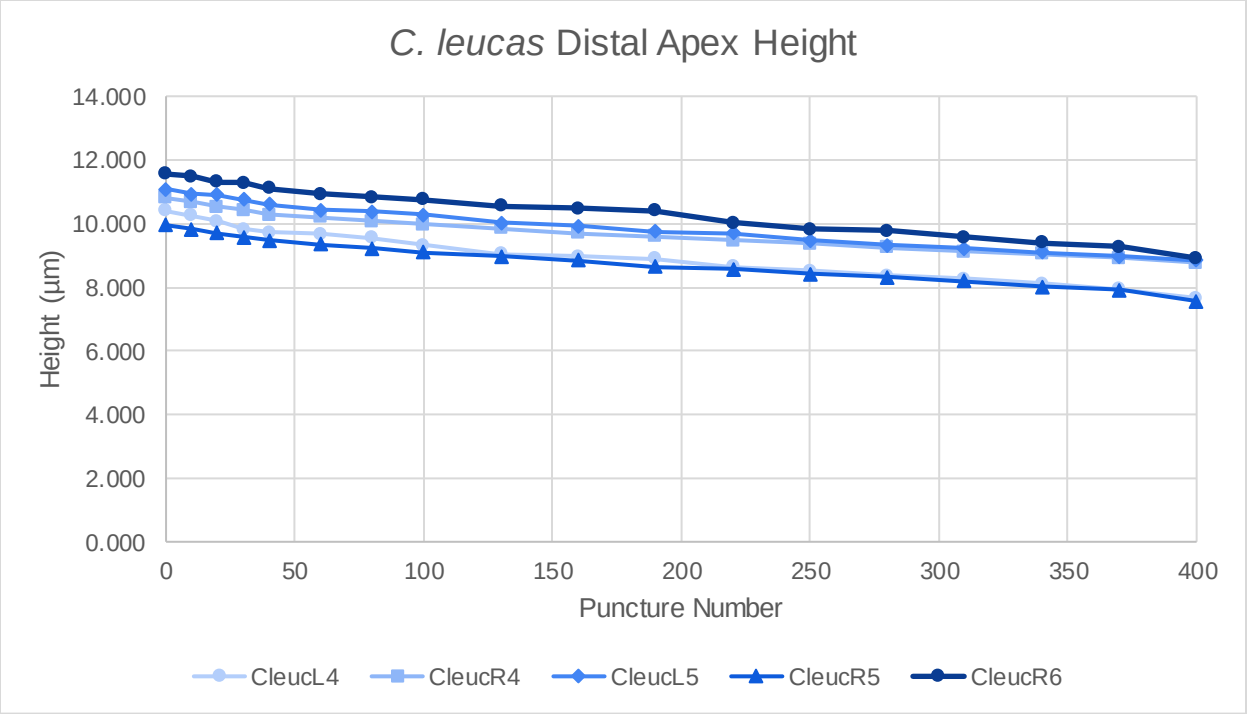
Appendix E: Distal Apex

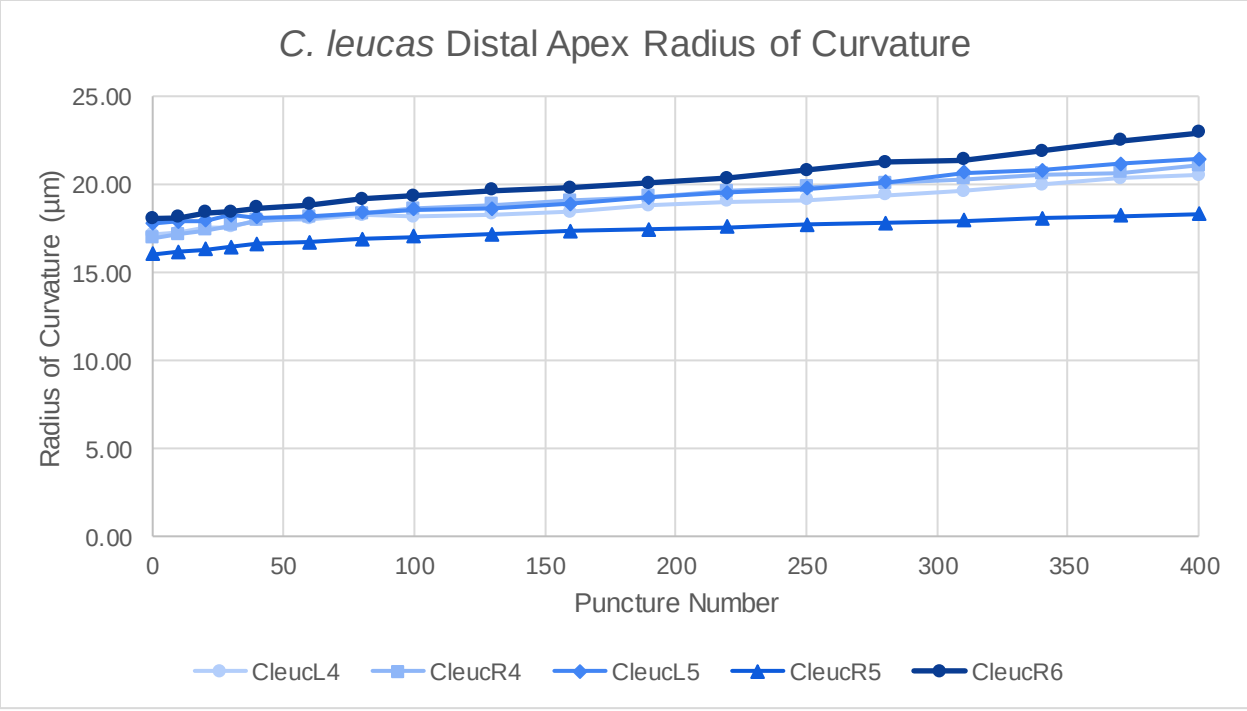


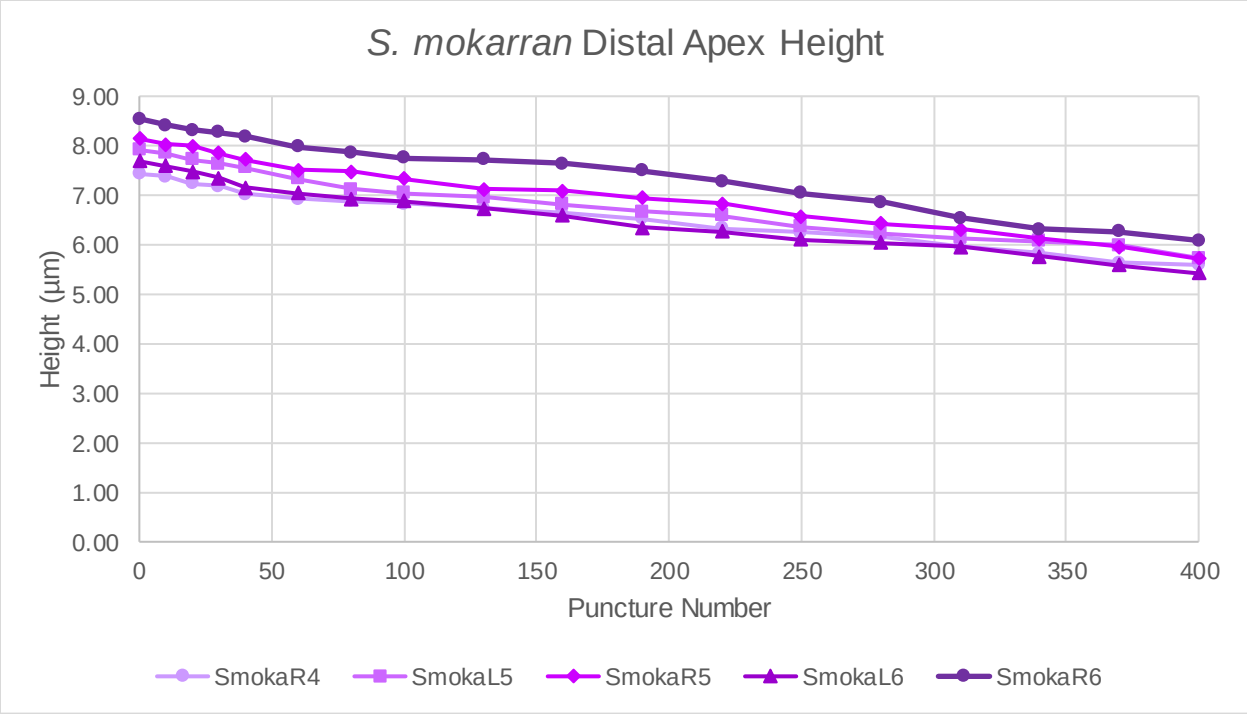


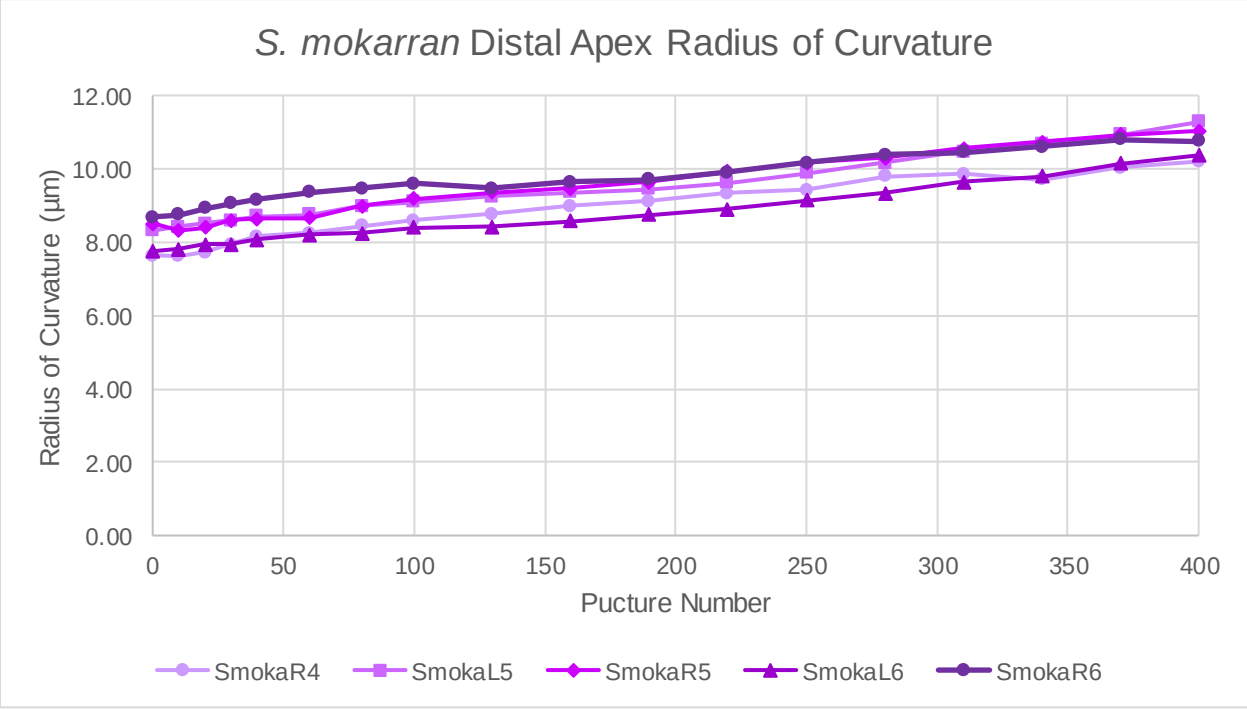

C. limbatus Distal Apex Height
Height (µm)
8.00
7.00
6.00
5.00
4.00
3.00
2.00
1.00
0.00
0
50
100
150
200
250
300
350
400
Puncture Number
ClimbL4
ClimbR4
ClimbL5
ClimbR5
ClimbL6

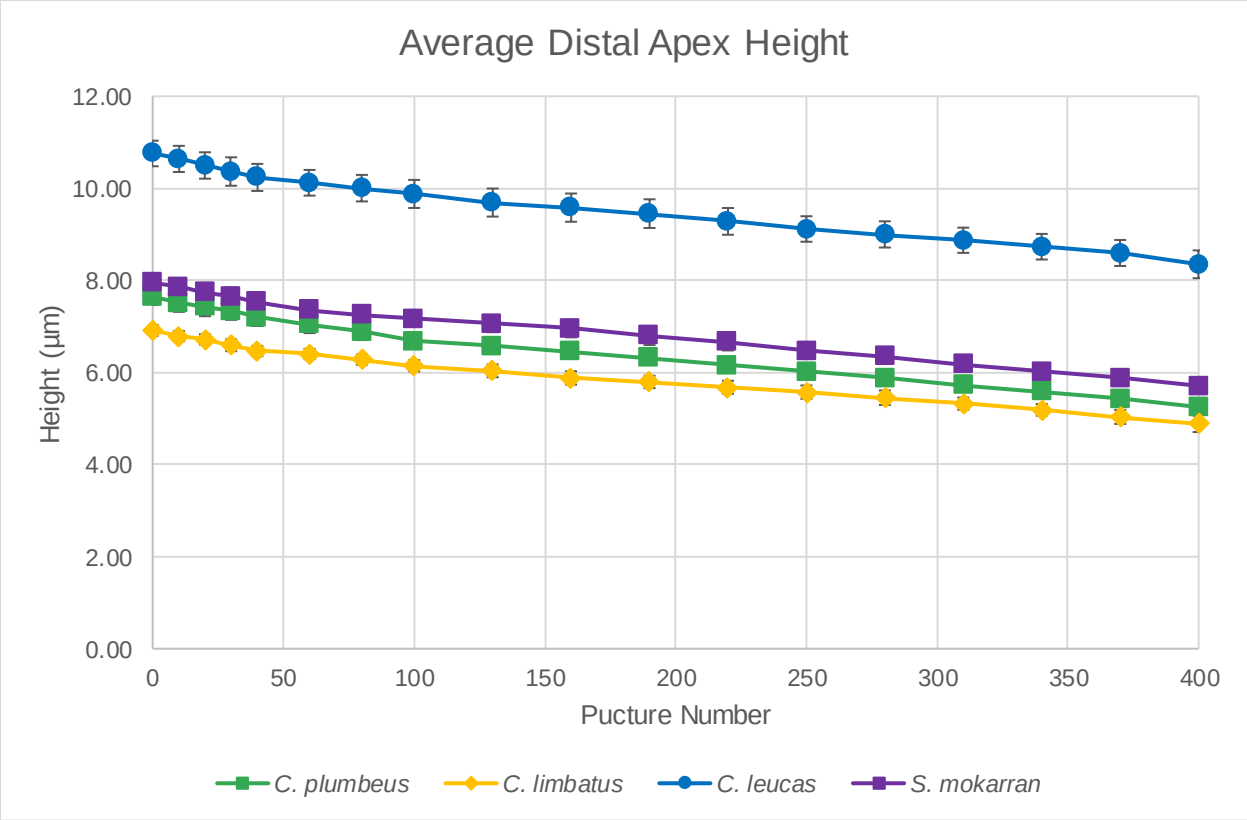

C. limbatus Distal Apex Radius of Curvature
Radius of Curvature (µm)
18.00
16.00
14.00
12.00
10.00
8.00
6.00
4.00
2.00
0.00
0
50
100
150
200
250
300
350
400
Puncture Number
ClimbL4
ClimbR4
ClimbL5
ClimbR5
ClimbL6

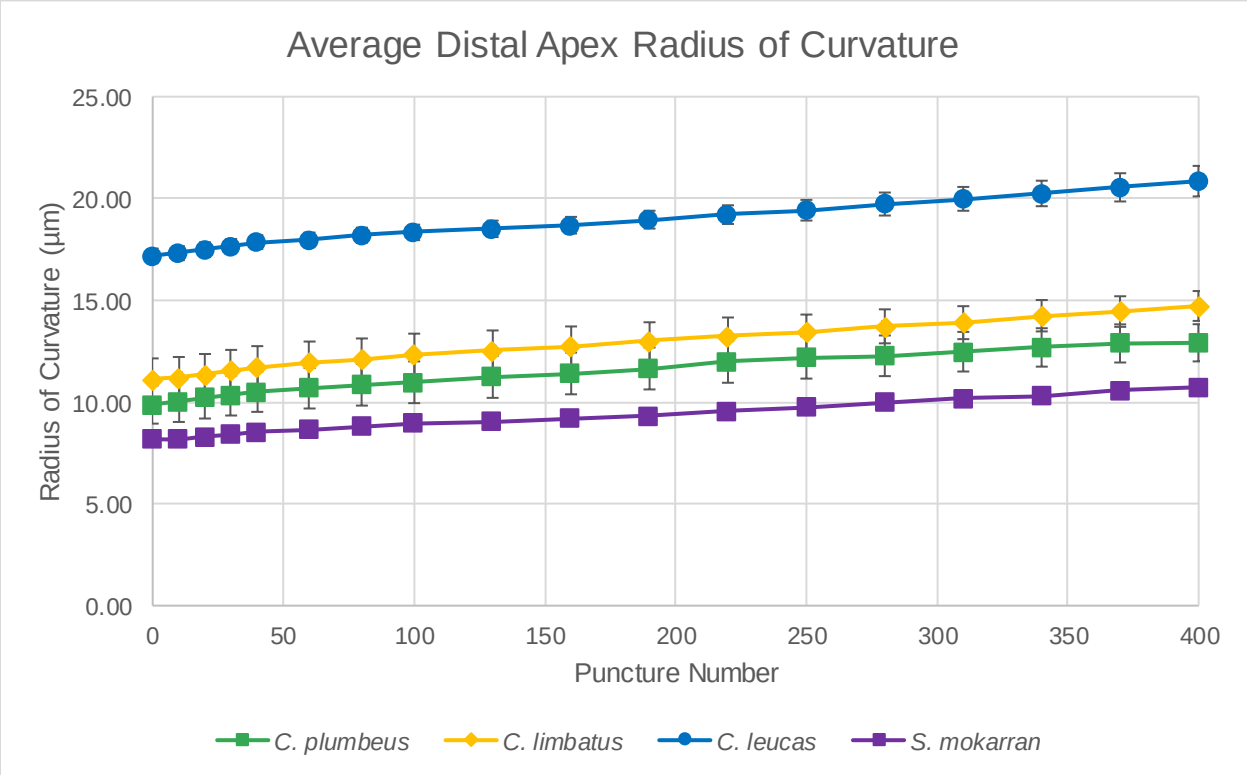

C. leucas Distal Apex Height
14.000
12.000
10.000
8.000
6.000
4.000
2.000
0.000
Height (µm)
0
50
100
150
200
250
300
350
400
Puncture Number
CleucL4
CleucR4
CleucL5
CleucR5
CleucR6


C. leucas Distal Apex Radius of Curvature
25.00
20.00
15.00
10.00
5.00
0.00
Radius of Curvature (µm)
0
50
100
150
200
250
300
350
400
Puncture Number
CleucL4
CleucR4
CleucL5
CleucR5
CleucR6

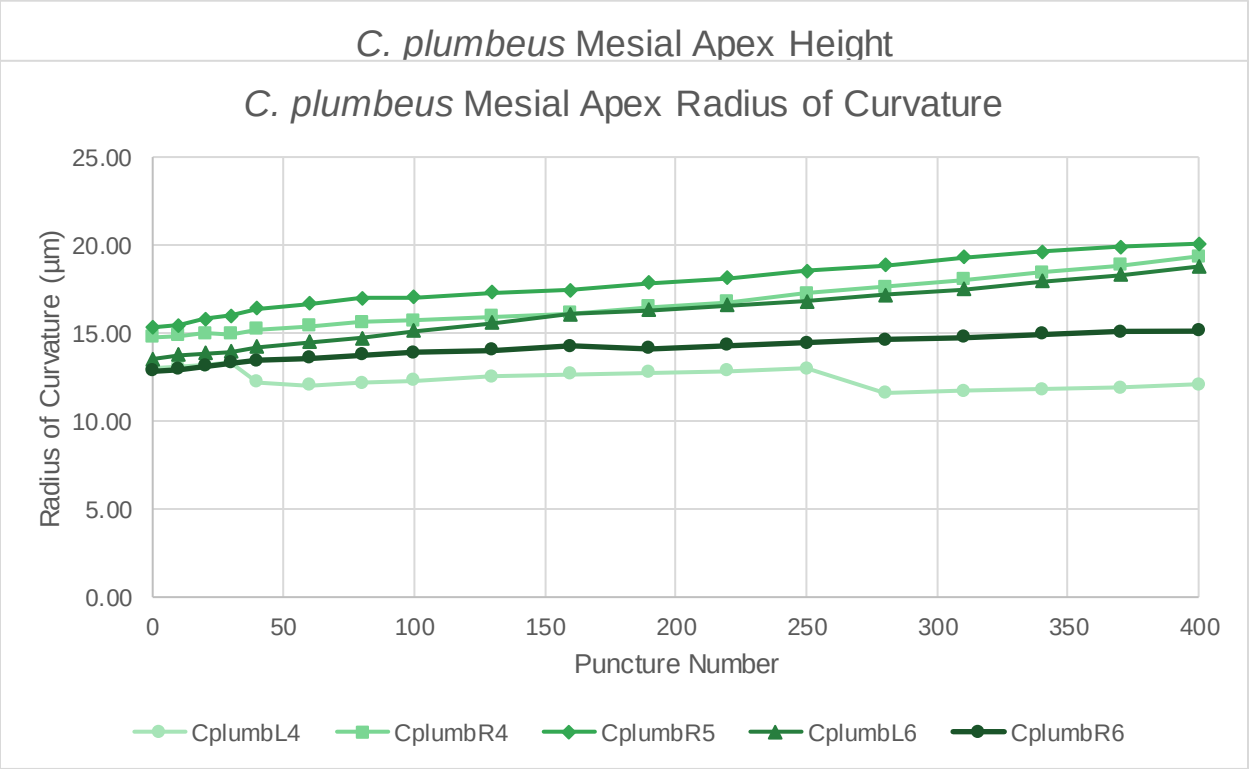

S. mokarran Distal Apex Height
9.00
8.00
7.00
6.00
5.00
4.00
3.00
2.00
1.00
0.00
Height (µm)
0
50
100
150
200
250
300
350
400
Puncture Number
SmokaR4
SmokaL5
SmokaR5
SmokaL6
SmokaR6

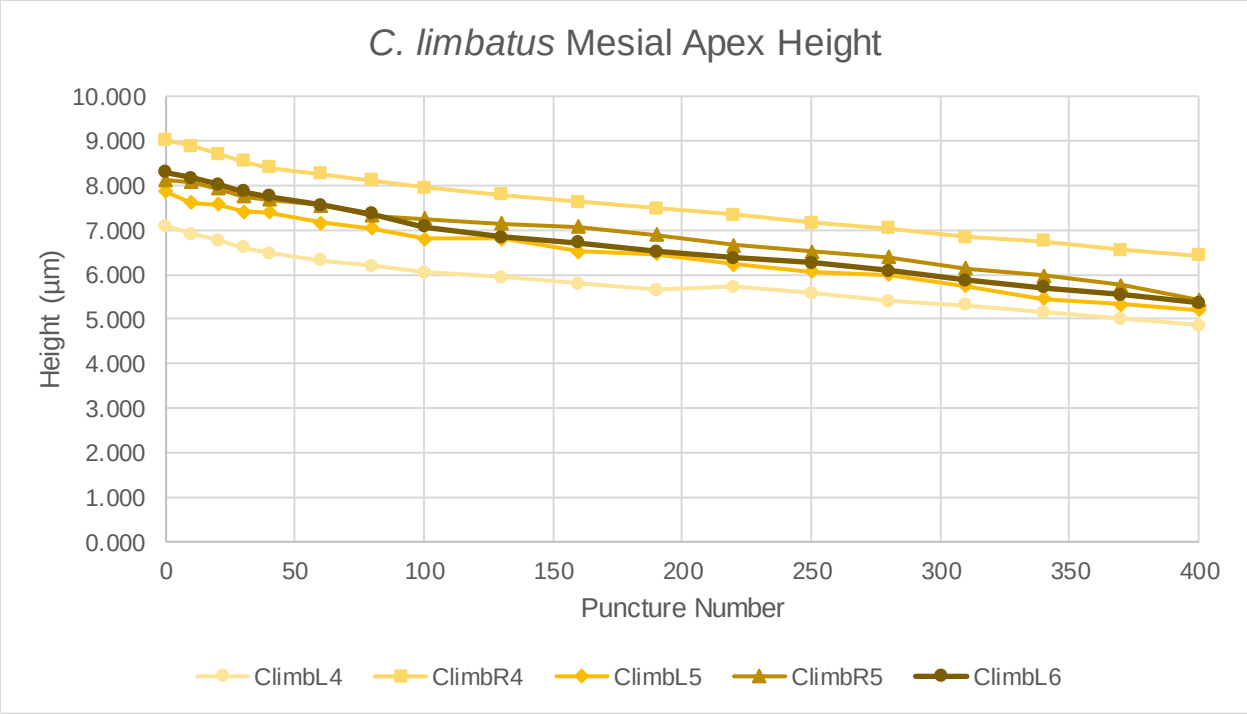

S. mokarran Distal Apex Radius of Curvature
12.00
10.00
8.00
6.00
4.00
2.00
0.00
Radius of Curvature (µm)
0
50
100
150
200
250
300
350
400
Pucture Number
SmokaR4
SmokaL5
SmokaR5
SmokaL6
SmokaR6

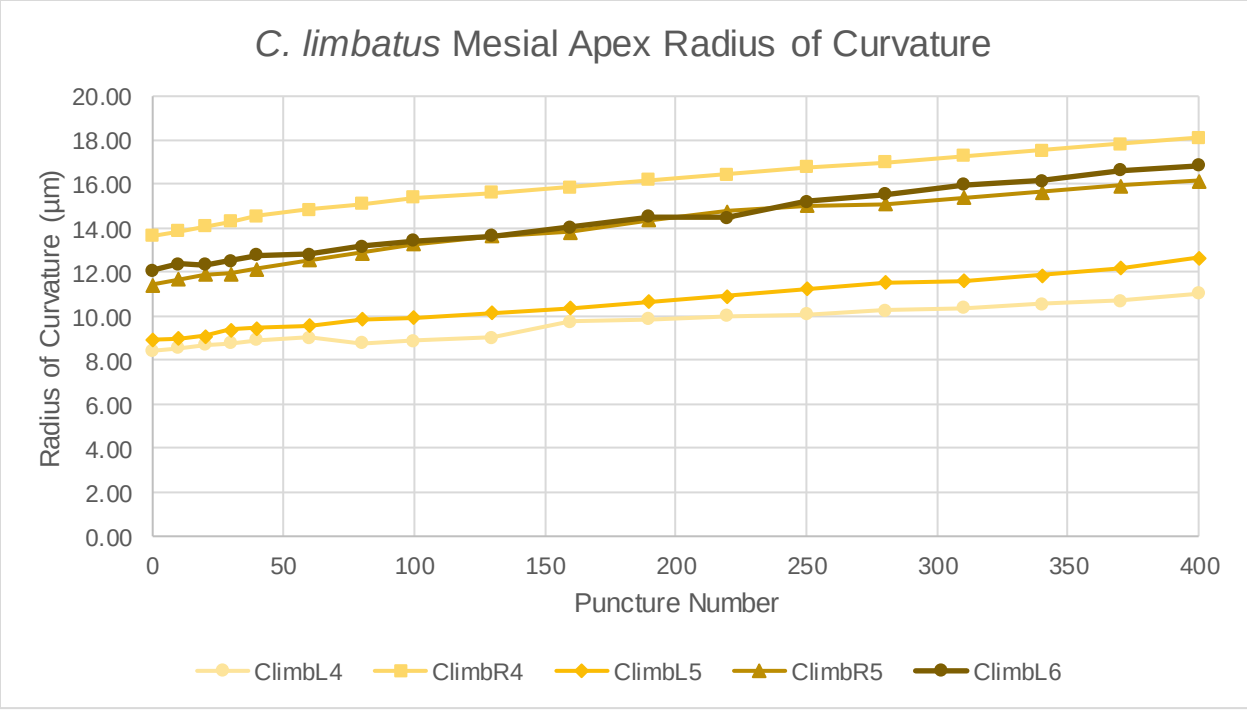

Average Distal Apex Height
12.00
10.00
8.00
6.00
4.00
2.00
0.00
Height (µm)
0
50
100
150
200
250
300
350
400
Pucture Number
C. plumbeus
C. limbatus
C. leucas
S. mokarran

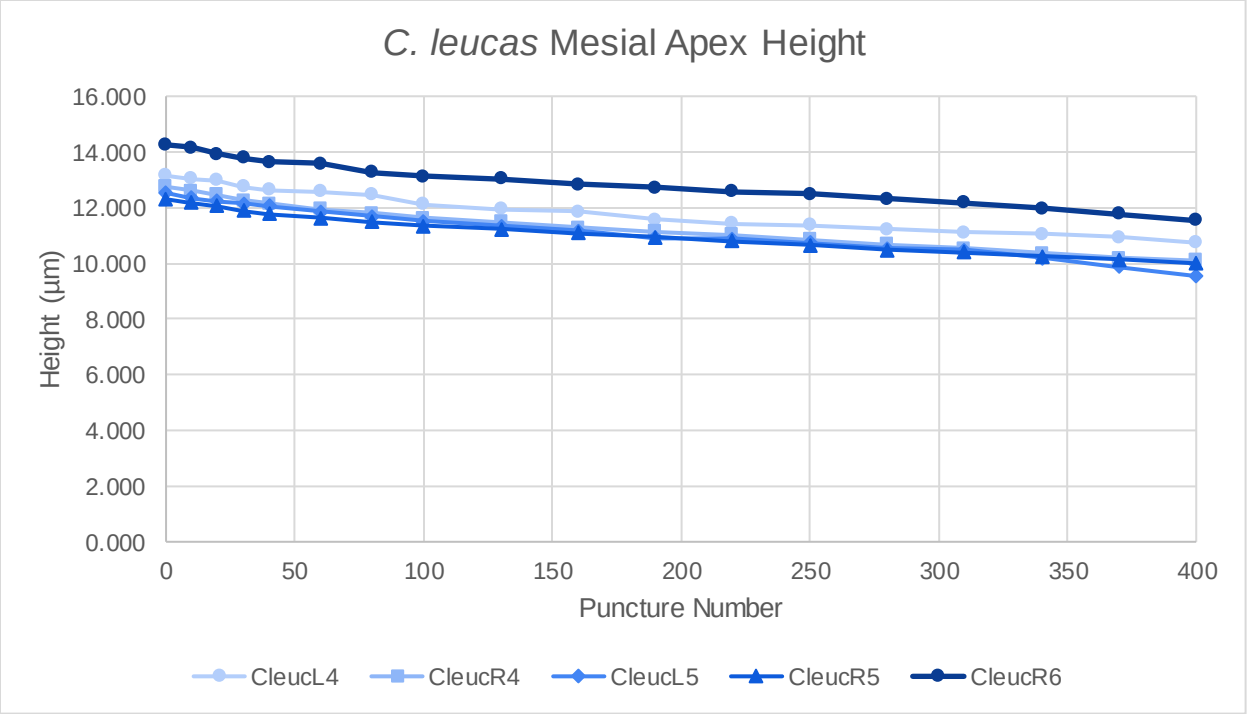

Average Distal Apex Radius of Curvature
25.00
20.00
15.00
10.00
5.00
0.00
Radius of Curvature (µm)
0
50
100
150
200
250
300
350
400
Puncture Number
C. plumbeus
C. limbatus
C. leucas
S. mokarran

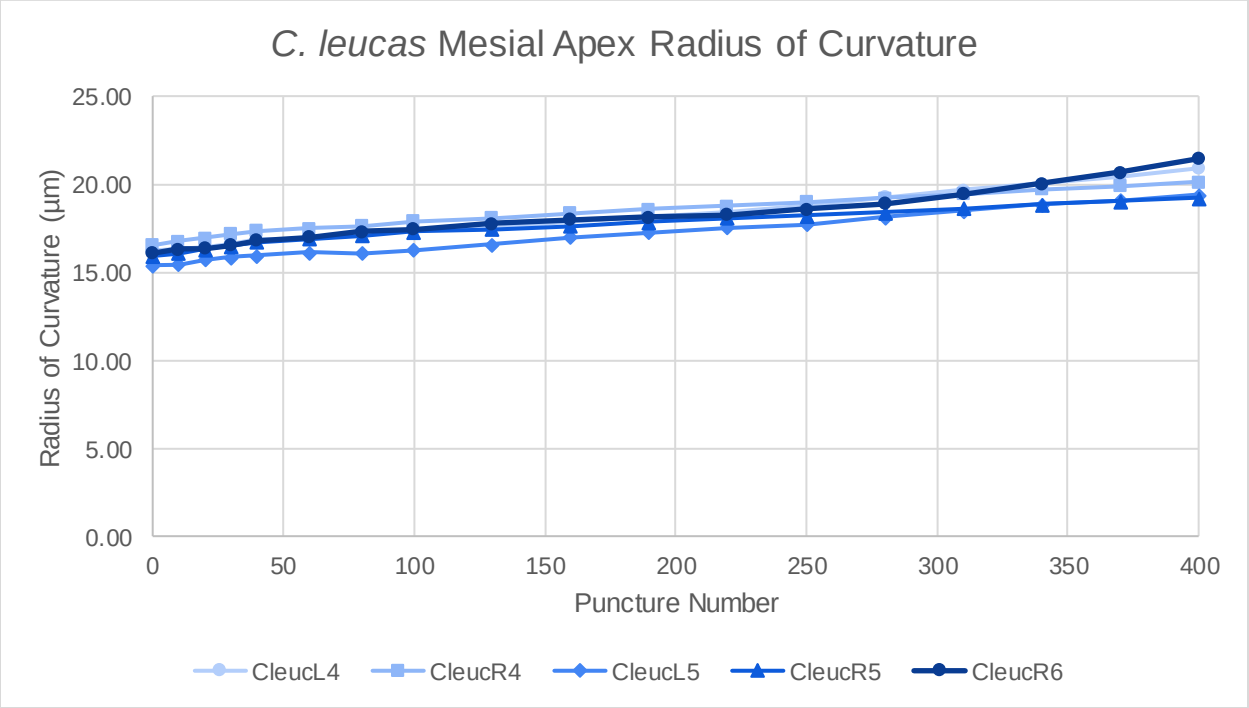
Appendix F: Mesial Apex

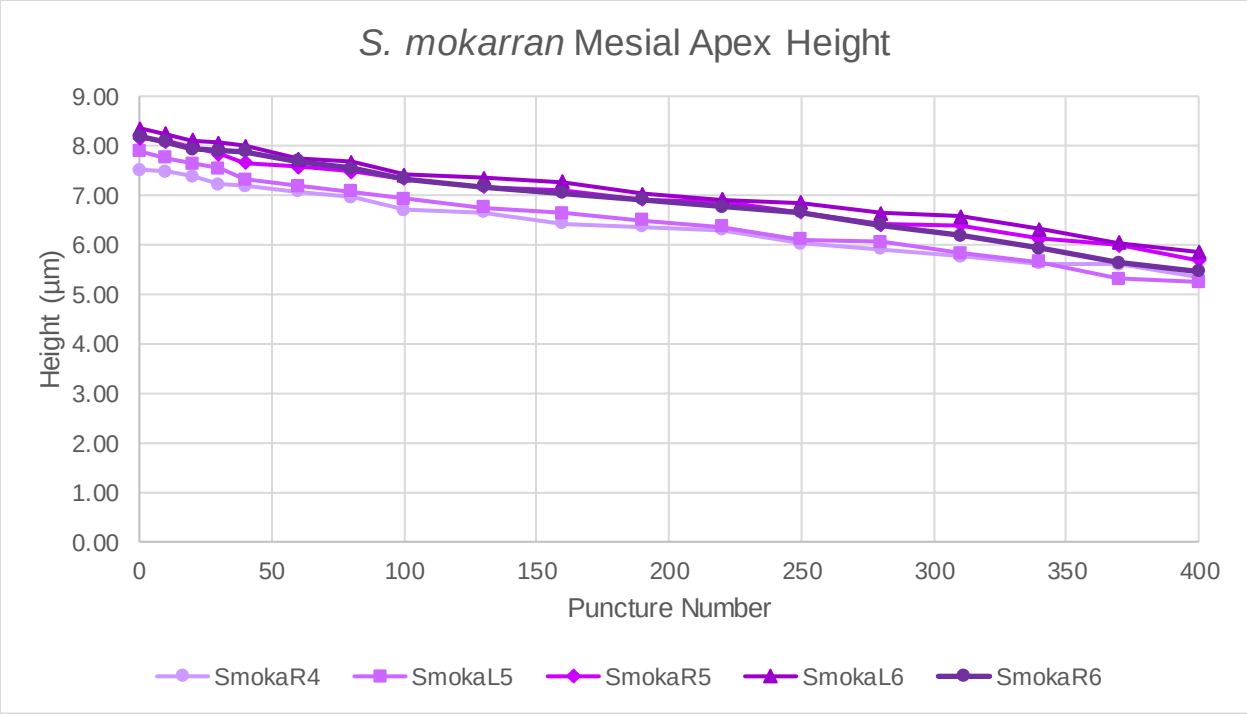


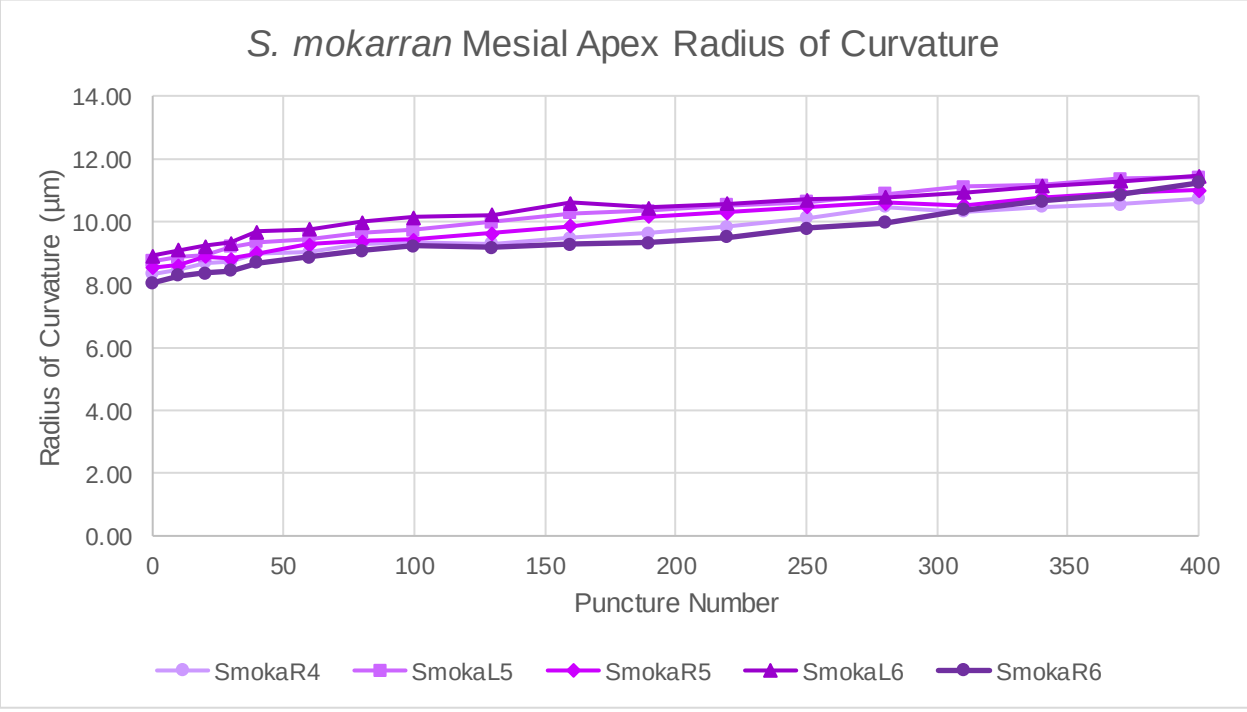

C. limbatus Mesial Apex Height
Height (µm)
10.000
9.000
8.000
7.000
6.000
5.000
4.000
3.000
2.000
1.000
0.000
0
50
100
150
200
250
300
350
400
Puncture Number
ClimbL4
ClimbR4
ClimbL5
ClimbR5
ClimbL6

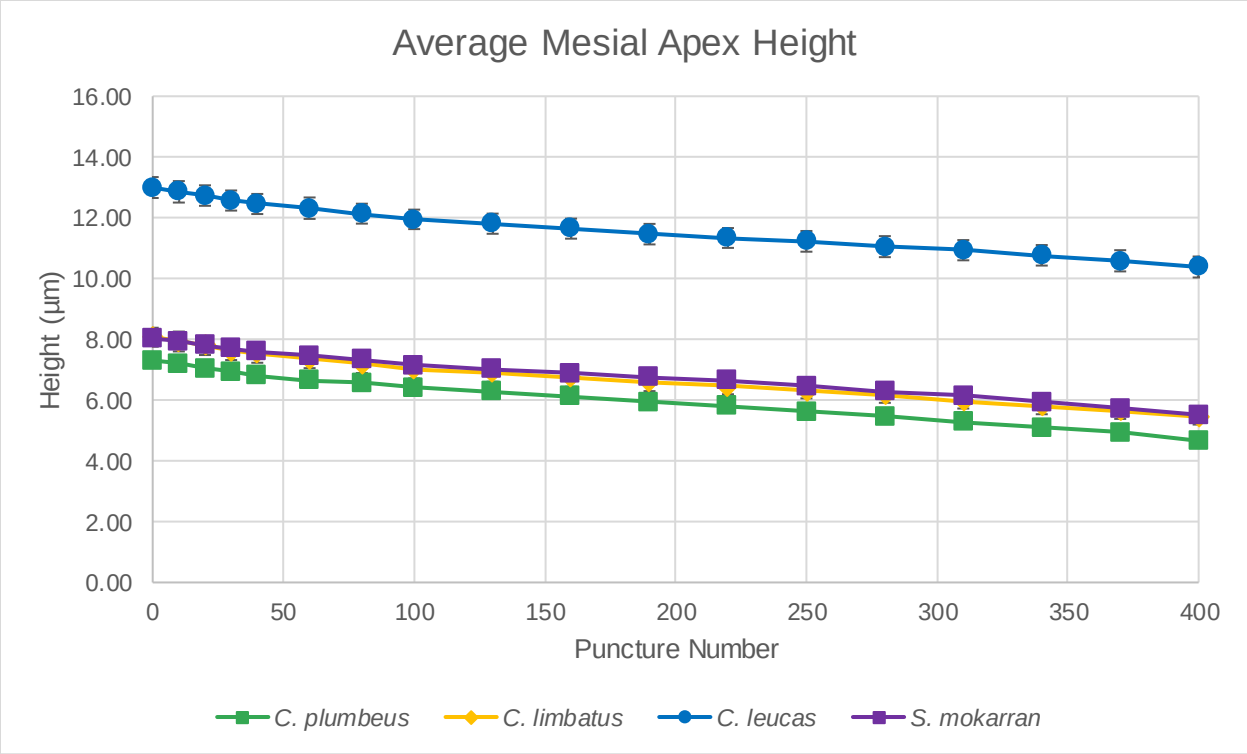

C. limbatus Mesial Apex Radius of Curvature
Radius of Curvature (µm)
20.00
18.00
16.00
14.00
12.00
10.00
8.00
6.00
4.00
2.00
0.00
0
50
100
150
200
250
300
350
400
Puncture Number
ClimbL4
ClimbR4
ClimbL5
ClimbR5
ClimbL6

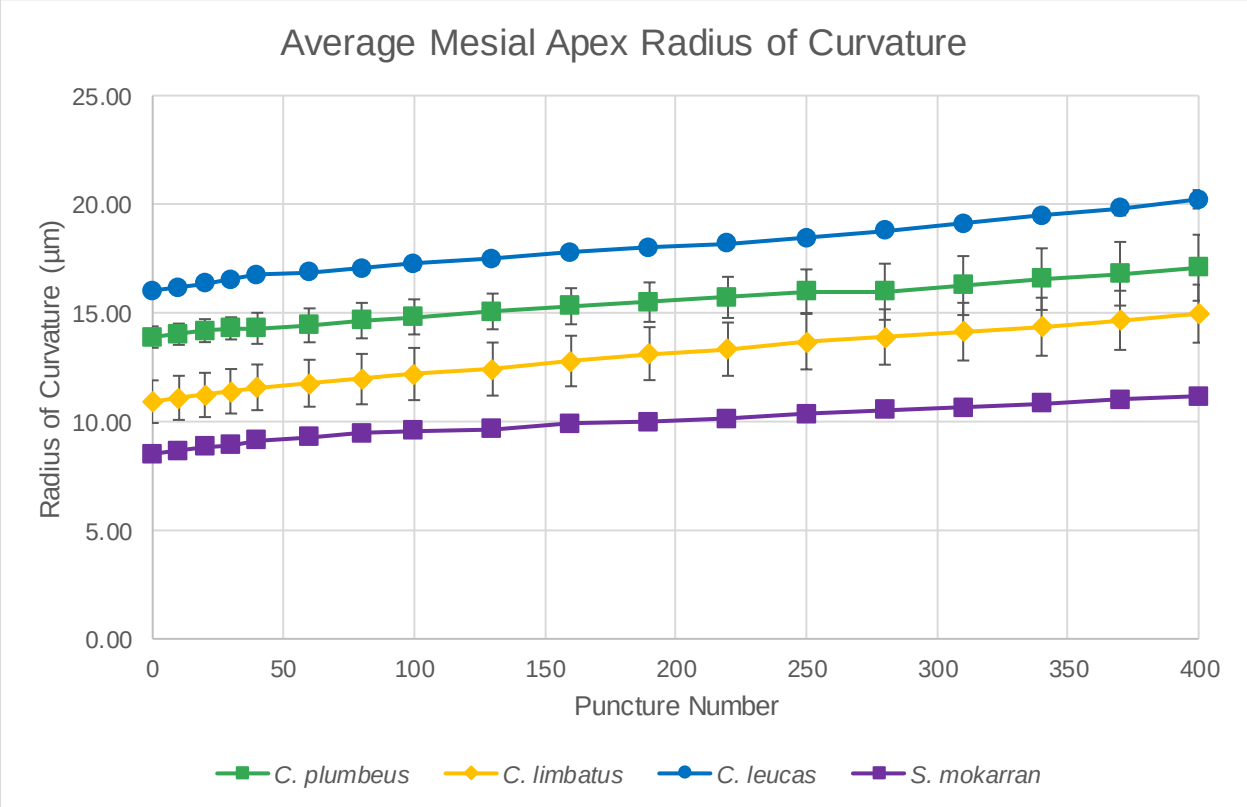

C. leucas Mesial Apex Height
16.000
14.000
12.000
10.000
8.000
6.000
4.000
2.000
0.000
Height (µm)
0
50
100
150
200
250
300
350
400
Puncture Number
CleucL4
CleucR4
CleucL5
CleucR5
CleucR6


C. leucas Mesial Apex Radius of Curvature
25.00
20.00
15.00
10.00
5.00
0.00
Radius of Curvature (µm)
0
50
100
150
200
250
300
350
400
Puncture Number
CleucL4
CleucR4
CleucL5
CleucR5
CleucR6

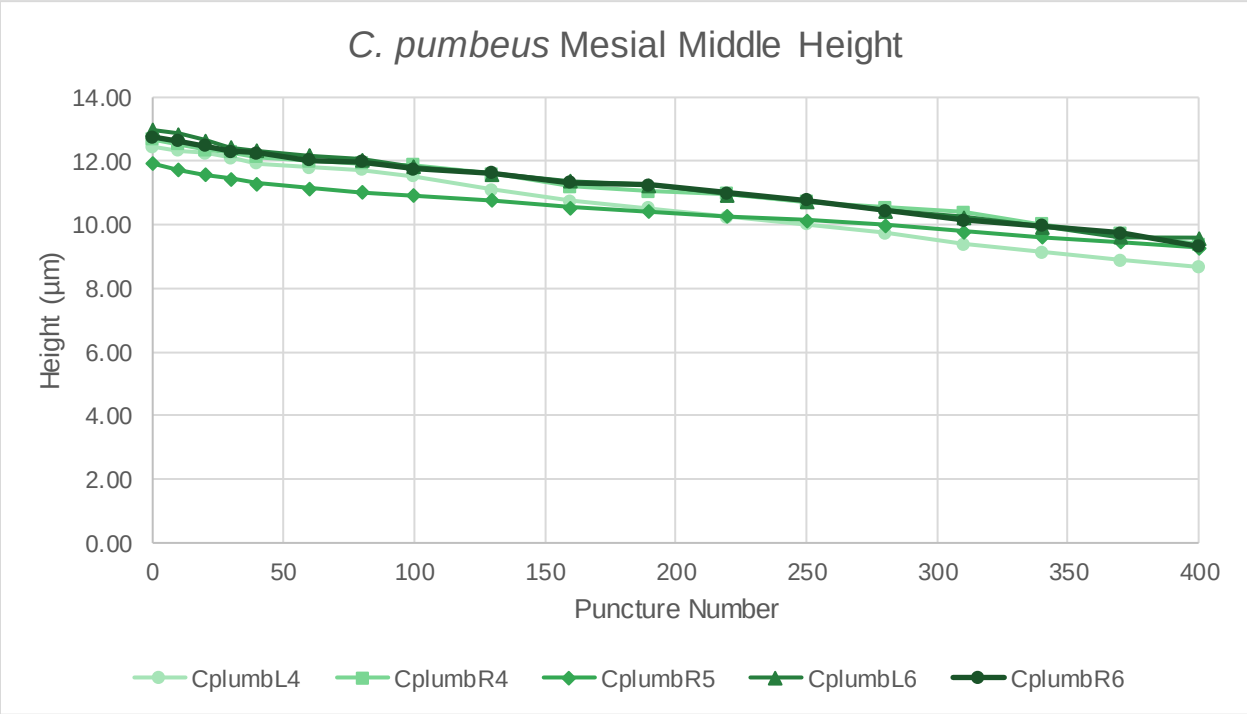

S. mokarran Mesial Apex Height
9.00
8.00
7.00
6.00
5.00
4.00
3.00
2.00
1.00
0.00
Height (µm)
0
50
100
150
200
250
300
350
400
Puncture Number
SmokaR4
SmokaL5
SmokaR5
SmokaL6
SmokaR6

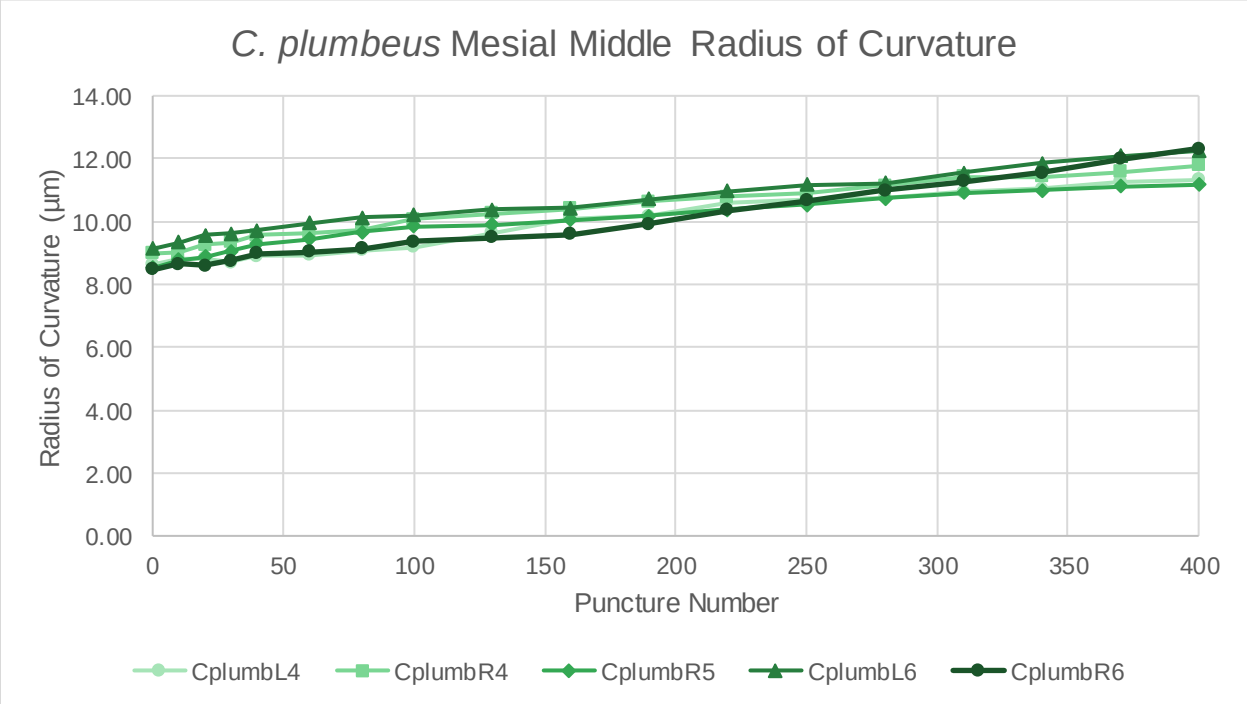

S. mokarran Mesial Apex Radius of Curvature
14.00
12.00
10.00
8.00
6.00
4.00
2.00
0.00
Radius of Curvature (µm)
0
50
100
150
200
250
300
350
400
Puncture Number
SmokaR4
SmokaL5
SmokaR5
SmokaL6
SmokaR6

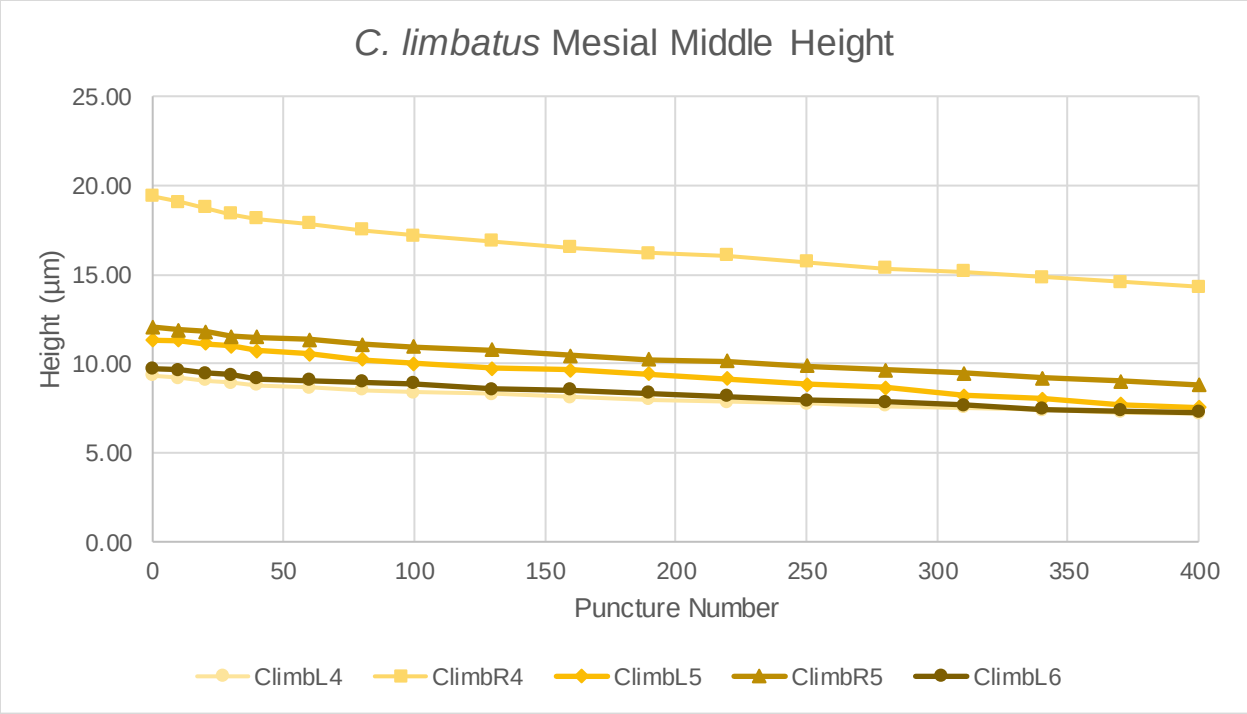

Average Mesial Apex Height
16.00
14.00
12.00
10.00
8.00
6.00
4.00
2.00
0.00
Height (µm)
0
50
100
150
200
250
300
350
400
Puncture Number
C. plumbeus
C. limbatus
C. leucas
S. mokarran

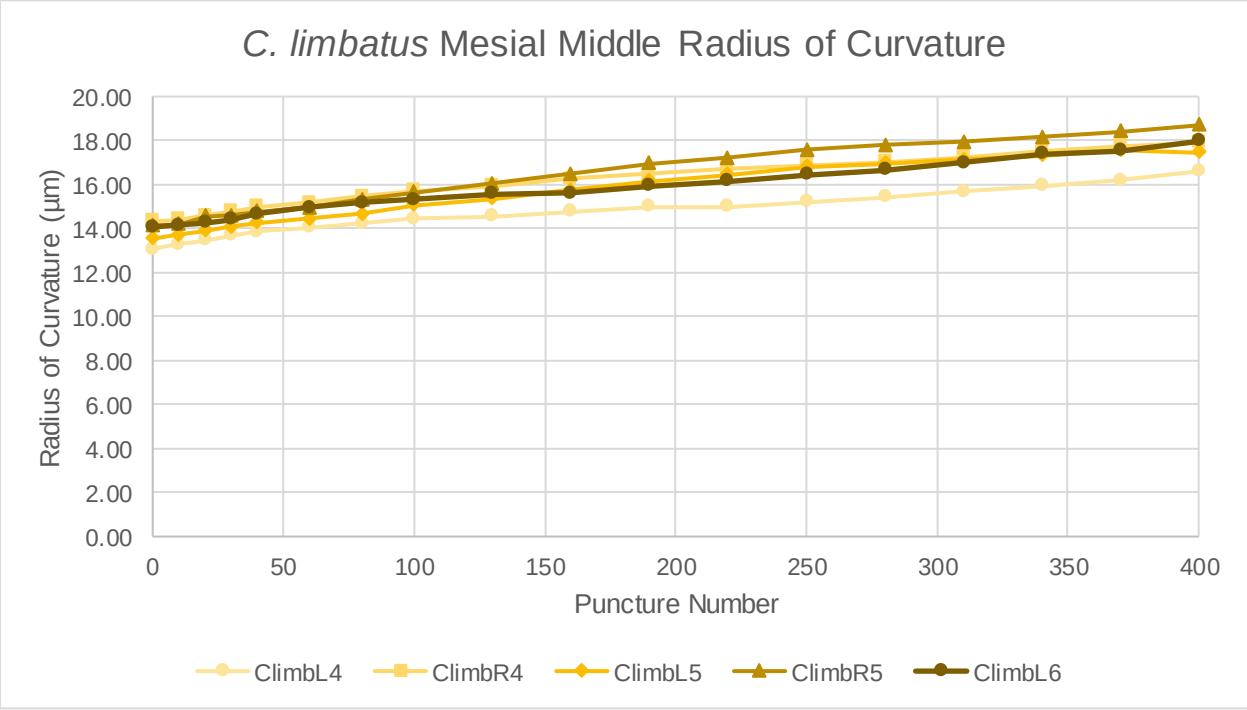

Average Mesial Apex Radius of Curvature
25.00
20.00
15.00
10.00
5.00
0.00
Radius of Curvature (µm)
0
50
100
150
200
250
300
350
400
Puncture Number
C. plumbeus
C. limbatus
C. leucas
S. mokarran

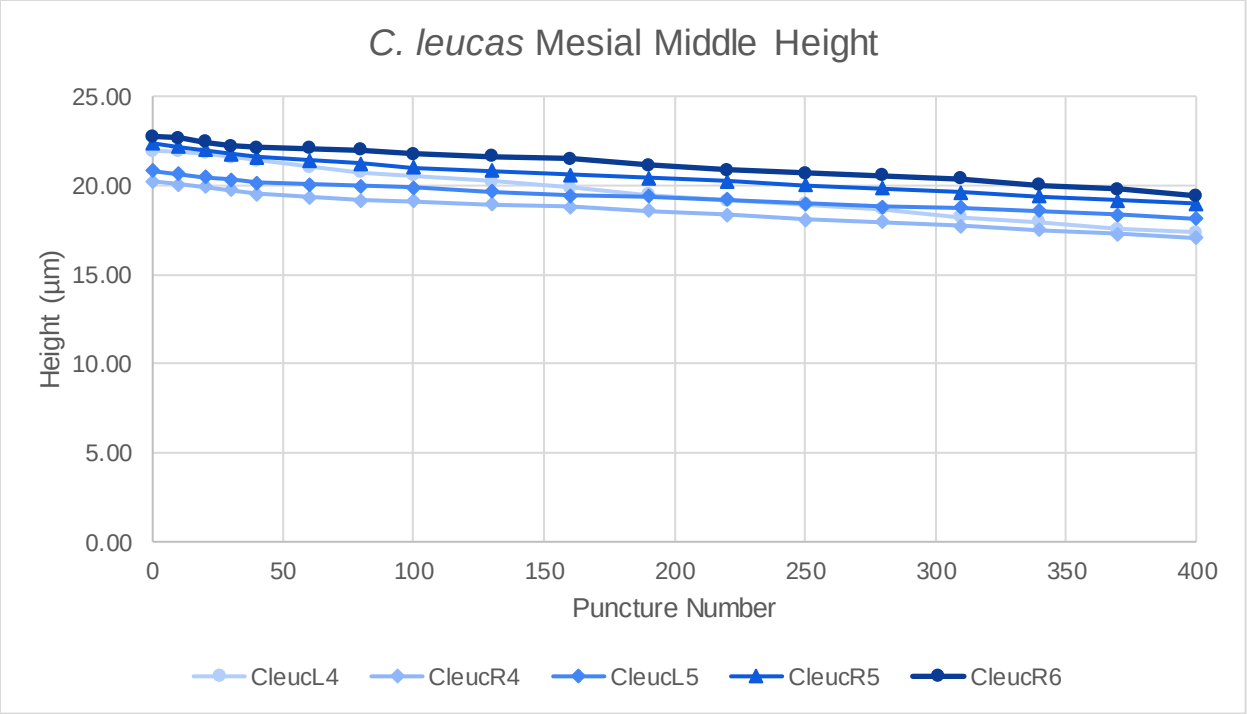
Appendix G: Mesial Middle

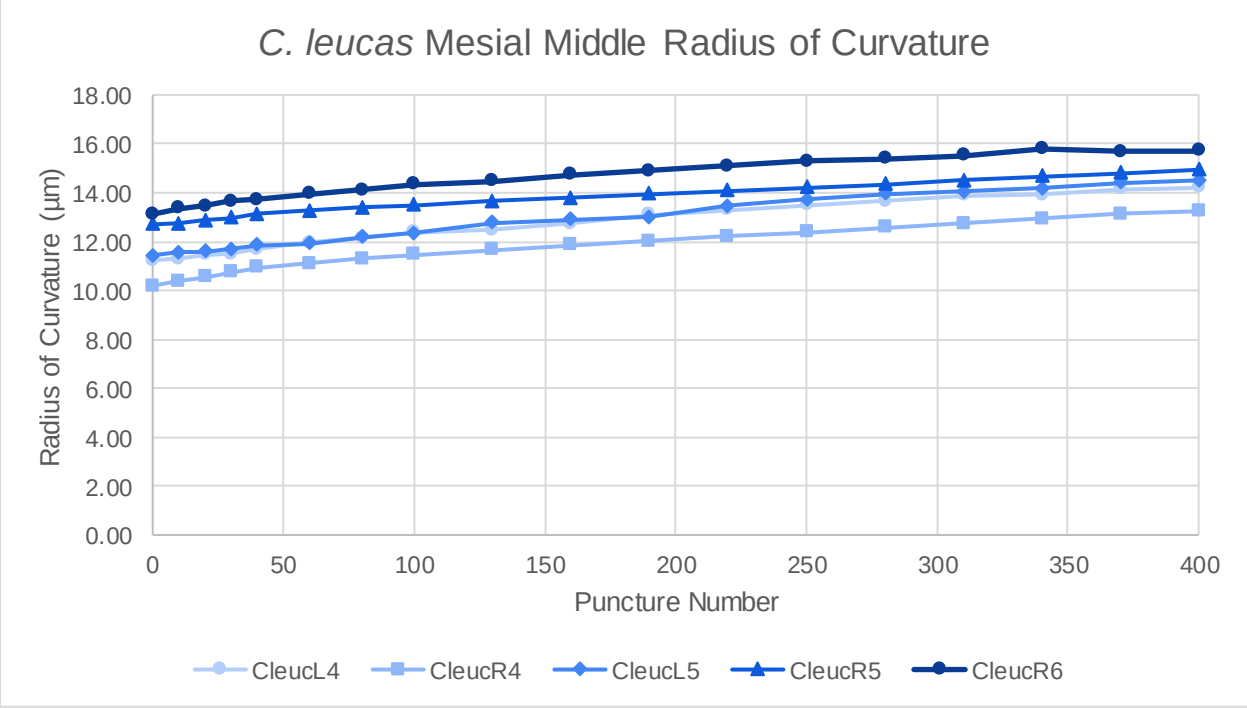


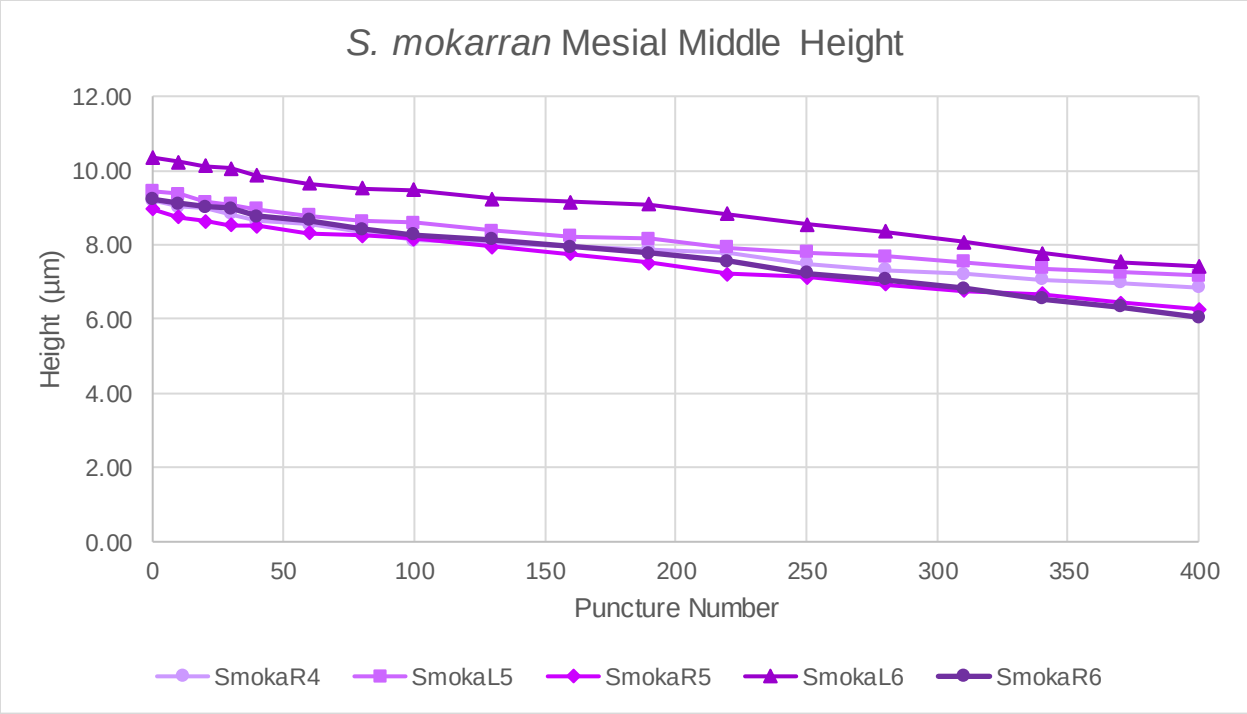


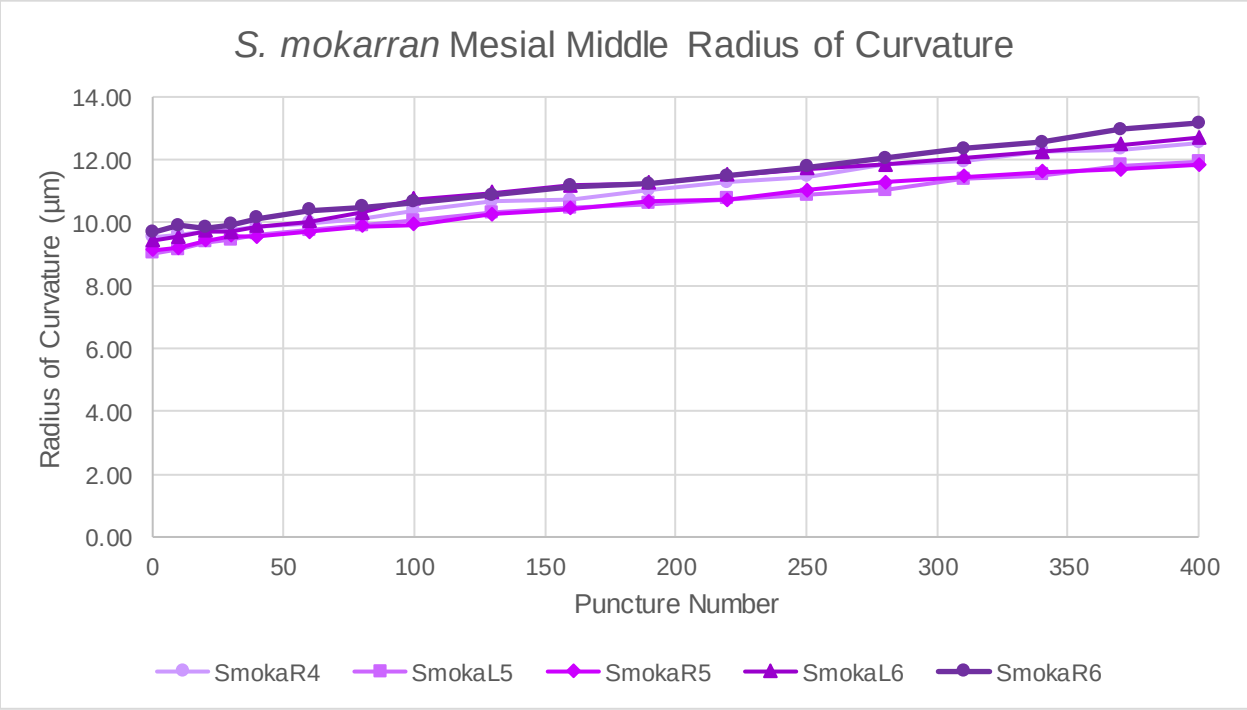

C. limbatus Mesial Middle Height
25.00
20.00
15.00
10.00
5.00
0.00
Height (µm)
0
50
100
150
200
250
300
350
400
Puncture Number
ClimbL4
ClimbR4
ClimbL5
ClimbR5
ClimbL6

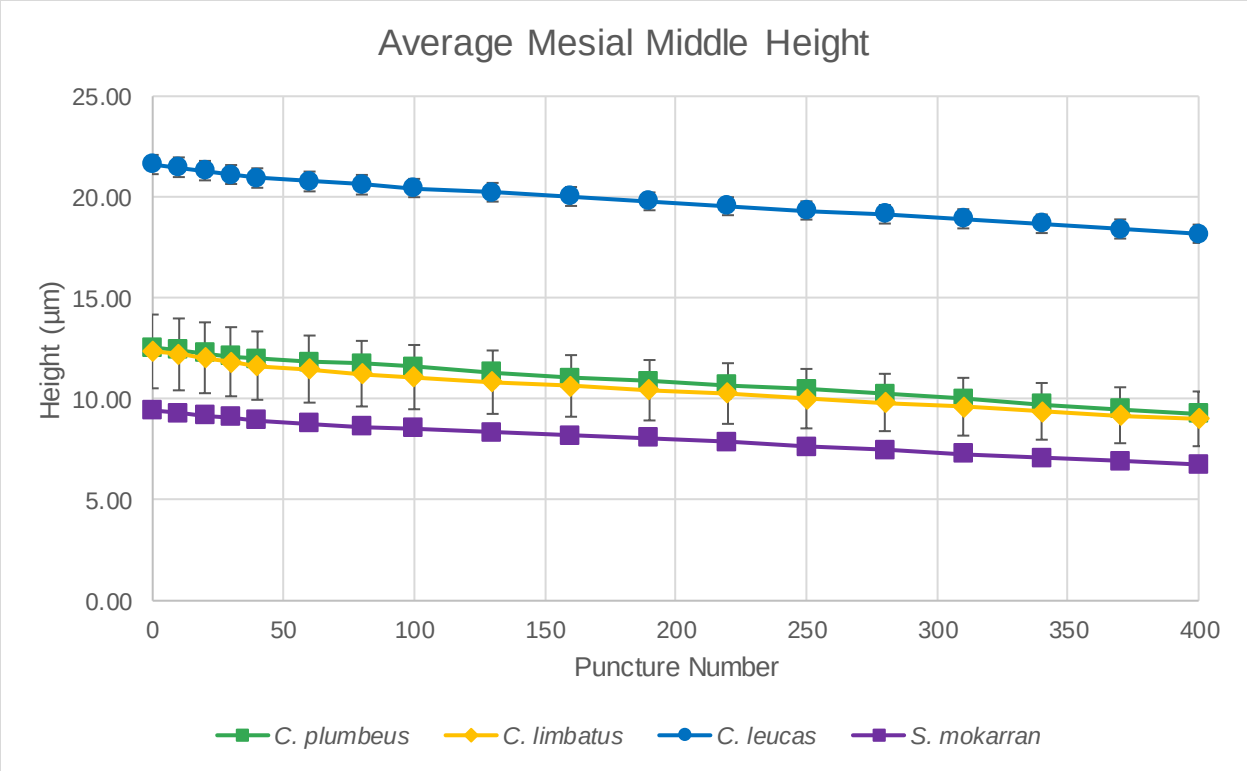

C. limbatus Mesial Middle Radius of Curvature
20.00
18.00
16.00
14.00
12.00
10.00
8.00
6.00
4.00
2.00
0.00
Radius of Curvature (µm)
0
50
100
150
200
250
300
350
400
Puncture Number
ClimbL4
ClimbR4
ClimbL5
ClimbR5
ClimbL6

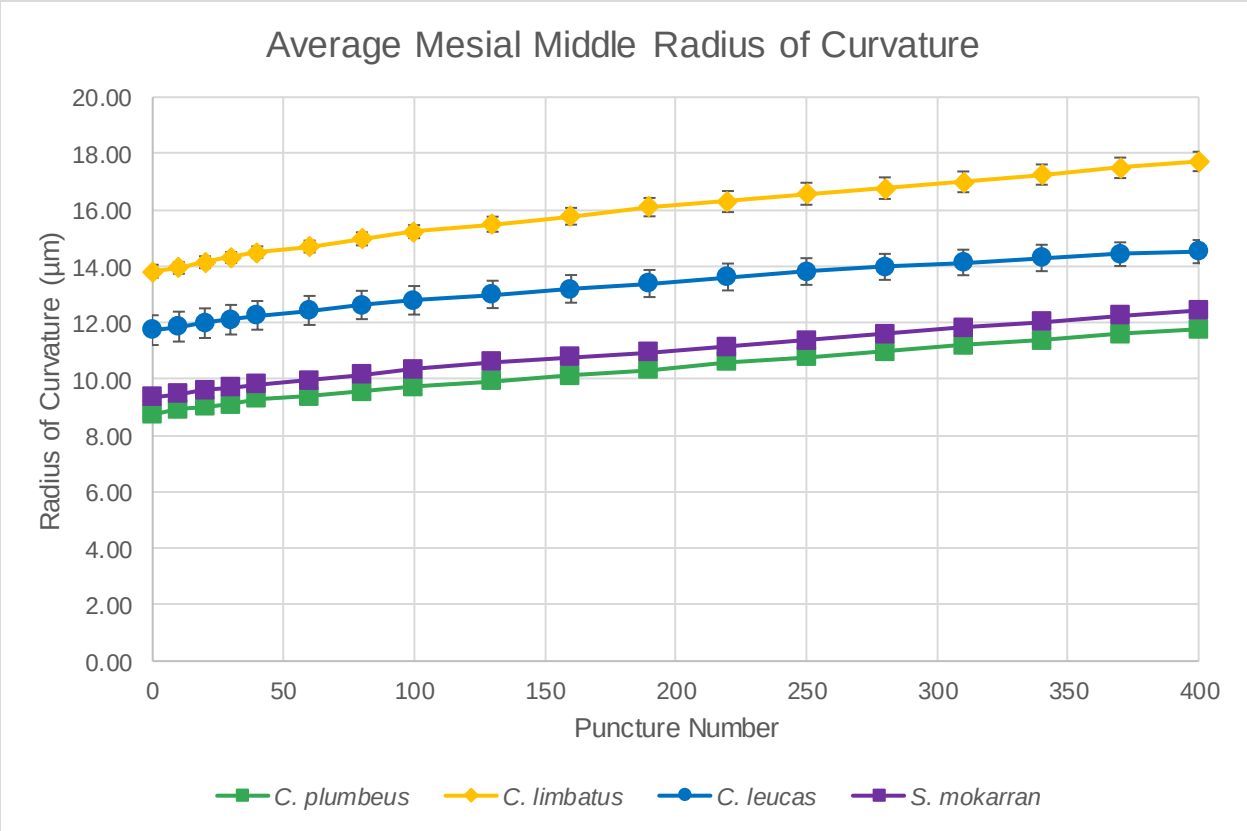

C. leucas Mesial Middle Height
25.00
20.00
15.00
10.00
5.00
0.00
Height (µm)
0
50
100
150
200
250
300
350
400
Puncture Number
CleucL4
CleucR4
CleucL5
CleucR5
CleucR6


C. leucas Mesial Middle Radius of Curvature
18.00
16.00
14.00
12.00
10.00
8.00
6.00
4.00
2.00
0.00
Radius of Curvature (µm)
0
50
100
150
200
250
300
350
400
Puncture Number
CleucL4
CleucR4
CleucL5
CleucR5
CleucR6

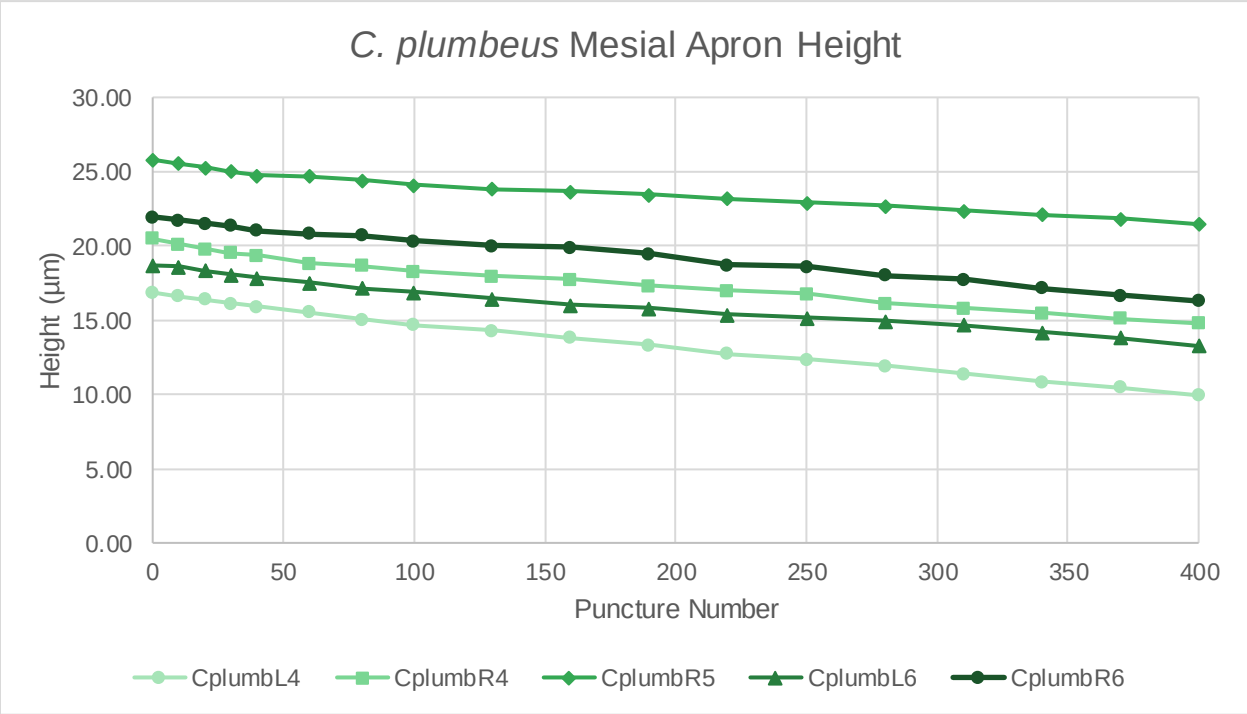

S. mokarran Mesial Middle Height
12.00
10.00
8.00
6.00
4.00
2.00
0.00
Height (µm)
0
50
100
150
200
250
300
350
400
Puncture Number
SmokaR4
SmokaL5
SmokaR5
SmokaL6
SmokaR6

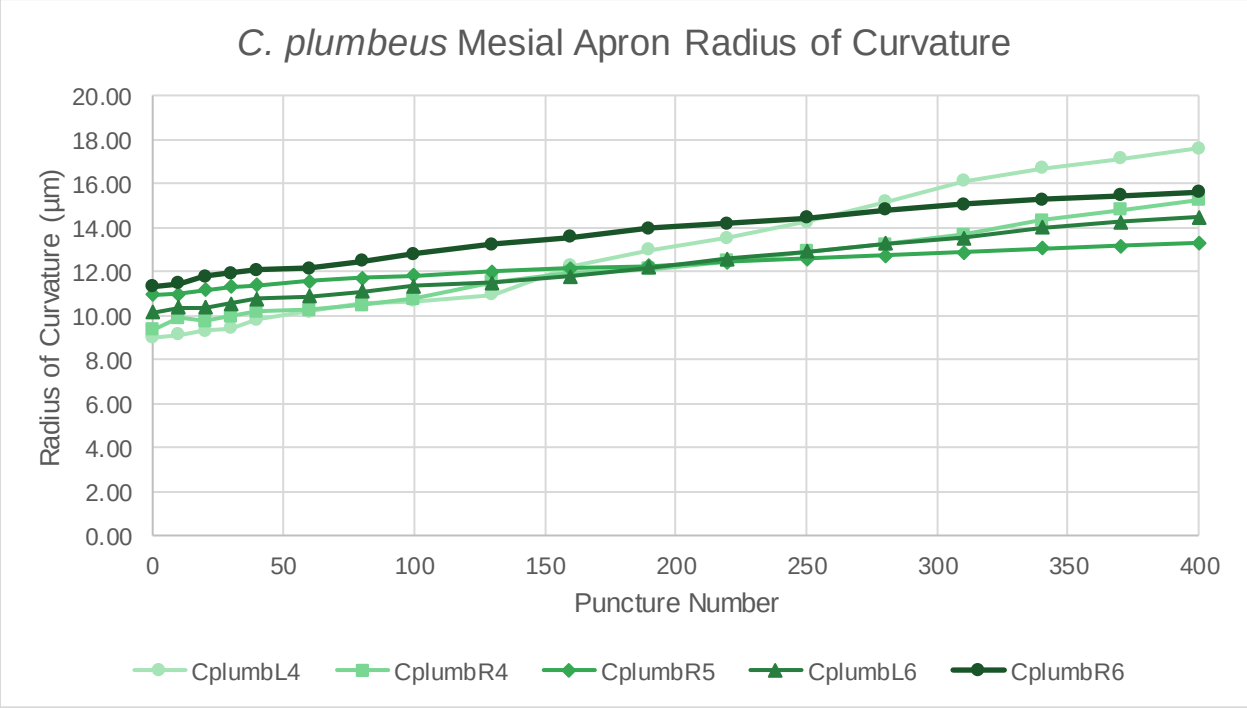

S. mokarran Mesial Middle Radius of Curvature
14.00
12.00
10.00
8.00
6.00
4.00
2.00
0.00
Radius of Curvature (µm)
0
50
100
150
200
250
300
350
400
Puncture Number
SmokaR4
SmokaL5
SmokaR5
SmokaL6
SmokaR6

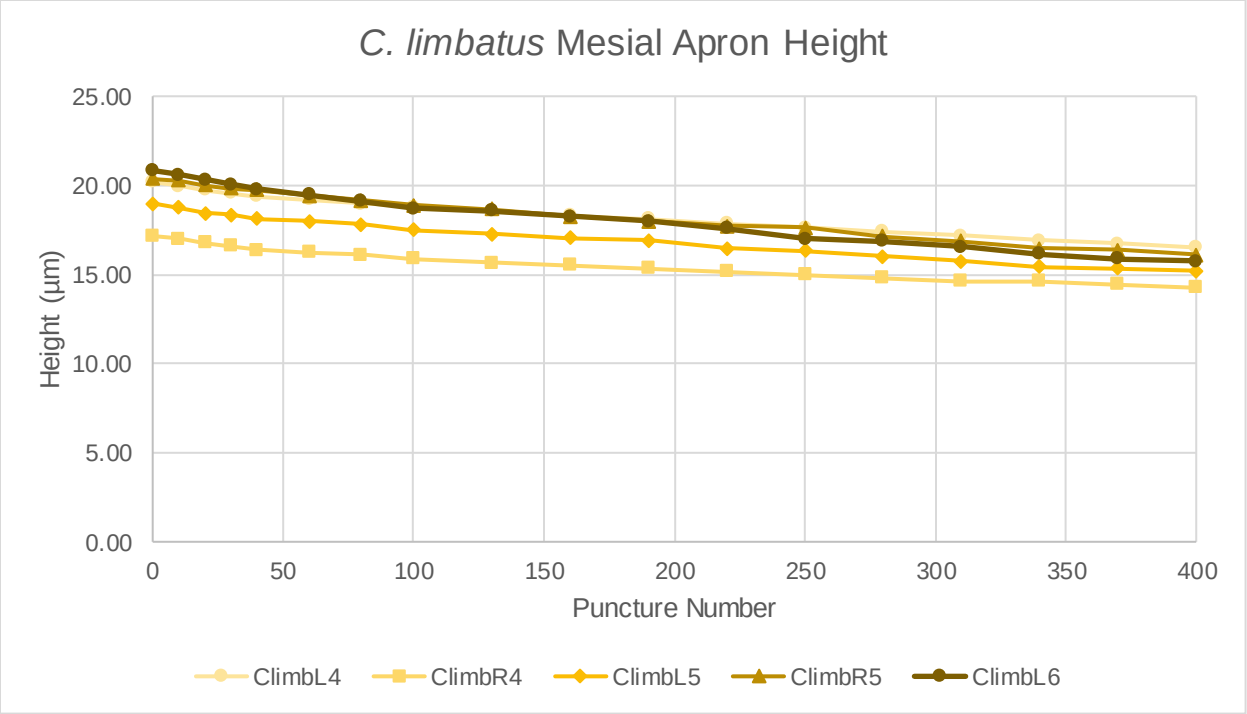

Average Mesial Middle Height
Height (µm)
25.00
20.00
15.00
10.00
5.00
0.00
0
50
100
150
200
250
300
350
400
Puncture Number
C. plumbeus
C. limbatus
C. leucas
S. mokarran

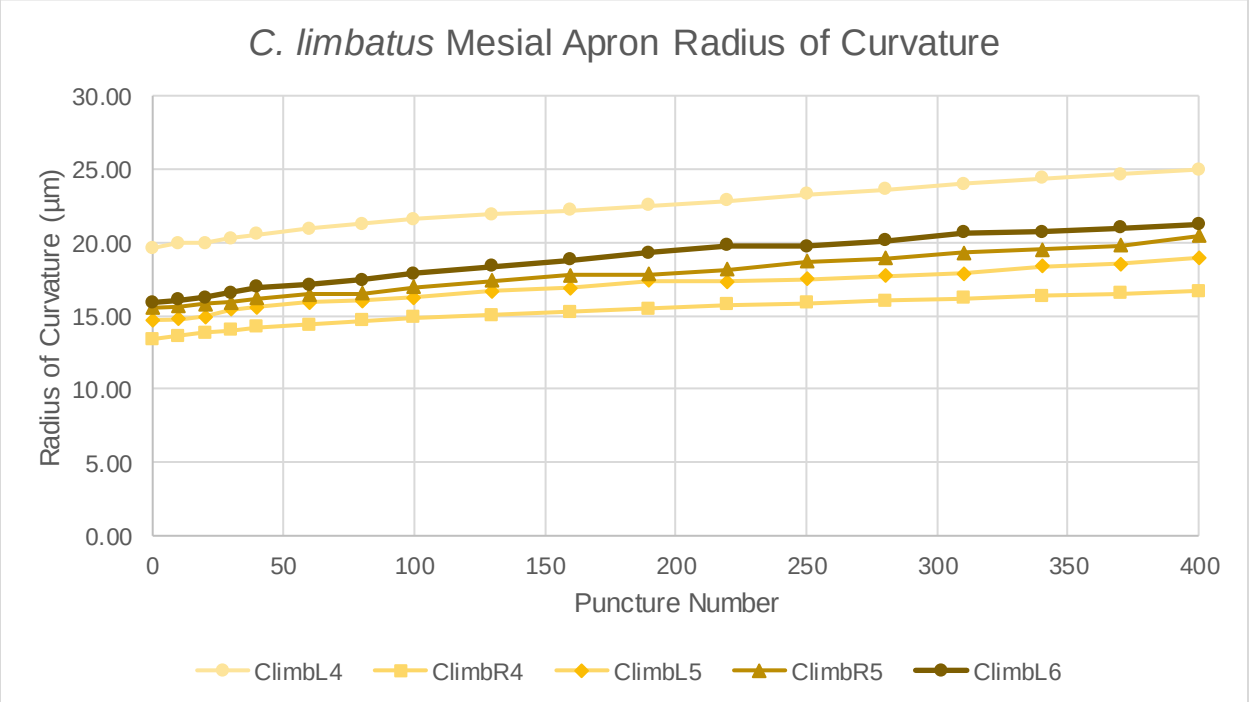

Average Mesial Middle Radius of Curvature
Radius of Curvature (µm)
20.00
18.00
16.00
14.00
12.00
10.00
8.00
6.00
4.00
2.00
0.00
0
50
100
150
200
250
300
350
400
Puncture Number
C. plumbeus
C. limbatus
C. leucas
S. mokarran

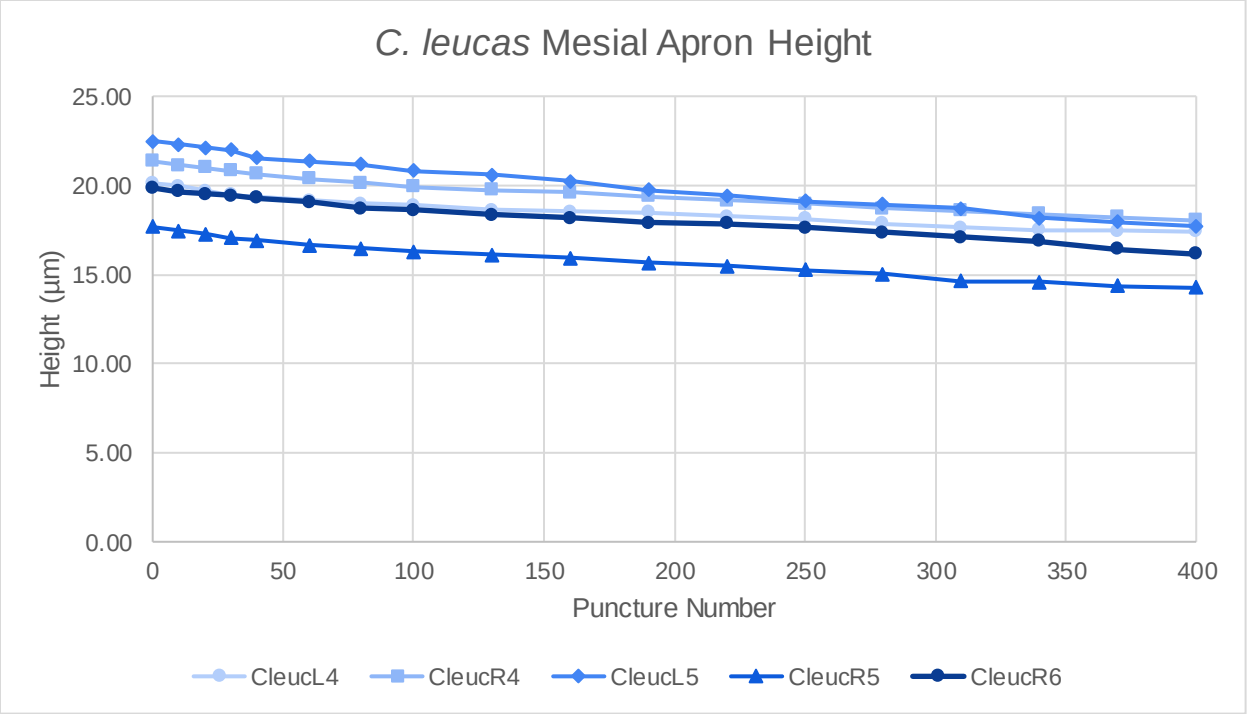
Appendix H: Mesial Apron

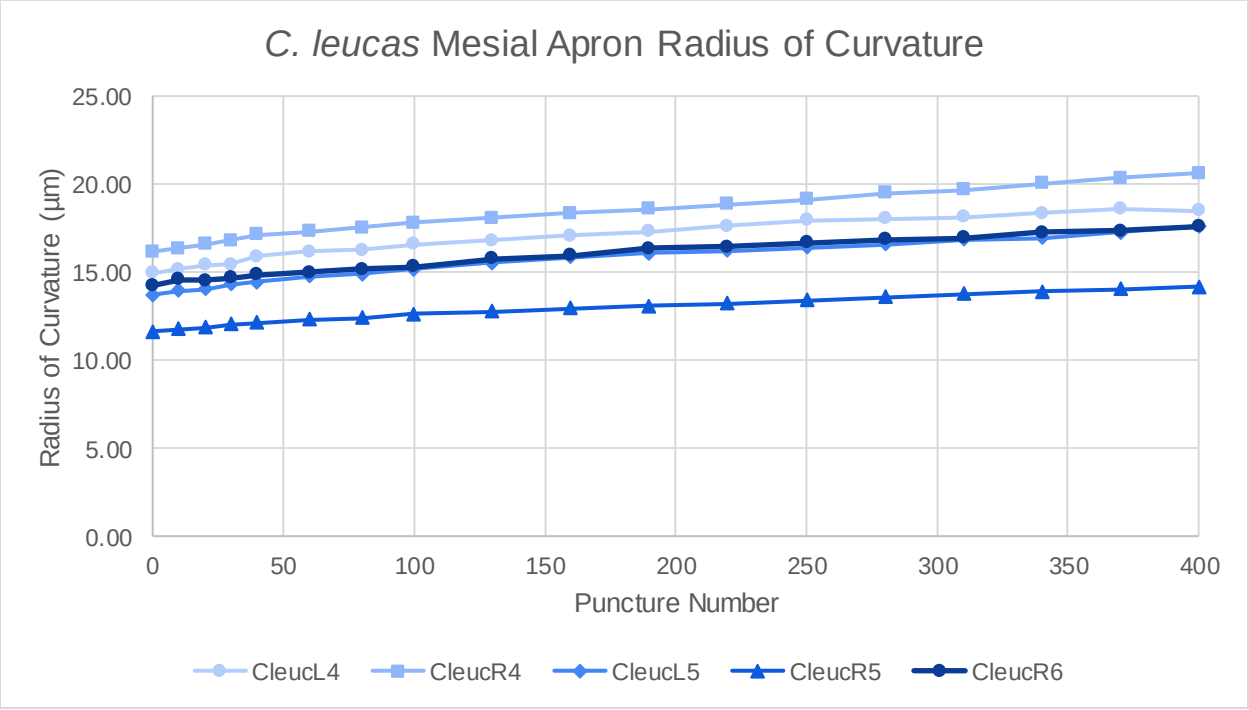


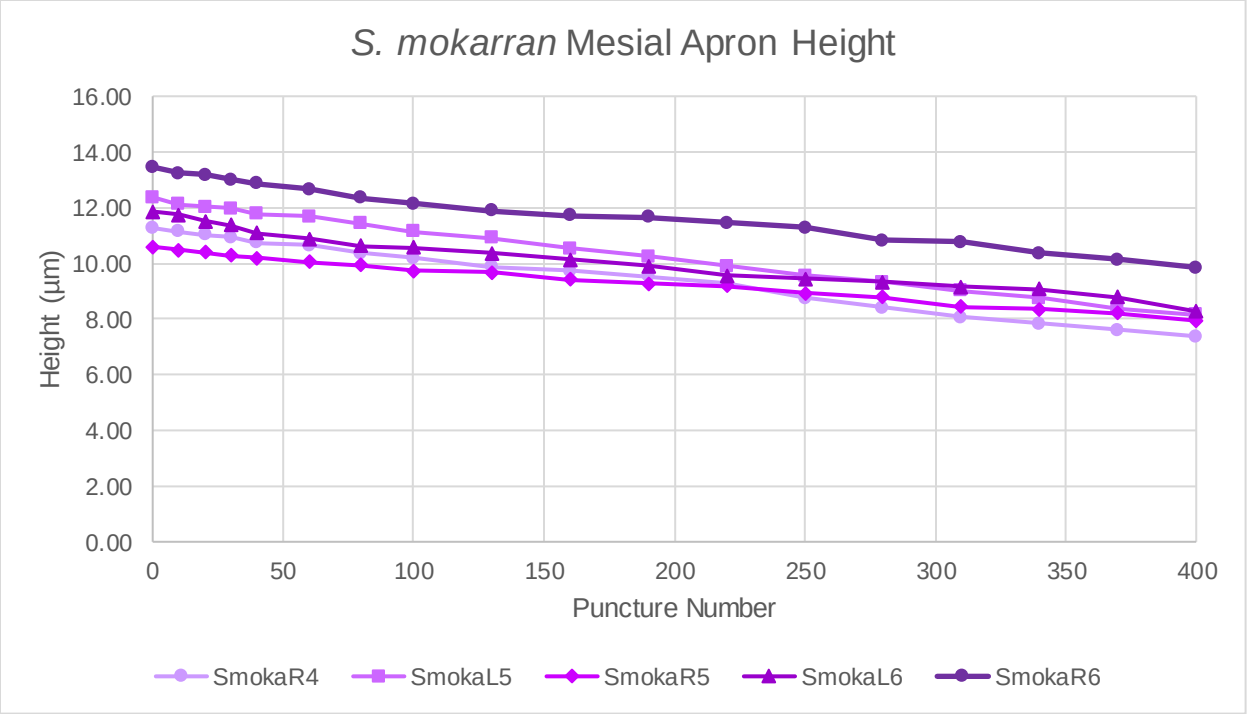


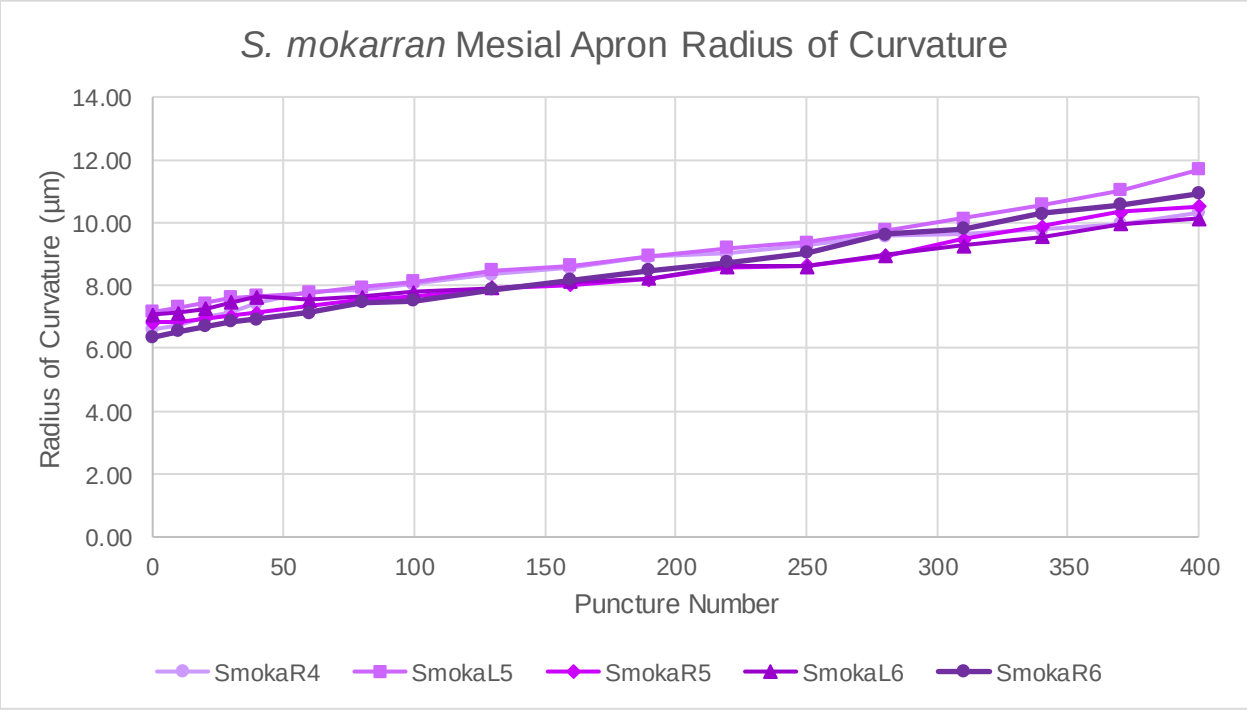

C. limbatus Mesial Apron Height
25.00
20.00
15.00
10.00
5.00
0.00
Height (µm)
0
50
100
150
200
250
300
350
400
Puncture Number
ClimbL4
ClimbR4
ClimbL5
ClimbR5
ClimbL6

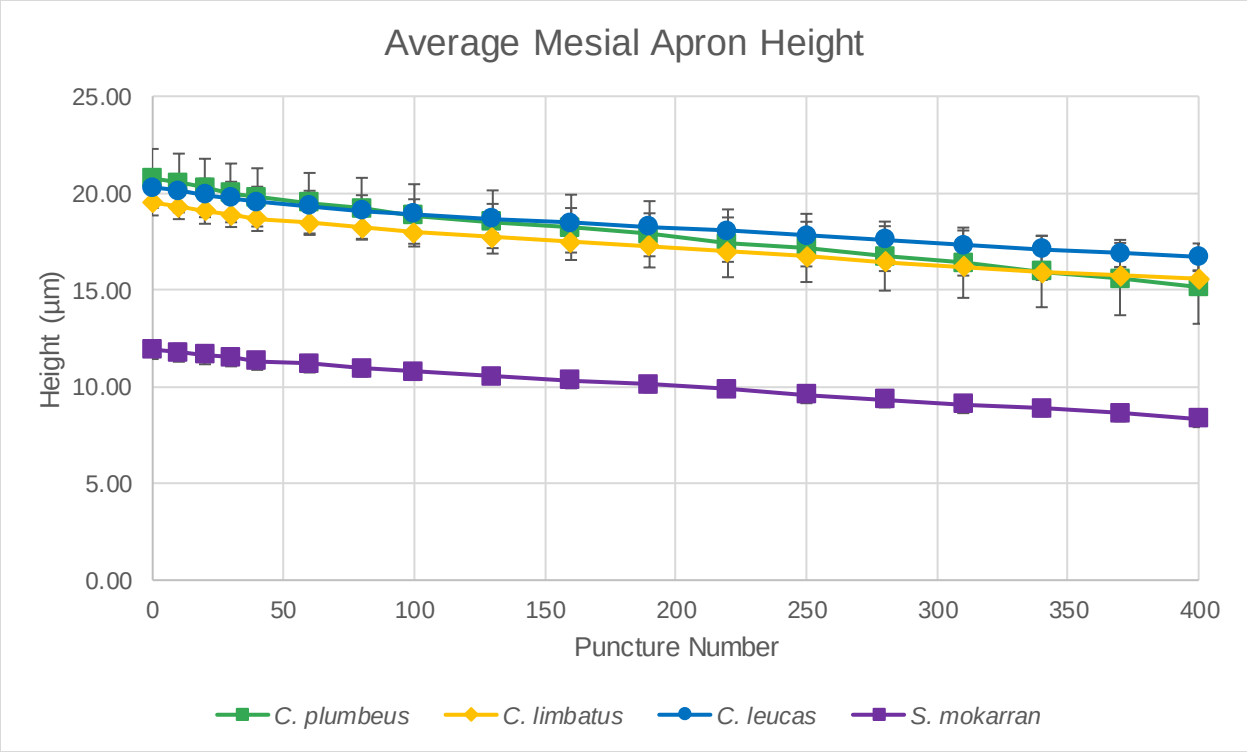

C. limbatus Mesial Apron Radius of Curvature
30.00
25.00
20.00
15.00
10.00
5.00
0.00
Radius of Curvature (µm)
0
50
100
150
200
250
300
350
400
Puncture Number
ClimbL4
ClimbR4
ClimbL5
ClimbR5
ClimbL6

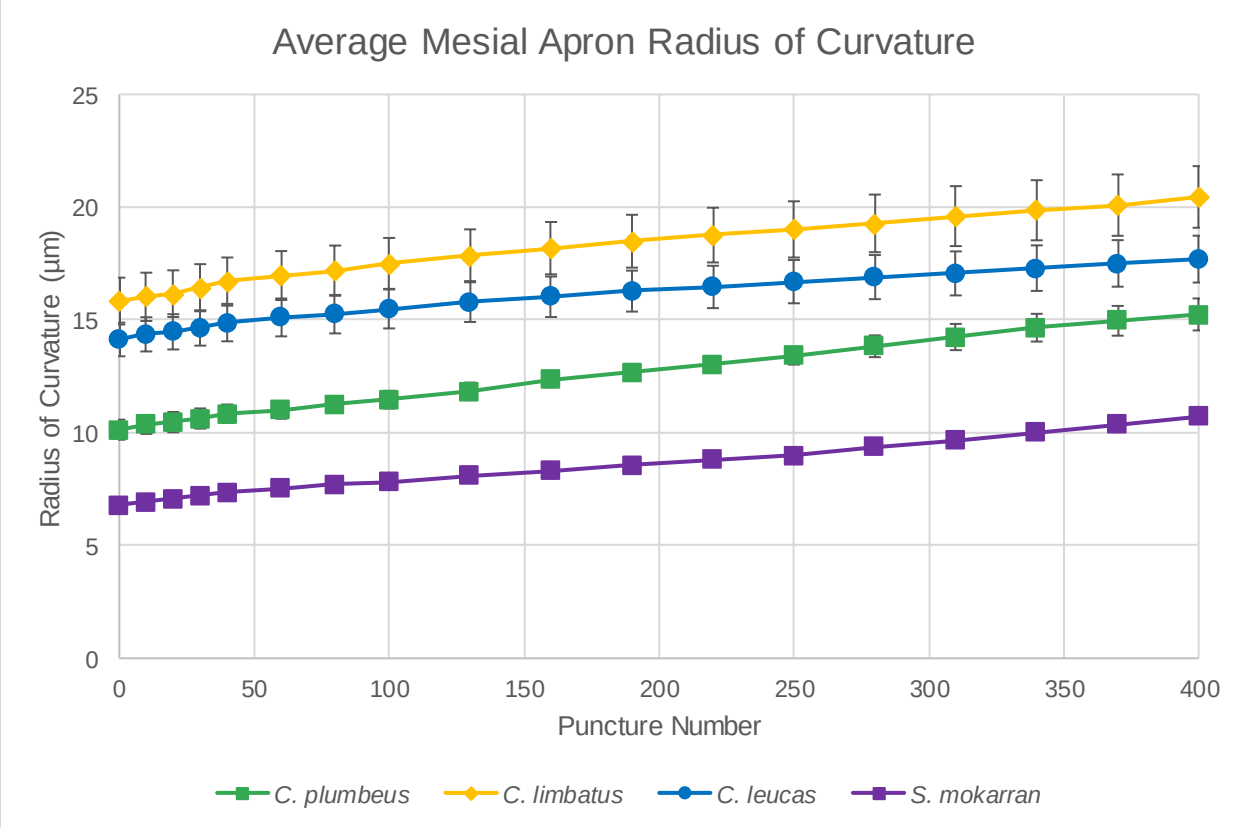

C. leucas Mesial Apron Height
25.00
20.00
15.00
10.00
5.00
0.00
Height (µm)
0
50
100
150
200
250
300
350
400
Puncture Number
CleucL4
CleucR4
CleucL5
CleucR5
CleucR6


C. leucas Mesial Apron Radius of Curvature
25.00
20.00
15.00
10.00
5.00
0.00
Radius of Curvature (µm)
0
50
100
150
200
250
300
350
400
Puncture Number
CleucL4
CleucR4
CleucL5
CleucR5
CleucR6


S. mokarran Mesial Apron Height
16.00
14.00
12.00
10.00
8.00
6.00
4.00
2.00
0.00
Height (µm)
0
50
100
150
200
250
300
350
400
Puncture Number
SmokaR4
SmokaL5
SmokaR5
SmokaL6
SmokaR6


S. mokarran Mesial Apron Radius of Curvature
14.00
12.00
10.00
8.00
6.00
4.00
2.00
0.00
Radius of Curvature (µm)
0
50
100
150
200
250
300
350
400
Puncture Number
SmokaR4
SmokaL5
SmokaR5
SmokaL6
SmokaR6


Average Mesial Apron Height
25.00
20.00
15.00
10.00
5.00
0.00
Height (µm)
0
50
100
150
200
250
300
350
400
Puncture Number
C. plumbeus
C. limbatus
C. leucas
S. mokarran


Average Mesial Apron Radius of Curvature
25
20
15
10
5
0
Radius of Curvature (µm)
0
50
100
150
200
250
300
350
400
Puncture Number
C. plumbeus
C. limbatus
C. leucas
S. mokarran

Appendix I: Rate of Wear Linear Regressions

For each linear regression, the degrees of freedom was 17.

Measurement Type	Species	Slope	*y*-intercept	R^2 value	*P*-value
Puncture Force	*C. plumbeus*	0.0319	3.9187	0.9961	<0.0001
	C. limbatus	0.0196	2.9413	0.9853	<0.0001
	C. leucas	0.0343	10.703	0.9895	<0.0001
	I. oxyrinchus	0.0283	10.095	0.9953	<0.0001
	S. mokarran	0.008	3.5738	0.99	<0.0001
Tip Radius of Curvature	*C. plumbeus*	0.0121	6.2968	0.9903	<0.0001
	C. limbatus	0.0168	16.806	0.9622	<0.0001
	C. leucas	0.0191	18.717	0.9598	<0.0001
	I. oxyrinchus	0.0185	25.099	0.9501	<0.0001
	S. mokarran	0.0076	12.566	0.9737	<0.0001
Distal Apron Height	*C. plumbeus*	-0.0137	22.236	0.9779	<0.0001
	C. limbatus	-0.0187	18.813	0.9869	<0.0001
	C. leucas	-0.0096	23.26	0.9847	<0.0001
	S. mokarran	-0.0069	10.585	0.9716	<0.0001
Distal Apron Radius of Curvature	*C. plumbeus*	0.0167	10.989	0.992	<0.0001
	C. limbatus	0.0095	14.246	0.9823	<0.0001
	C. leucas	0.01	12.646	0.9829	<0.0001
	S. mokarran	0.011	7.4143	0.9932	<0.0001
Distal Middle Height	*C. plumbeus*	-0.0089	14.69	0.9761	<0.0001
	C. limbatus	-0.007	9.6226	0.978	<0.0001
	C. leucas	-0.0095	21.296	0.9918	<0.0001
	S. mokarran	-0.0052	8.499	0.9815	<0.0001

Measurement Type	Species	Slope	*y*-intercept	R^2 value	*P*-value
Distal Middle Radius of Curvature	*C. plumbeus*	0.0093	9.8935	0.9836	<0.0001
	C. limbatus	0.0099	11.684	0.9893	<0.0001
	C. leucas	0.0095	12.692	0.9865	<0.0001
	S. mokarran	0.0053	9.8373	0.9908	<0.0001
Distal Apex Height	*C. plumbeus*	-0.0056	7.442	0.9829	<0.0001
	C. limbatus	-0.0047	6.7277	0.984	<0.0001
	C. leucas	-0.0055	10.533	0.9833	<0.0001
	S. mokarran	-0.0052	7.7936	0.9896	<0.0001
Distal Apex Radius of Curvature	*C. plumbeus*	0.0076	10.138	0.9841	<0.0001
	C. limbatus	0.0086	11.311	0.9925	<0.0001
	C. leucas	0.0085	17.366	0.9936	<0.0001
	S. mokarran	0.0062	8.224	0.9947	<0.0001
Mesial Apex Height	*C. plumbeus*	-0.0061	7.1273	0.9906	<0.0001
	C. limbatus	-0.006	7.818	0.9812	<0.0001
	C. leucas	-0.006	12.737	0.9782	<0.0001
	S. mokarran	-0.0058	7.8746	0.9907	<0.0001
Mesial Apex Radius of Curvature	*C. plumbeus*	0.0076	14.01	0.9949	<0.0001
	C. limbatus	0.0098	11.114	0.9949	<0.0001
	C. leucas	0.0097	16.19	0.9936	<0.0001
	S. mokarran	0.0061	8.7884	0.9784	<0.0001
Mesial Middle Height	*C. plumbeus*	-0.0078	12.392	0.996	<0.0001
	C. limbatus	-0.008	12.054	0.9826	<0.0001
	C. leucas	-0.0081	21.38	0.9911	<0.0001
	S. mokarran	-0.0064	9.2627	0.9929	<0.0001

Measurement Type	Species	Slope	*y*-intercept	R^2 value	*P*-value
Mesial Middle Radius of Curvature	*C. plumbeus*	0.0074	8.9167	0.9953	<0.0001
	C. limbatus	0.0095	14.089	0.9866	<0.0001
	C. leucas	0.007	11.964	0.9817	<0.0001
	S. mokarran	0.0076	9.4942	0.9954	<0.0001
Mesial Apron Height	*C. plumbeus*	-0.0133	20.413	0.9931	<0.0001
	C. limbatus	-0.0095	19.14	0.9838	<0.0001
	C. leucas	-0.0085	19.965	0.9836	<0.0001
	S. mokarran	-0.0086	11.739	0.9956	<0.0001
Mesial Apron Radius of Curvature	*C. plumbeus*	0.0128	10.229	0.999	<0.0001
	C. limbatus	0.0111	16.177	0.9847	<0.0001
	C. leucas	0.0085	14.474	0.9805	<0.0001
	S. mokarran	0.0092	6.8813	0.9948	<0.0001